

NONLINEAR ASSIMILATION WITH SCORE-BASED SEQUENTIAL LANGEVIN SAMPLING

ZHAO DING¹, CHENGUANG DUAN¹, YULING JIAO¹, JERRY ZHIJIAN YANG¹, CHENG YUAN²,
AND PINGWEN ZHANG^{1,3}

ABSTRACT. This paper presents a novel approach for nonlinear assimilation called score-based sequential Langevin sampling (SSLS) within a recursive Bayesian framework. SSLS decomposes the assimilation process into a sequence of prediction and update steps, utilizing dynamic models for prediction and observation data for updating via score-based Langevin Monte Carlo. An annealing strategy is incorporated to enhance convergence and facilitate multi-modal sampling. The convergence of SSLS in TV-distance is analyzed under certain conditions, providing insights into error behavior related to hyper-parameters. Numerical examples demonstrate its outstanding performance in high-dimensional and nonlinear scenarios, as well as in situations with sparse or partial measurements. Furthermore, SSLS effectively quantifies the uncertainty associated with the estimated states, highlighting its potential for error calibration.

1. INTRODUCTION

Data assimilation aims to estimate the time-varying latent states given noisy observation data and the state transition dynamics (Law et al., 2015, Reich and Cotter, 2015, Reich, 2019). This task is essential in various application scenarios such as weather forecasting (Katsafados et al., 2020, Evensen et al., 2022), digital twin technology (Thelen et al., 2022, 2023), and mathematical finance (Bhar, 2010, Frey and Schmidt, 2012, Elliott and Siu, 2013). Despite its importance and widespread application, data assimilation remains a challenging task. The major difficulties in data assimilation lie in the nonlinear nature of both the state transition dynamics and the measurement model, as well as the high dimensionality of the state. Moreover, in many cases, only noisy and sparse observation data are available, introducing further difficulties to the data assimilation. Apart from estimating the latent states, researchers also need to quantify the uncertainties of the estimated states, which is crucial for assessing and calibrating the estimation error (Sullivan, 2015). These constraints and requirements pose significant challenges for data assimilation.

Various methods have been proposed to address the data assimilation, broadly categorized into variational methods (Evensen et al., 2022) and the Bayesian filtering (Särkkä and Svensson, 2023). The variational methods, such as 3D-Var and 4D-Var (Le Dimet and Talagrand, 1986), estimate the latent states through maximum-a-posteriori. In contrast, Bayesian filtering, including the ensemble Kalman filter (EnKF) (Houtekamer and Mitchell, 1998) and the particle filter (PF) (Gordon et al., 1993, Kitagawa, 1996, Doucet et al., 2001), aims to sample from the posterior distribution. Despite their widespread use, these methods face challenges when

1. WUHAN UNIVERSITY, 2. CENTRAL CHINA NORMAL UNIVERSITY, 3. PEKING UNIVERSITY.

E-mail addresses: zd1998@whu.edu.cn, cgduan.math@whu.edu.cn, yulingjiaomath@whu.edu.cn, zjyang.math@whu.edu.cn, yuancheng@ccnu.edu.cn, pzhang@pku.edu.cn.

Date: November 21, 2024.

Key words and phrases. Data assimilation, Langevin Monte Carlo, Bayesian inverse problems, convergence analysis.

dealing with complex assimilation problems. Specifically, the rationale behind variational methods and EnKF invokes a Gaussian approximation to the posterior distribution (Särkkä and Svensson, 2023). To this end, they assume a Gaussian prior and a Gaussian measurement noise, as well as linearize the dynamics and measurement models. However, in the highly nonlinear assimilation scenarios with non-Gaussian prior and likelihood, the posterior may be far away from a Gaussian distribution (Mandel et al., 2012), leading to poor performance of the Gaussian approximation. On the other hand, the PF suffers from a particle degeneracy or impoverishment in high-dimensional assimilations (Snyder et al., 2008, Bengtsson et al., 2008, Bickel et al., 2008), although the PF does not rely on the linear and Gaussian assumptions. This refers to the phenomenon that when the number of ensemble particles is restricted, with high probability many of the particles in the ensemble will turn out to have the same value (Snyder et al., 2008). This mode collapse arises due to the limited number of particles utilized in the PF, which are inadequate to fully capture the intricate structure of the high-dimensional posterior distribution.

Recently, score-based generative models (Song and Ermon, 2019, Song et al., 2021) have achieved tremendous success in diverse applications (Yang et al., 2023, Chen et al., 2024) such as vision and audio generation (Croitoru et al., 2023, Zhang et al., 2023), medical imaging (Song et al., 2022, Chung and Ye, 2022), as well as life science (Weiss et al., 2023, Watson et al., 2023, Guo et al., 2024c). Their exceptional performance in high-dimensional problems has sparked a surge of interest in utilizing diffusion models for data assimilation (Rozet and Louppe, 2023a, Li et al., 2024, Bao et al., 2024, Si and Chen, 2024). However, a key challenge arises when estimating the time-dependent likelihood (Chung et al., 2023), as existing methods rely on either linear Gaussian assumptions or biased approximations. For example, in Li et al. (2024), the authors propose an unbiased estimation for the time-dependent likelihood assuming a Gaussian prior and likelihood. Rozet and Louppe (2023a) estimate the time-dependent likelihood by exchanging the expectation with likelihood, introducing a bias term known as Jensen’s gap (Chung et al., 2023). In contrast, Bao et al. (2024), Si and Chen (2024) approximate the time-dependent likelihood by scaling the time-independent likelihood with a time-dependent damping function. See Section 5.1 for a detailed review of the related work. While these biased estimations have been empirically validated in specific application scenarios, the precise impact of these biases on assimilation and strategies to mitigate them remain largely mysterious. Consequently, these line of methods may lack reliability.

In order to address the current challenges and benefit from existing approaches, two crucial questions arise:

How to develop a provable method for the high-dimensional and nonlinear data assimilation with only sparse or partial measurements? How to quantify the uncertainty associated with the states estimated by this method?

In this work, we attempt to offer answers to these questions. Our main contributions are summarized as follows:

- (i) We present a novel method for nonlinear assimilation, named score-based sequential Langevin sampling (SSLS), within a recursive Bayesian framework. SSLS decomposes the assimilation process into a sequence of iterations invoking prediction and update steps. During the prediction step, we utilize the dynamics model to predict states, from which the score of the prior distribution can be learned. Subsequently, in the update step, we incorporate the observation data as the likelihood and sample from the posterior distribution using the score-based Langevin Monte Carlo. To improve

convergence and facilitate multi-modal sampling, an annealing strategy is integrated into the Langevin algorithm.

- (ii) We analyze the convergence of SSSL in TV-distance under certain mild conditions. Our theoretical findings characterize precisely how the assimilation error is affected by the various hyper-parameters including the terminal time, the score estimation error, the discretization error, and the initial distribution shift (Theorem 3.5). In addition, our theoretical results provide valuable insights into the convergence of score-based Langevin-type algorithms for posterior sampling (Theorem 3.3), which is of independent interest.
- (iii) We utilize SSSL in various numerical examples to assess its performance and compare it with baseline approaches from multiple perspectives. According to our experimental results, SSSL yields significant advantages in high-dimensional and nonlinear data assimilation, even with only sparse observations. Furthermore, the standard deviation of SSSL accurately indicates estimation errors, highlighting the proficiency of our method in quantifying uncertainty.

1.1. Notations. We now introduce some basic notations. The set of positive integers is denoted by $\mathbb{N} = \{1, 2, \dots\}$. Denote $\mathbb{N}_0 = \{0\} \cup \mathbb{N}$ for convenience. For a positive integer $k \in \mathbb{N}$, let $[k]$ denote the set $\{1, \dots, k\}$. We employ the notations $A \lesssim B$ and $B \gtrsim A$ to signify that there exists an absolute constant $c > 0$ such that $A \leq cB$. Appendix A summarizes the notations used in Sections 2 and 3 for easy reference and cross-checking.

1.2. Organization. The rest of this paper is organized as follows. Section 2 presents the score-based sequential Langevin sampling for data assimilation, while Section 3 provides a thorough theoretical guarantee. The efficiency of our methods is demonstrated through a series of numerical experiments in Section 4. Existing approaches are reviewed in Section 5. Finally, Section 6 summarizes the conclusions and outlines future work. The complete proofs of the theoretical results and the details of the experiments are provided in the appendices.

2. SCORE-BASED SEQUENTIAL LANGEVIN SAMPLING

This section introduces the concept of the data assimilation in Section 2.1, followed by the introduction to the recursive Bayesian framework in Section 2.2. Then Sections 2.3 and 2.4 propose the prediction and update procedures, respectively. The complete assimilation algorithm is summarized in Section 2.5.

2.1. Problem formulation. The data assimilation refers to a class of problems that aim to estimate the state of a time-varying system that is indirectly observed through noisy measurements. Let $(\mathbf{X}_k)_{k \in \mathbb{N}}$ be a sequence of unobservable latent states taking values in \mathbb{R}^d , which satisfies the dynamics model

$$(2.1) \quad \mathbf{X}_{k+1} = \mathcal{F}_k(\mathbf{X}_k, \mathbf{V}_k).$$

Here $k \in \mathbb{N}$ is the time index, \mathcal{F}_k is a time-dependent forward propagation operator, and $(\mathbf{V}_k)_{k \in \mathbb{N}}$ is a sequence of independent random variables with known distribution. The dynamics model (2.1) implies that $(\mathbf{X}_k)_{k \in \mathbb{N}}$ is a non-homogeneous Markov chain, defined in terms of the transition probability density $\rho_k(\mathbf{x}|\mathbf{x}_k) := p_{\mathbf{X}_{k+1}|\mathbf{X}_k}(\mathbf{x}|\mathbf{x}_k)$. The stochastic process $(\mathbf{Y}_k)_{k \in \mathbb{N}}$ represents the indirect and noisy observations, linked with the latent states $(\mathbf{X}_k)_{k \in \mathbb{N}}$ by the measurement model

$$(2.2) \quad \mathbf{Y}_k = \mathcal{G}_k(\mathbf{X}_k, \mathbf{W}_k),$$

where \mathcal{G}_k is a time-dependent measurement operator, and $(\mathbf{W}_k)_{k \in \mathbb{N}}$ is a sequence of independent noise with known distribution. Denote the conditional density associated with the measurement model (2.2) by $g_k(\mathbf{y}|\mathbf{x}) := p_{\mathbf{Y}_k|\mathbf{X}_k}(\mathbf{y}|\mathbf{x})$, which is known as the measurement likelihood. The dynamics model (2.1) together the measurement model (2.2) characterize a state-space model illustrated in Figure 1.

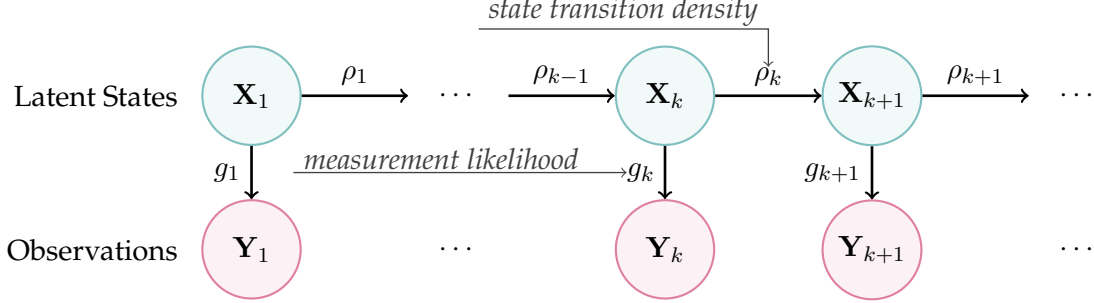


FIGURE 1. A illustrative schematic of the state-space model. The latent states $(\mathbf{X}_k)_{k \in \mathbb{N}}$ are unobservable and evolves according to known transition densities $(\rho_k)_{k \in \mathbb{N}}$, which are specified by a dynamics model (2.1). The observations $(\mathbf{Y}_k)_{k \in \mathbb{N}}$ are linked with states by a known likelihood g_k characterized by the measurement model (2.2).

The goal of the data assimilation is to estimate the posterior distribution of the latent state \mathbf{X}_{k+1} conditioned on all available observations $\mathbf{Y}_{[k+1]}$, that is,

$$(2.3) \quad \pi_{k+1}(\mathbf{x}|\mathbf{y}_{[k+1]}) := p_{\mathbf{X}_{k+1}|\mathbf{Y}_{[k+1]}}(\mathbf{x}|\mathbf{y}_{[k+1]}), \quad k \in \mathbb{N}.$$

It is worth noting that in practical scenarios, one is typically interested in the particle approximation to the posterior distribution (2.3), rather than the values of the posterior density function. Therefore, the data assimilation is reformulated to a sequence of posterior sampling problems.

2.2. Recursive Bayesian framework. In this subsection, we introduce the recursive Bayesian framework (Särkkä and Svensson, 2023). The posterior distribution in (2.3) can be expressed as the product of the measurement likelihood g_{k+1} (2.2) and the prior on \mathbf{X}_{k+1} given previous observations via the Bayes' rule

$$(2.4) \quad \pi_{k+1}(\mathbf{x}|\mathbf{y}_{[k+1]}) \propto g_{k+1}(\mathbf{y}_{k+1}|\mathbf{x})p_{\mathbf{X}_{k+1}|\mathbf{Y}_{[k]}}(\mathbf{x}|\mathbf{y}_{[k]}),$$

where we omit the constant independent of \mathbf{x} . The conditional distribution $q_{k+1} := p_{\mathbf{X}_{k+1}|\mathbf{Y}_{[k]}}$ is known as the prediction distribution, which is linked to the previous posterior distribution and the dynamics model (2.1) by Chapman-Kolmogorov identity

$$(2.5) \quad q_{k+1}(\mathbf{x}|\mathbf{y}_{[k]}) = \int \rho_k(\mathbf{x}|\mathbf{x}_k)\pi_k(\mathbf{x}_k|\mathbf{y}_{[k]}) d\mathbf{x}_k.$$

The prediction (2.5) and update (2.4) stages can be combined to characterize a recursion from the previous posterior π_k to the current posterior π_{k+1} as

$$(2.6) \quad \pi_{k+1}(\mathbf{x}|\mathbf{y}_{[k+1]}) \propto g_{k+1}(\mathbf{y}_{k+1}|\mathbf{x}) \int \rho_k(\mathbf{x}|\mathbf{x}_k)\pi_k(\mathbf{x}_k|\mathbf{y}_{[k]}) d\mathbf{x}_k.$$

This recursion serves as the central object throughout our method, which enables us to decompose the data assimilation into a sequence of posterior sampling problems. Each of these sub-problems can be solved by alternating between prediction (2.5) and update (2.4)

steps. The complete procedure of the prediction-update recursion is illustrated in Figure 2. We will present these two steps in detail as Sections 2.3 and 2.4, respectively.

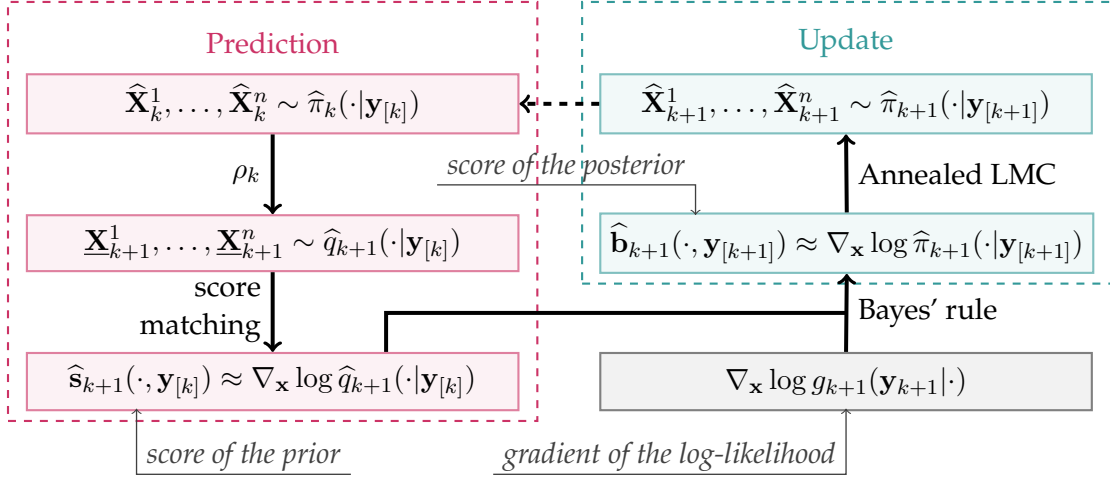


FIGURE 2. A illustrative schematic of the score-based sequential Langevin sampling. (a) In the prediction step, we sample from the approximated prediction distribution and then estimate the prediction score, which serves as the prior score. Combining the prior score and the gradient of the log-likelihood yields the posterior score as (2.13). (b) In the update step, we sample from the posterior distribution through the ALMC. This procedure characterizes a recursion from the previous posterior to the current posterior.

2.3. Prediction and score matching. This section focuses on estimating the score, i.e., the gradient of log-density, of the prediction distribution (2.5), given an estimator $\widehat{\pi}_k(\cdot | \mathbf{y}_{[k]})$ of the previous posterior distribution $\pi_k(\cdot | \mathbf{y}_{[k]})$. The prediction score estimator will be utilized in the update step for sampling through Langevin-type algorithms, as demonstrated in the subsequent subsection.

To begin with, we introduce an approximated prediction distribution

$$(2.7) \quad \widehat{q}_{k+1}(\mathbf{x} | \mathbf{y}_{[k]}) := \int \rho_k(\mathbf{x} | \mathbf{x}_k) \widehat{\pi}_k(\mathbf{x}_k | \mathbf{y}_{[k]}) d\mathbf{x}_k \approx q_{k+1}(\mathbf{x} | \mathbf{y}_{[k]}).$$

It is apparent that (2.7) closely approximates the prediction distribution (2.5), provided that $\widehat{\pi}_k(\cdot | \mathbf{y}_{[k]})$ closely resembles the previous posterior distribution $\pi_k(\cdot | \mathbf{y}_{[k]})$. Therefore, it remains to estimate the score of the approximated prediction distribution (2.7).

According to the dynamics model (2.1), a particle approximation to the approximated prediction distribution (2.7) can be constructed by the dynamics model

$$(2.8) \quad \widehat{\mathbf{X}}_{k+1}^i = \mathcal{F}_k(\widehat{\mathbf{X}}_k^i, \mathbf{V}_k^i), \quad 1 \leq i \leq n,$$

where $\widehat{\mathbf{X}}_k^1, \dots, \widehat{\mathbf{X}}_k^n$ are independent random variables drawn from the previous estimated posterior $\widehat{\pi}_k(\cdot | \mathbf{y}_{[k]})$, and $\mathbf{V}_k^1, \dots, \mathbf{V}_k^n$ are independent random copies of \mathbf{V}_k . There have been several approaches that can estimate the score from a particle approximation, such as the implicit score matching (Hyvärinen, 2005), the sliced score matching (Song et al., 2020), and the denoising score matching (Vincent, 2011, Ho et al., 2020, Song and Ermon, 2019, Song et al., 2021). In this work, we introduce a Gaussian smoothing to the approximated prediction distribution (2.7), and then estimate the score of smoothed density from a particle approximation using the denoising score matching.

For a fixed noise level $\sigma > 0$, define the Gaussian smoothed prediction density as

$$(2.9) \quad q_{k+1}^\sigma(\mathbf{x}|\mathbf{y}_{[k]}) = \int N(\mathbf{x}; \mathbf{x}_0, \sigma^2 \mathbf{I}_d) \widehat{q}_{k+1}(\mathbf{x}_0|\mathbf{y}_{[k]}) d\mathbf{x}_0 \approx \widehat{q}_{k+1}(\mathbf{x}|\mathbf{y}_{[k]}).$$

The score function of the smoothed distribution is an approximation to that of the original prediction density $\widehat{q}_{k+1}(\cdot|\mathbf{y}_{[k]})$ for sufficiently small noise level $\sigma > 0$ (Tang and Yang, 2024). We therefore use the score function of (2.9) as the surrogate score. According to the denoising score matching (Vincent, 2011), the score function of the smoothed density (2.9) minimizes the objective functional

$$L_{k+1}(\mathbf{s}) = \mathbb{E}_{\mathbf{X}_{k+1} \sim \widehat{q}_{k+1}(\cdot|\mathbf{y}_{[k]})} \mathbb{E}_{\boldsymbol{\varepsilon} \sim N(0, \mathbf{I}_d)} [\|\sigma \mathbf{s}(\mathbf{X}_{k+1} + \sigma \boldsymbol{\varepsilon}, \mathbf{y}_{[k]}) + \boldsymbol{\varepsilon}\|_2^2].$$

However, in practical applications, this population risk is analytically intractable. Hence one needs to estimate the score function by the empirical risk minimization

$$(2.10) \quad \widehat{\mathbf{s}}_{k+1} \in \arg \min_{\mathbf{s} \in \mathcal{S}} \widehat{L}_{k+1}(\mathbf{s}) = \frac{1}{n} \sum_{i=1}^n \|\sigma \mathbf{s}(\mathbf{X}_{k+1}^i + \sigma \boldsymbol{\varepsilon}_i, \mathbf{y}_{[k]}) + \boldsymbol{\varepsilon}_i\|_2^2,$$

where \mathcal{S} is a deep neural network class, $\{\mathbf{X}_{k+1}^i\}_{i=1}^n$ is a set of independent predicted states defined as (2.8), and $\{\boldsymbol{\varepsilon}_i\}_{i=1}^n$ is a set of independent standard Gaussian variables.

Remark 2.1 (Inflation). The Gaussian smoothing equation (2.9) is commonly known as inflation in the field of data assimilation, and has demonstrated empirical success in practical applications (Anderson and Anderson, 1999, Anderson, 2009, Sacher and Bartello, 2008, Evensen et al., 2022). Inflation serves two main purposes: firstly, it is necessary to mitigate the excessive reduction of variance resulting from spurious correlations in the update step. Secondly, inflation provides a means to account for model errors that may not be captured in the dynamics model (2.1).

2.4. Update via annealed Langevin Monte Carlo. In the previous subsection, we have estimated the score of the prediction distribution. This subsection introduces an annealed Langevin Monte Carlo (ALMC) to sample from the posterior distribution $\pi_{k+1}(\cdot|\mathbf{y}_{[k+1]})$ in (2.4).

Before proceeding, we introduce the Langevin Monte Carlo (LMC) for the posterior sampling. The Langevin diffusion associated with the target distribution $\pi_{k+1}(\cdot|\mathbf{y}_{[k+1]})$ is defined as the solution to the stochastic differential equation

$$(2.11) \quad d\mathbf{Z}_t = \nabla_{\mathbf{x}} \log \pi_{k+1}(\mathbf{Z}_t|\mathbf{y}_{[k+1]}) dt + \sqrt{2} d\mathbf{B}_t, \quad \mathbf{Z}_0 \sim \widehat{q}_{k+1}(\cdot|\mathbf{y}_{[k]}),$$

where $(\mathbf{B}_t)_{t \geq 0}$ is a Brownian motion. Classically, if π_{k+1} satisfies a functional inequality such as Poincaré's inequality or log-Sobolev inequality, then the law of Langevin diffusion (2.11) converges exponentially fast to the target distribution π_{k+1} (Bakr et al., 2014). However, in most of the cases, Langevin diffusion (2.11) can not be simulated analytically, and the exact score function is intractable. The Euler-Maruyama discretization (Kloeden and Platen, 1992) of the Langevin diffusion with the estimated score (2.10) leads to the score-based LMC, which defines a discrete-time non-homogeneous Markov chain

$$(2.12) \quad \widehat{\mathbf{Z}}_{(\ell+1)h} = \widehat{\mathbf{Z}}_{\ell h} + h \widehat{\mathbf{b}}_{k+1}(\widehat{\mathbf{Z}}_{\ell h}|\mathbf{y}_{[k+1]}) + \sqrt{2h} \boldsymbol{\xi}_\ell, \quad \widehat{\mathbf{Z}}_0 \sim \widehat{q}_{k+1}(\cdot|\mathbf{y}_{[k]}),$$

where $h > 0$ is the step size, $(\boldsymbol{\xi}_\ell)_{\ell \in \mathbb{N}}$ is a sequence of independent standard Gaussian variables, and the drift term is the sum of the log-likelihood and the estimated prediction score function (2.10)

$$(2.13) \quad \widehat{\mathbf{b}}_{k+1}(\mathbf{Z}_t, \mathbf{y}_{[k+1]}) = \nabla_{\mathbf{x}} \log g_{k+1}(\mathbf{y}_{k+1}|\mathbf{x}) + \widehat{\mathbf{s}}_{k+1}(\mathbf{x}|\mathbf{y}_{[k]}).$$

The LMC is also known as the unadjusted Langevin algorithm (ULA) in the computational statistics literature (Roberts and Tweedie, 1996).

Recall the setting of data assimilation, the Bayes' rule characterizes a distribution transition from the prediction distribution q_{k+1} to the posterior distribution π_{k+1} via the likelihood,

$$\pi_{k+1}(\mathbf{x}|\mathbf{y}_{[k+1]}) \propto g_{k+1}(\mathbf{y}_{k+1}|\mathbf{x})q_{k+1}(\mathbf{x}|\mathbf{y}_{[k]}).$$

However, as the posterior may be far from the prediction distribution, sampling from the posterior through LMC (2.12) is typically perceived as inefficient. To overcome this difficulties, we propose an annealing procedure for the posterior sampling. The rationale behind annealing involves a gradual transition from the prediction distribution to the target posterior distribution. Specifically, we construct a sequence of interpolations between the prediction distribution and the posterior (Del Moral et al., 2006, Guo et al., 2024a)

$$\pi_{k+1}^m(\mathbf{x}|\mathbf{y}_{[k+1]}) \propto \pi_{k+1}(\mathbf{y}_{k+1}|\mathbf{x})^{\beta_m} q_{k+1}(\mathbf{x}|\mathbf{y}_{[k]})^{1-\beta_m}, \quad 0 \leq m \leq M,$$

where $0 \equiv \beta_0 < \beta_1 < \dots < \beta_M \equiv 1$ is inverse temperatures with $\beta_0 = 0$ corresponding to the prior and $\beta_M = 1$ corresponding to the full posterior. It is evident that when β_m is small, the interpolation distribution π_{k+1}^m is dominated by the prediction distribution q_{k+1} , making it easy to sample from it starting from the sampleable prediction distribution. On the other hand, as β_m becomes sufficiently close to 1, the interpolation π_{k+1}^m approximates the target distribution π_{k+1} closely. With the gradual increase of the annealing schedule β_m from 0 to 1, the readily sampleable prediction distribution q_{k+1} slowly transport towards the target posterior distribution π_{k+1} . It has been shown that the annealing procedure not only accelerates the convergence of the sampling algorithm (Guo et al., 2024a), but also makes it possible to sample from multi-modal data (Wu and Xie, 2024).

At each inverse temperature β_m , we aim to sample from $\pi_{k+1}^m(\cdot|\mathbf{y}_{[k+1]})$ through LMC. The prior is set as the distribution $\pi_{k+1}^{m-1}(\cdot|\mathbf{y}_{[k]})$ at the previous inverse temperature β_{m-1} , and the likelihood is given by Radon-Nikodym derivative

$$\frac{\pi_{k+1}^m(\mathbf{x}|\mathbf{y}_{[k+1]})}{\pi_{k+1}^{m-1}(\mathbf{x}|\mathbf{y}_{[k+1]})} \propto \frac{\pi_{k+1}(\mathbf{y}_{k+1}|\mathbf{x})^{\beta_m} q_{k+1}(\mathbf{x}|\mathbf{y}_{[k]})^{1-\beta_m}}{\pi_{k+1}(\mathbf{y}_{k+1}|\mathbf{x})^{\beta_{m-1}} q_{k+1}(\mathbf{x}|\mathbf{y}_{[k]})^{1-\beta_{m-1}}} \propto g_{k+1}(\mathbf{y}_{k+1}|\mathbf{x})^{\beta_m - \beta_{m-1}}.$$

Then the sampling scheme is given as

$$(2.14) \quad \widehat{\mathbf{Z}}_{(\ell+1)h}^m = \widehat{\mathbf{Z}}_{\ell h}^m + h \widehat{\mathbf{b}}_{k+1}^m(\widehat{\mathbf{Z}}_{\ell h}^m|\mathbf{y}_{[k+1]}) + \sqrt{2h} \boldsymbol{\xi}_{\ell}^m, \quad \widehat{\mathbf{Z}}_0^m \sim \widehat{\pi}_{k+1}^{m-1}(\cdot|\mathbf{y}_{[k+1]}),$$

where $h > 0$ is the step size, $(\boldsymbol{\xi}_{\ell}^m)_{\ell \in \mathbb{N}}$ is a sequence of independent standard Gaussian variables, and the drift term is a weighted linear combination of the log-likelihood and the estimated prediction score function (2.10)

$$(2.15) \quad \widehat{\mathbf{b}}_{k+1}^m(\mathbf{x}) = \beta_m \nabla_{\mathbf{x}} \log g_{k+1}(\mathbf{y}_{k+1}|\mathbf{x}) + \widehat{\mathbf{s}}_{k+1}(\mathbf{x}|\mathbf{y}_{[k]}) \approx \nabla_{\mathbf{x}} \log \pi_{k+1}^m(\mathbf{x}).$$

Since distributions at two neighboring temperatures are very close, the LMC (2.14) converges easily. The detailed algorithm for the $(k+1)$ -th time step is summarized as Algorithm 1.

Remark 2.2 (Annealing). The convergence of the standard LMC (2.12) is proven under certain isoperimetric and warm-start assumptions. Refer to Section 3 for a comprehensive explanation. In order to address these limitations, the method of annealing is commonly utilized to enhance sampling algorithms (Del Moral et al., 2006, Brosse et al., 2018, Song and Ermon, 2019, 2020, Ge et al., 2020, Jalal et al., 2021, Guo et al., 2024a, Wu and Xie, 2024). However, existing approaches typically generate interpolation distributions through products (Brosse et al., 2018, Ge et al., 2020, Guo et al., 2024a, Wu and Xie, 2024) or convolutions (Song and Ermon,

Algorithm 1: Update by Annealed Langevin Monte Carlo.

-
- 1 **Input:** Prediction samples $\underline{\mathbf{X}}_{k+1}^1, \dots, \underline{\mathbf{X}}_{k+1}^n$, an estimator of the prediction score $\widehat{\mathbf{s}}_{k+1}$, the measurement likelihood g_{k+1} .
 - 2 **Output:** A particle approximation $\widehat{\mathbf{X}}_{k+1}^1, \dots, \widehat{\mathbf{X}}_{k+1}^n$ of the posterior distribution π_{k+1} .
 - 3 Set inverse temperatures $0 \equiv \beta_0 < \beta_1 < \dots < \beta_M \equiv 1$, and a step size $h > 0$.
 - 4 Initialize the particles $\widehat{\mathbf{Z}}_0^{1,i} \leftarrow \underline{\mathbf{X}}_{k+1}^i$ for each $1 \leq i \leq n$.
 - 5 **for** $m = 1, \dots, M$ **do**
 - 6 **for** $\ell = 0, \dots, K - 1$ **do**
 - 7 Sample independent Gaussian noises $\boldsymbol{\xi}_\ell^{m,1}, \dots, \boldsymbol{\xi}_\ell^{m,n} \sim \text{i.i.d. } N(0, \mathbf{I})$.
 - 8 Compute the estimated posterior score
 $\widehat{\mathbf{b}}_{k+1}^m(\cdot | \mathbf{y}_{[k+1]}) \leftarrow \beta_m \nabla_{\mathbf{x}} \log g_{k+1}(\mathbf{y}_{k+1} | \cdot) + \widehat{\mathbf{s}}_{k+1}(\cdot | \mathbf{y}_{[k]})$.
 - 9 Update by the LMC, for $1 \leq i \leq n$,
 $\widehat{\mathbf{Z}}_{(\ell+1)h}^{m,i} \leftarrow \widehat{\mathbf{Z}}_{\ell h}^{m,i} + h \widehat{\mathbf{b}}_{k+1}^m(\widehat{\mathbf{Z}}_{\ell h}^{m,i} | \mathbf{y}_{[k+1]}) + \sqrt{2h} \boldsymbol{\xi}_\ell^{m,i}$.
 - 10 **end**
 - 11 Initialize the particles for the next round $\widehat{\mathbf{Z}}_0^{m+1,i} \leftarrow \widehat{\mathbf{Z}}_{Kh}^{m,i}$ for $1 \leq i \leq n$.
 - 12 **end**
 - 13 $\widehat{\mathbf{X}}_{k+1}^i \leftarrow \widehat{\mathbf{Z}}_{Kh}^{M,i}$ for $1 \leq i \leq n$.
-

2019, 2020, Jalal et al., 2021) of the target distribution with a Gaussian distribution, which limits their ability to incorporate prior information in the posterior sampling. In contrast, the annealing method (2.14) proposed in this study involves interpolating between the target posterior distribution and the prior distribution. Moreover, our approach is closely related to sequential Monte Carlo methods (Del Moral et al., 2006, Kantas et al., 2014, Beskos et al., 2015). Unlike previous methods in this area, the score-based LMC has better empirical performance in high-dimensional problems by exploiting the advantages of deep neural networks.

2.5. Summary of the procedure. With the help of Sections 2.3 and 2.4, one can sample from the current posterior distribution $\pi_{k+1}(\cdot | \mathbf{y}_{[k+1]})$ given a particle approximation to the previous posterior distribution $\pi_k(\cdot | \mathbf{y}_{[k]})$.

We now illustrate how to achieve a particle approximation to the initial posterior distribution $\pi_1(\cdot | \mathbf{y}_1)$. Applying the Bayes' rule, one has

$$(2.16) \quad \nabla_{\mathbf{x}} \log \pi_1(\mathbf{x} | \mathbf{y}_1) = \nabla_{\mathbf{x}} \log q_1(\mathbf{y}_1 | \mathbf{x}) + \nabla_{\mathbf{x}} \log p_{\mathbf{X}_1}(\mathbf{x}),$$

where $q_1 = p_{\mathbf{X}_1}$ denotes the initial prior distribution. Hence, sampling from the initial posterior distribution $\pi_1(\cdot | \mathbf{y}_1)$ only requires estimating the score of the initial prior distribution $\nabla_{\mathbf{x}} \log q_1$. In practical scenarios, one may have a set of samples independently drawn from \widehat{q}_1 , a guess of the initial prior q_1 . The initial prior score $\nabla_{\mathbf{x}} \log q_1$ can then be estimated from these samples using Gaussian smoothing and denoising score matching as (2.10), denoted as $\widehat{\mathbf{s}}_1$.

The complete algorithm of the score-based sequential Langevin sampling is summarized in Algorithm 2.

Remark 2.3 (Reduction of the computational cost). In each time step of Algorithm 2, it is necessary to learn a score network from the predicted states, which results in a substantial computational burden. However, in practical applications, it is often sufficient to fine-tune the score network that has been trained in the previous time step, rather than retrain it from

Algorithm 2: Score-based sequential Langevin sampling for data assimilation.

1 **Input:** The observations $(\mathbf{y}_k)_{k \in \mathbb{N}}$, the dynamics model $(\mathcal{F}_k)_{k \in \mathbb{N}}$, the measurement likelihood $(g_k)_{k \in \mathbb{N}}$.

2 **Output:** A particle approximation $\widehat{\mathbf{X}}_{k+1}^1, \dots, \widehat{\mathbf{X}}_{k+1}^n$ to the distribution $\pi_{k+1}(\cdot | \mathbf{y}_{[k+1]})$.

3 **# Initial posterior sampling.**

4 Choose a prior distribution \widehat{q}_1 for assimilation.

5 Sample from the prior distribution $\mathbf{X}_1^1, \dots, \mathbf{X}_1^n \sim \text{i.i.d. } \widehat{q}_1$.

6 Estimate the prior score from $\{\mathbf{X}_1^i\}_{i=1}^n$ by denoising score matching $\widehat{\mathbf{s}}_1$.

7 Sample from the posterior distribution $\widehat{\pi}_1(\cdot | \mathbf{y}_1)$ by the ALMC:
 $\widehat{\mathbf{X}}_1^1, \dots, \widehat{\mathbf{X}}_1^n \leftarrow \text{ALMC}(\mathbf{X}_1^1, \dots, \mathbf{X}_1^n, \widehat{\mathbf{s}}_1, g_1)$.

8 **# Recursive posterior sampling.**

9 **for** $k = 1, 2, \dots$ **do**

10 **# Prediction step.**

11 Sample from the known distribution: $\mathbf{V}_k^i \sim p_{\mathbf{V}}$ for $1 \leq i \leq n$.

12 Run the dynamics model: $\mathbf{X}_{k+1}^i \leftarrow \mathcal{F}_k(\widehat{\mathbf{X}}_k^i, \mathbf{V}_k^i)$ for $1 \leq i \leq n$.

13 Estimate the prediction score from $\{\mathbf{X}_{k+1}^i\}_{i=1}^n$ by denoising score matching $\widehat{\mathbf{s}}_{k+1}$.

14 **# Update step.**

15 Sample from the posterior distribution $\pi_{k+1}(\cdot | \mathbf{y}_{[k+1]})$ by the ALMC:
 $\widehat{\mathbf{X}}_{k+1}^1, \dots, \widehat{\mathbf{X}}_{k+1}^n \leftarrow \text{ALMC}(\mathbf{X}_{k+1}^1, \dots, \mathbf{X}_{k+1}^n, \widehat{\mathbf{s}}_{k+1}, g_{k+1})$.

16 **end**

scratch with random parameter initialization. This approach allows us to significantly reduce the computational cost.

3. CONVERGENCE ANALYSIS

In this section, we present a convergence analysis for score-based sequential Langevin sampling (SSLS). In Section 3.1, we introduce several assumptions regarding the assimilation. Under these assumptions, an error analysis for posterior sampling using score-based LMC is established in Section 3.2. Furthermore, we demonstrate a comprehensive convergence analysis for the assimilation using SSLS in Section 3.3.

Let $\pi_{k+1}^0(\cdot | \mathbf{y}_{[k+1]})$ be the initial distribution of the $(k+1)$ -th time step. We focus on the score-based LMC, that is, for each $0 \leq \ell \leq K-1$,

$$(3.1) \quad \widehat{\mathbf{Z}}_{(\ell+1)h} = \widehat{\mathbf{Z}}_{\ell h} + h \widehat{\mathbf{b}}_{k+1}(\widehat{\mathbf{Z}}_{\ell h} | \mathbf{y}_{[k+1]}) + \sqrt{2h} \boldsymbol{\xi}_{\ell}, \quad \widehat{\mathbf{Z}}_0 \sim \pi_{k+1}^0(\cdot | \mathbf{y}_{[k+1]}),$$

where the estimated posterior score is given as

$$\widehat{\mathbf{b}}_{k+1}(\mathbf{x} | \mathbf{y}_{[k+1]}) = \nabla_{\mathbf{x}} \log g_{k+1}(\mathbf{y}_{k+1} | \mathbf{x}) + \widehat{\mathbf{s}}_{k+1}(\mathbf{x}, \mathbf{y}_{[k]}).$$

Here the prediction score $\widehat{\mathbf{s}}_{k+1}$ is estimated by score matching (2.10). Denote by $\widehat{\pi}_{k+1} := \widehat{\pi}_{k+1}^T$ the law of $\widehat{\mathbf{Z}}_T$ for $T = Kh$. The objective of this section is to provide an upper bound on the TV-distance between the posterior distribution $\pi_{k+1}(\cdot | \mathbf{y}_{[k+1]})$ and its estimation $\widehat{\pi}_{k+1}^T(\cdot | \mathbf{y}_{[k+1]})$, that is,

$$(3.2) \quad \varepsilon_{\text{TV}}^k := \text{TV}(\pi_k(\cdot | \mathbf{y}_{[k]}), \widehat{\pi}_k^T(\cdot | \mathbf{y}_{[k]})), \quad k \in \mathbb{N}.$$

3.1. Assumptions. Before proceeding, we introduce some assumptions.

Assumption 1 (Lipschitz score). For each $k \in \mathbb{N}$, the posterior score is λ -Lipschitz on \mathbb{R}^d , that is, for each $\mathbf{x}_1, \mathbf{x}_2 \in \mathbb{R}^d$,

$$\|\nabla_{\mathbf{x}} \log \pi_{k+1}(\mathbf{x}_1 | \mathbf{y}_{[k+1]}) - \nabla_{\mathbf{x}} \log \pi_{k+1}(\mathbf{x}_2 | \mathbf{y}_{[k+1]})\|_2 \leq \lambda \|\mathbf{x}_1 - \mathbf{x}_2\|_2.$$

Assumption 1 is a fundamental requirement in the convergence analysis of Langevin-type sampling methods (Chewi et al., 2024, Chewi, 2024, Lee et al., 2022). This assumption guarantees the existence and uniqueness of strong solution to the Langevin diffusion (2.11). Further, it is crucial for the analysis of discretization errors in LMC.

Our analysis heavily depends on some isoperimetric property of the target posterior distribution stated as the following assumption.

Assumption 2 (Log-Sobolev inequality). For each $k \in \mathbb{N}$, the posterior distribution satisfies a log-Sobolev inequality with constant C_{LSI} , that is, for each function $f \in C_0^\infty(\mathbb{R}^d)$,

$$\text{Ent}(f^2) \leq 2C_{\text{LSI}} \mathbb{E}[\|\nabla_{\mathbf{x}} f\|_2^2],$$

where the entropy is defined as $\text{Ent}(g) = \mathbb{E}[g \log g] - \mathbb{E}[g] \log \mathbb{E}[g]$, and the expectation and variance are taken with respect to the posterior distribution $\pi_{k+1}(\cdot | \mathbf{y}_{[k+1]})$.

Assumption 2 plays an important role in ensuring the convergence of Langevin diffusion and LMC (Chewi et al., 2024, Chewi, 2024, Lee et al., 2022, Tang and Yang, 2024). This assumption is mild in the context of posterior sampling. Indeed, the Bernstein-von Mises theorem states that as the number of samples tends to infinity, the posterior distribution is close to a Gaussian distribution and thus satisfies the log-Sobolev inequality (Nickl and Wang, 2024).

Assumption 3 (Boundedness). For each $k \in \mathbb{N}$,

- (i) there exists $B \geq 1$ such that $\rho_k(\mathbf{x} | \mathbf{x}_k), \|\nabla_{\mathbf{x}} \rho_k(\mathbf{x} | \mathbf{x}_k)\|_\infty \leq B$ for $\mathbf{x} \in \mathbb{R}^d$,
- (ii) there exists $D \geq 1$ such that $q_{k+1}(\mathbf{x} | \mathbf{y}_{[k]}) \geq D^{-1}$ for $\mathbf{x} \in \Omega_{k+1} := \text{supp}(q_{k+1}(\cdot | \mathbf{y}_{[k]}))$,
- (iii) there exists $G \geq 1$ such that $g_k(\mathbf{y} | \mathbf{x}) \leq G$ for $\mathbf{x} \in \mathbb{R}^d$, and
- (iv) $q_1(\mathbf{x}), \|\nabla_{\mathbf{x}} q_1(\mathbf{x})\|_\infty \leq B$ and $q_1(\mathbf{x}) \geq D^{-1}$ for $\mathbf{x} \in \Omega_1 := \text{supp}(q_1)$.

Assumption 3 offers regularity properties for the state transition density, the prediction density, the measurement likelihood, and the initial prior score. The upper and lower boundedness of the density plays a critical role in bounding the prediction score and controlling the error coming from the prior distribution. The significance of the boundedness of the density is emphasized in the literature, such as Tsybakov (2009), as distributions lacking boundedness may exhibit arbitrarily poor properties.

Remark 3.1. Suppose that the dynamics model is with Gaussian additive noise, that is, there exists $F_k : \mathbb{R}^d \rightarrow \mathbb{R}^d$, such that

$$\mathcal{F}_k(\mathbf{X}_k, \mathbf{V}_k) := F_k(\mathbf{X}_k) + \mathbf{V}_k, \quad \mathbf{V}_k \sim N(\mathbf{0}, \Sigma_k),$$

where $\Sigma_k \in \mathbb{R}^{d \times d}$ is symmetric and positive definite. Then the prediction distribution

$$q_{k+1}(\mathbf{x} | \mathbf{y}_{[k]}) \propto \int \exp\left(-\frac{1}{2}(\mathbf{x} - F_k(\mathbf{x}_k))^\top \Sigma_k^{-1}(\mathbf{x} - F_k(\mathbf{x}_k))\right) \pi_k(\mathbf{x}_k | \mathbf{y}_{[k]}) d\mathbf{x}_k$$

satisfies (iii) in Assumption 3, provided that the previous posterior $\pi_k(\cdot | \mathbf{y}_{[k]})$ has a compact support.

We next introduce a ‘‘black-box’’ assumption on score matching.

Assumption 4 (Error of score matching). There exists a score matching tolerance $\Delta \in (0, 1)$ such that

$$\begin{aligned} \mathbb{E}_{\underline{\mathbf{X}}_1} [\|\nabla_{\mathbf{x}} \log \hat{q}_1(\underline{\mathbf{X}}_1) - \hat{\mathbf{s}}_1(\underline{\mathbf{X}}_1)\|_2^2] &\leq \Delta^2, \\ \mathbb{E}_{\underline{\mathbf{X}}_{k+1}} [\|\nabla_{\mathbf{x}} \log \hat{q}_{k+1}(\underline{\mathbf{X}}_{k+1} | \mathbf{y}_{[k]}) - \hat{\mathbf{s}}_{k+1}(\underline{\mathbf{X}}_{k+1}, \mathbf{y}_{[k]})\|_2^2] &\leq \Delta^2, \end{aligned}$$

for each $k \in \mathbb{N}$. Here the expectation $\mathbb{E}_{\underline{\mathbf{X}}_1}[\cdot]$ is taken with respect to $\underline{\mathbf{X}}_1 \sim \hat{q}_1$, and the expectation $\mathbb{E}_{\underline{\mathbf{X}}_{k+1}}[\cdot]$ is taken with respect to $\underline{\mathbf{X}}_{k+1} \sim \hat{q}_{k+1}(\cdot | \mathbf{y}_{[k]})$.

Assumption 4 requires the L^2 -error of prediction score estimator $\hat{\mathbf{s}}_{k+1}$ (2.10) to be sufficiently small, where the L^2 -error is with respect to the approximated prediction distribution $\hat{q}_{k+1}(\cdot | \mathbf{y}_{[k]})$. Although Assumption 4 can be replaced by directly utilizing some score matching bounds, our results are established on this assumption for the simplicity of presentation.

Remark 3.2 (Score matching bounds). According to some standard techniques of nonparametric regression using deep neural networks (Schmidt-Hieber, 2020, Kohler and Langer, 2021, Jiao et al., 2023), it can be shown that

$$\mathbb{E}_{\underline{\mathbf{X}}_{k+1}} [\|\nabla_{\mathbf{x}} \log \hat{q}_{k+1}(\underline{\mathbf{X}}_{k+1} | \mathbf{y}_{[k]}) - \hat{\mathbf{s}}_{k+1}(\underline{\mathbf{X}}_{k+1}, \mathbf{y}_{[k]})\|_2^2] \rightarrow 0$$

with high probability, as the number of samples n approaches infinity and the denoising parameter σ in (2.9) tends to zero. A detailed proof of this convergence can be found in Tang and Yang (2024, Theorem 1).

3.2. Convergence analysis for posterior sampling. Our main theoretical result for posterior sampling is stated as the following theorem.

Theorem 3.3 (Posterior sampling). *Suppose Assumptions 1, 2, 3, and 4 hold. Then for each time step $k \in \mathbb{N}$ and each terminal time $T = Kh$,*

$$(\varepsilon_{\text{TV}}^{k+1})^2 \lesssim \underbrace{\exp\left(-\frac{T}{5C_{\text{LSI}}}\right)\eta_{\chi}^2}_{\text{convergence of LD}} + \underbrace{dC_{\text{LSI}}\lambda^2 h}_{\text{discretization error}} + \underbrace{\sqrt{GB^3D^3}(T + C_{\text{LSI}}\eta_{\chi})\Delta}_{\text{score estimation error}} + \underbrace{B^4D^4T(\varepsilon_{\text{TV}}^k)^2}_{\text{prior error}},$$

where the step size h and the initial distribution $\pi_k^0(\cdot | \mathbf{y}_{[k]})$ satisfies

$$h \leq \mathcal{O}\left(\frac{1}{dC_{\text{LSI}}\lambda^2}\right), \quad \chi^2(\pi_{k+1}^0(\cdot | \mathbf{y}_{[k+1]}) \| \pi_{k+1}(\cdot | \mathbf{y}_{[k+1]})) \leq \eta_{\chi}^2.$$

Error decomposition. Theorem 3.3 provides a decomposition of the total variation error into four distinct terms: the convergence of the Langevin diffusion, the discretization error, the score estimation error, and the prior error.

- (i) The first term demonstrates that the Langevin diffusion (2.11) converges to the stationary distribution exponentially as the terminal time T increases (Vempala and Wibisono, 2019, Chewi et al., 2024).
- (ii) The discretization error arises from the Euler-Maruyama approximation (3.1), which converges linearly with respect to the step size h .
- (iii) The score estimation error diminishes as the score matching tolerance Δ in Assumption 4 approaches zero.
- (iv) The prior error comes from inaccuracies in the prior distribution, which are influenced by the error of the previous posterior distribution estimation $\varepsilon_{\text{TV}}^k$.

Early-stopping. Notice that the first term of Theorem 3.3 decreases as the terminal time T increases. In contrast, the score estimation error and the prior error increase as T grows. Therefore, there exists a trade-off with respect to the terminal time T , indicating the necessity of early-stopping in score-based LMC (Lee et al., 2022). Based on this trade-off, the optimal number of iterations will be given in Corollary 3.4.

It is evident that the error of the LMC with an exact score comprises only the first two terms in Theorem 3.3, which decrease monotonically as the terminal time T increases. Consequently, early stopping distinguishes LMC with inexact score from that with exact score. This observation is consistent with Lee et al. (2022, Theorem D.1), which demonstrates that the stationary distribution of Langevin diffusion with an inexact score can deviate significantly from the original stationary distribution.

The following corollary gives a prior guidance for the selection of hyper-parameters in the score-based LMC.

Corollary 3.4. *Suppose Assumptions 1, 2, 3, and 4 hold. Then for each time step $k \in \mathbb{N}$ and each error tolerance $\varepsilon \in (0, 1)$,*

$$(\varepsilon_{\text{TV}}^{k+1})^2 \lesssim C_{\text{LSI}} B^4 D^4 \log\left(\frac{\eta_{\chi}^2}{\varepsilon^2}\right) (\varepsilon_{\text{TV}}^k)^2 + \varepsilon^2,$$

where the number of the Langevin iterations K , and the score matching error Δ are set, respectively, as

$$K = \Theta\left(\frac{d\lambda^2 C_{\text{LSI}}^2}{\varepsilon^2} \log\left(\frac{\eta_{\chi}^2}{\varepsilon^2}\right)\right), \quad \Delta = \Theta\left(\frac{\varepsilon^2}{\sqrt{GB^3 D^3}(T + C_{\text{LSI}}\eta_{\chi})}\right).$$

Warm-start. In Theorem 3.3, a warm-start in χ^2 -divergence is necessary, indicating that the initial distribution should not be significantly far from the target posterior distribution

$$(3.3) \quad \chi^2(\pi_{k+1}^0(\cdot|\mathbf{y}_{[k+1]})\|\pi_{k+1}(\cdot|\mathbf{y}_{[k+1]})) \leq \eta_{\chi}^2.$$

The convergence of Langevin diffusion and the score estimation error in Theorem 3.3 are both influenced by the warm-start condition (3.3). It is important to note that the score estimator $\hat{\mathbf{s}}_{k+1}$ (2.10) serves as an approximation of the prediction score in L^2 -norm (Assumption 4), where the L^2 -error is with respect to the approximated prediction distribution $\hat{q}_{k+1}(\cdot|\mathbf{y}_{[k]})$. However, as per the Girsanov theorem (Chen et al., 2023), the error between the law of LMC and score-based LMC is bounded by the L^2 -error of the score with respect to the law of the LMC. The warm-start condition in χ^2 -divergence is crucial as it ensures the out-of-distribution generalization of the score estimator from the approximated prediction distribution to the law of the LMC (Lee et al., 2022, Chewi et al., 2024, Tang and Yang, 2024).

The convergence of the Langevin diffusion in Theorem 3.3 is only weakly affected by the warm-start condition (3.3), since the number of iterations K given by Corollary 3.4 grows logarithmically with the initial χ^2 -divergence. In contrast, the score estimation error is highly sensitive to the warm-start condition. Specifically, the score matching tolerance Δ diminishes polynomially with an increase in the initial χ^2 -divergence. Consequently, addressing the challenge posed by a substantial initial χ^2 -divergence necessitates the use of larger deep neural networks and an augmented number of training samples, leading to a significant increase in computational costs.

Annealing. In our method, the initial distribution of the score-based LMC is chosen as the approximated prediction distribution (Section 2.4). However, the approximated prediction distribution may be far from the target posterior distribution. To ensure the warm-start condition (3.3), we employ the ALMC (2.14) in practical scenarios. Specifically, at each inverse

temperature β_m , we sample from $\pi_{k+1}^m(\cdot|\mathbf{y}_{[k+1]})$ through LMC. The initial distribution of LMC is set as the distribution $\pi_{k+1}^{m-1}(\cdot|\mathbf{y}_{[k+1]})$ at the previous inverse temperature β_{m-1} . Notice that

$$\chi^2(\pi_{k+1}^{m-1}(\cdot|\mathbf{y}_{[k+1]})\|\pi_{k+1}^m(\cdot|\mathbf{y}_{[k+1]})) = \int \frac{\pi_{k+1}^m(\mathbf{x}|\mathbf{y}_{[k+1]})}{g_{k+1}(\mathbf{y}_{k+1}|\mathbf{x})^{2(\beta_m-\beta_{m-1})}} d\mathbf{x} - 1 \rightarrow 0,$$

as $\beta_m - \beta_{m-1}$ tends to zero. Consequently, by selecting appropriate temperatures, we can ensure that each LMC in the annealing procedure meets the warm-start condition.

3.3. Convergence analysis for assimilation. With the aid of the convergence of score-based LMC for the posterior sampling derived in the preceding subsection, we now proceed to analyze the convergence of SSLs. Let q_1 represent the ground truth prior distribution of the initial state in the assimilation, and let \hat{q}_1 denote the prior distribution utilized in score-based sequential Langevin sampling. This initial distribution shift can be described as follows:

$$\varepsilon_{\text{init}} := \|\nabla_{\mathbf{x}} \log q_1 - \nabla_{\mathbf{x}} \log \hat{q}_1\|_{L^\infty(\mathbb{R}^d)}.$$

The convergence of the assimilation with score-based sequential Langevin sampling is stated as the following theorem.

Theorem 3.5 (Assimilation). *Suppose Assumptions 1, 2, 3, and 4 hold. Then for each time step $k \in \mathbb{N}$ and each error tolerance $\varepsilon \in (0, 1)$,*

$$(\varepsilon_{\text{TV}}^{k+1})^2 \leq \mathcal{O}((\varepsilon_{\text{init}}^2 + \varepsilon^2) \log^{k+1}(\varepsilon^{-1})),$$

where the constant behind the big \mathcal{O} notation is independent of $\varepsilon_{\text{init}}$ and ε . The number of the Langevin iterations K , and the score matching error Δ are set, respectively, as

$$K = \Theta\left(\frac{d\lambda^2 C_{\text{LSI}}^2}{\varepsilon^2} \log\left(\frac{\eta_\chi^2}{\varepsilon^2}\right)\right), \quad \Delta = \Theta\left(\frac{\varepsilon^2}{\sqrt{GB^3 D^3}(T + C_{\text{LSI}}\eta_\chi)}\right).$$

Consistency. Theorem 3.5 demonstrates that, in scenarios without initial distribution shift, the SSLs serves as a consistent estimator of the posterior distribution. Indeed, discussions in Remark 3.2 indicate that the score matching error Δ diminishes towards zero as the ensemble size increases towards infinity. Consequently, Theorem 3.5 implies that the error of the SSLs vanishes as both the ensemble size and the number of iterations approach infinity simultaneously. In contrast, diffusion-based methods, as discussed in Section 5.1, are found to be inconsistent in assimilation scenarios without linear and Gaussian assumptions.

4. NUMERICAL EXPERIMENTS

In this section, we will illustrate the effectiveness of score-based sequential Langevin sampling (SSLs) through a series of numerical examples.

- (1) Section 4.1 showcases the application of SSLs to a linear Gaussian state-space model, highlighting its capability to accurately estimate the posterior distribution even in the presence of initial prior distribution shifts.
- (2) In Section 4.2, we delve into the assimilation of Langevin diffusion with a double-well potential. This section compares the performance of SSLs with the auxiliary particle filter (APF) and the ensemble Kalman filter (EnKF) in scenarios involving state mutations and model nonlinearity.

- (3) Section 4.3 focuses on applying SSLs to the Lorenz-96 model and comparing it with APF. The primary objective here is to assess the robustness of SSLs against initial prior distribution shifts, while also evaluating the impact of ensemble size on its performance across various metrics.
- (4) In Section 4.4, we utilize SSLs for assimilating Kolmogorov flow with sparse or partial observation data. Additionally, we illustrate how to quantify the uncertainty of states estimated by SSLs and emphasize the significance of the prior score in SSLs through comparisons with standard maximum likelihood estimation (MLE).

4.1. Linear Gaussian state-space model. To begin with, we look into a one-dimensional linear Gaussian state-space model, for which the ground truth posterior can be computed by the Kalman filter (Särkkä and Svensson, 2023). The state-space model is defined as

$$(4.1) \quad \begin{aligned} X_{k+1} &= X_k + V_k, & V_k &\sim N(0, 5), \\ Y_k &= X_k + W_k, & W_k &\sim N(0, 0.2), \end{aligned}$$

where $k \in \mathbb{N}$, and the initial prior distribution is set as $X_1 \sim N(0, 1)$. The SSLs ensemble size is 500.

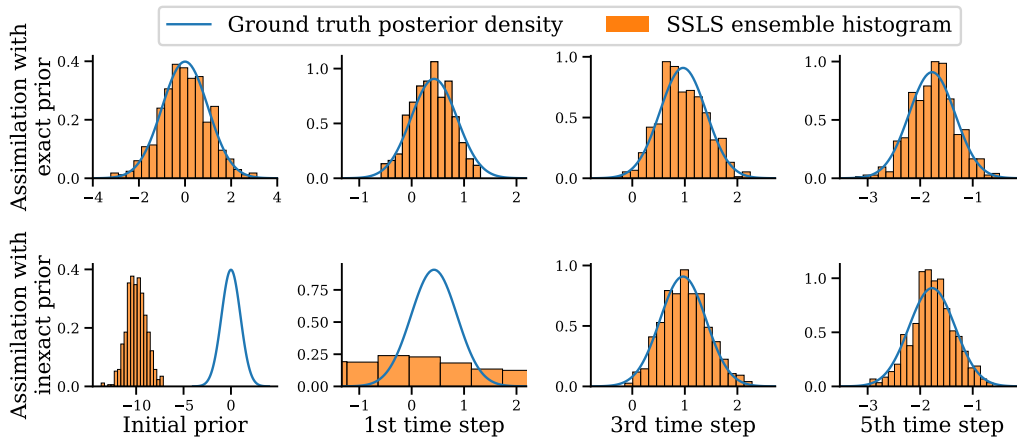


FIGURE 3. Posterior distributions estimated by SSLs in a linear Gaussian state-space model (4.1). (a) The top row shows the histogram of the SSLs ensemble with an exact initial prior distribution. (b) The bottom row demonstrates the histogram of the SSLs ensemble with an inexact initial prior distribution.

Assimilation with exact initial prior. We begin by considering the case where the SSLs is carried out with the exact initial prior. The experimental results are shown in the top row of Figure 3, indicating that the distribution of the SSLs ensemble closely aligns with the ground truth posterior throughout all time steps, given that the SSLs is conducted without the initial prior distribution shift. This empirical finding validates the theoretical conclusions outlined in Theorem 3.5.

Assimilation with inexact initial prior. In practical scenarios, the initial prior distribution is typically intractable. Therefore, it is essential to assess the robustness of the SSLs against the initial prior distribution shift. In this experiment, the SSLs is initialized by an inexact prior of $N(-10, 1)$, and the outcomes are presented in the bottom row of Figure 3. The results demonstrate that, even in the presence of an initial prior distribution shift, the SSLs

ensemble closely matches the ground truth posterior distribution after a small number of time steps, despite prominent estimation errors in initial few time steps.

Recall that Theorem 3.5 provides an error bound that increases with the number of time step. Nonetheless, this error bound may be too loose to accurately depict empirical findings, as it solely characterizes a worst-case scenario. Therefore, establishing a tighter error bound that precisely reflects experimental observations remains an open question. This gap between theoretical understandings and experimental observations will be explored in greater depth in future work.

4.2. The double-well potential. A typical problem in molecular dynamics considers a one-dimensional Langevin diffusion with a double-well potential, which is defined by the nonlinear SDE

$$(4.2) \quad dX_t = -\nabla U(X_t) dt + \beta dB_t,$$

where $U(x) := x^4 - 2x^2$ is a double-well potential, $\beta > 0$ is the temperature parameter, and $(B_t)_{t \geq 0}$ denotes the standard Brownian motion. In this experiment, we focus on the dynamics model defined as the Euler-Maruyama discretization of (4.2)

$$(4.3) \quad X_{k+1} = X_k - \delta t \nabla U(X_k) + \beta \sqrt{\delta t} V_k,$$

where $\delta t > 0$ and $V_k \sim N(0, 1)$. As we will demonstrate, there are state mutations present in this dynamic model. This experiment is designed to showcase the SSLS's ability to respond to these state mutations.

State mutations in dynamics model. Since the dynamics model (4.3) has similar behaviors as its time-continuous counterpart (4.2) when δt is sufficiently small, we illustrate state mutations in (4.2) for the sake of simplicity. The dynamics model (4.2) exhibits two local stable states at $x = -1$ and $x = 1$. Starting from an initial position, the particle is forced towards one of these stable states by the drift term in (4.2), while the diffusion term acts as thermal collisions with the environment, introducing stochasticity into the particle's motion. When the temperature β is sufficiently low, the particle tends to remain confined around one of the stable states, with occasional transitions to the another potential well. Conversely, when the temperature β is higher, the particle has a greater likelihood of transitions across two potential wells, leading to state mutations.

Reference states generation. We simulate the dynamics model (4.3) to generate true states at various time steps, with a temperature $\beta = 0.3$ and a time step $\delta t = 0.1$. Furthermore, to effectively showcase the responsiveness of different assimilation methods in dealing with state mutations, we manually switch the states X_k to $-X_k$ after each 20 steps.

Baseline. In addition to SSLS, we also employ two widely-used assimilation techniques for comparison: the auxiliary particle filter (APF) (Pitt and Shephard, 1999) and the ensemble Kalman filter (Houtekamer and Mitchell, 1998). In SSLS, the prediction score at each assimilation step are learned from 1000 particles. To ensure a fair comparison, the ensemble size for both APF and EnKF is also set to 1000. For further information on the network architecture and training parameters of these methods, please refer to Appendix I.

4.2.1. Linear measurement model. We first consider a linear measurement model with Gaussian additive noise

$$(4.4) \quad Y_k = X_k + \sigma_{\text{obs}} W_k,$$

where $k \in \mathbb{N}$ and $W_k \sim N(0, 1)$. Figure 4 plots the results of assimilation for the state-space model (4.3) and (4.4). The observation noise level is set as $\sigma_{\text{obs}} = 0.1$.

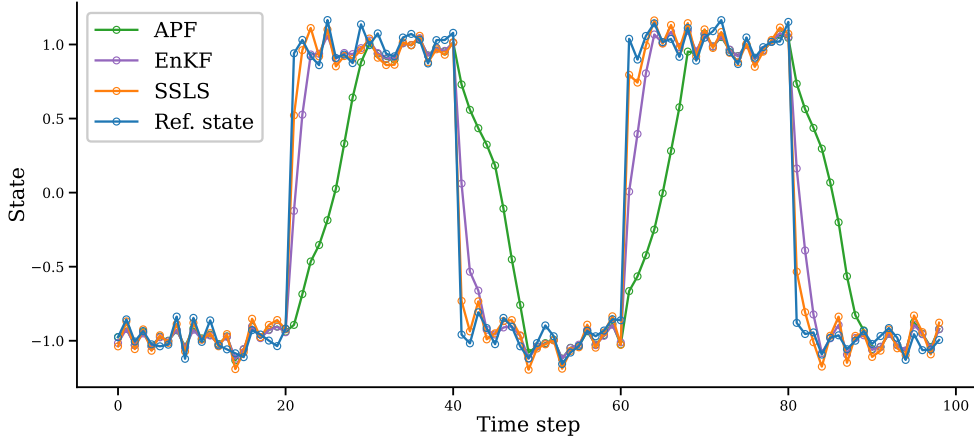


FIGURE 4. Results of assimilation for Langevin diffusion with a double-well potential (4.3). The linear measurement model (4.4). The ensemble mean of SSSL, APF, and EnKF at each time steps are shown in the figure.

According to Figure 4, it is evident that before a state mutation occurs, estimations of all assimilation methods closely align with the reference states. However, a noticeable delay appears in the APF following a state mutation. This delay can be attributed to the fact that APF approximates the prediction distribution using a weighted particle set. When a state mutation occurs, many particles sampled from the approximated prediction distribution may far from the observation. Consequently, these particles are likely to be assigned small weights, indicating that they have minimal impact on the approximation of the posterior distribution (Särkkä and Svensson, 2023, Chapter 11.6). This phenomenon is commonly referred to as particle degeneracy. While the APF can mitigate this issue in comparison to the standard PF, it is unable to fundamentally address this problem.

In contrast, SSSL and EnKF do not rely on particle approximations. SSSL utilizes a score network, while EnKF uses a Gaussian distribution to approximate the prediction distribution. Both of them have the ability to generalize to regions around the observation where predicted particles may not appear. As a result, SSSL and EnKF are able to respond more promptly to state mutations.

4.2.2. *Nonlinear measurement model.* As illustrated in Figure 4, SSSL demonstrates advantages compared to EnKF. This can be attributed to the nonlinearity of the dynamics model (4.3), since EnKF only captures the linear component of the dynamics model while disregarding its higher-order structures. To further highlight the benefits of using SSSL over EnKF in nonlinear state-space models, we consider a nonlinear measurement model given by

$$(4.5) \quad Y_k = \exp(X_k - \gamma_k) + \sigma_{\text{obs}} W_k,$$

where $\gamma_k = 0.6$, $\sigma_{\text{obs}} = 0.2$, and $W_k \sim N(0, 1)$.

Figure 5 illustrates the numerical results for this example, demonstrating that EnKF is unable to effectively assimilate the observation data in the fully nonlinear state-space model (4.3) and (4.5). In contrast, the nonlinearity of the measurement model barely affects

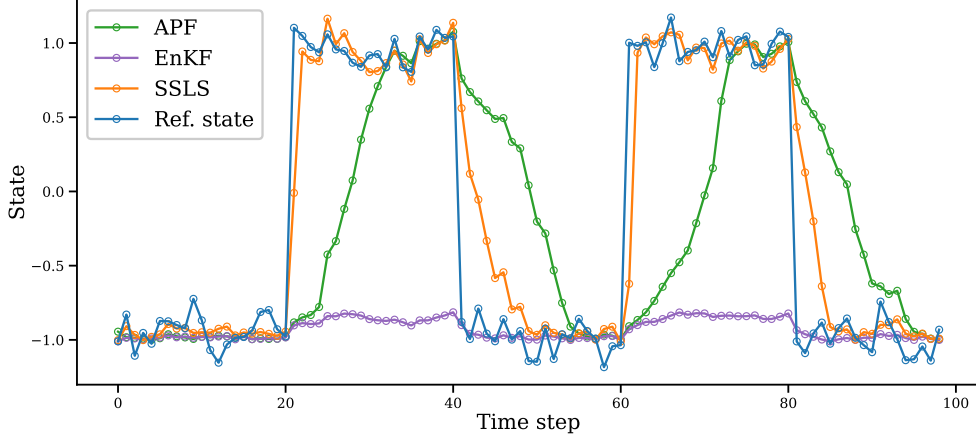


FIGURE 5. Results of assimilation for Langevin diffusion with a double-well potential (4.3). The nonlinear measurement model (4.5). The ensemble mean of SSSL, APF, and EnKF at each time steps are shown in the figure.

the performance of SSSL and APF. As a consequence, the SSSL proves to be a viable option for handling nonlinear scenarios, even in cases of full nonlinearity.

4.3. **Lorenz-96.** Lorenz-96 is a widely-used benchmark in the field of numerical weather forecasting (Majda and Harlim, 2012, Reich and Cotter, 2015, Evensen et al., 2022, Spantini et al., 2022), which is defined by a set of nonlinear ODEs representing the spatial discretization of a time-dependent PDE

$$(4.6) \quad \frac{d}{dt} Z_{t,i} = (Z_{t,i+1} - Z_{t,i-2})Z_{t,i-1} - Z_{t,i} + F, \quad 1 \leq i \leq d.$$

In this experiment, we consider the twenty-dimensional Lorenz-96 system. We set a constant forcing parameter $F = 8$, resulting in a fully chaotic dynamic (Majda and Harlim, 2012), where slightly different initial conditions lead to extremely different trajectories.

The dynamics model is defined by discretizing (4.6) using the fourth-order explicit Runge-Kutta method with time step δt . The states at discrete times are denoted by $(\mathbf{X}_k)_{k \in \mathbb{N}}$ with $\mathbf{X}_k = (Z_{k\delta t,1}, \dots, Z_{k\delta t,d})^\top$. At each time step $k \in \mathbb{N}$, we employ a linear measurement model with Gaussian additive noise

$$(4.7) \quad \mathbf{Y}_k = \mathbf{X}_k + \sigma_{\text{obs}} \mathbf{W}_k,$$

where $\mathbf{W}_k \sim N(\mathbf{0}, \mathbf{I}_d)$ denotes the measurement noise.

Baseline. To mitigate the degeneracy of the APF, a small amount of Gaussian noise $N(0, 10^{-1}\mathbf{I}_d)$ is incorporated into the state at each iteration of the Runge-Kutta method (Spantini et al., 2022). To ensure a fair comparison, the ensemble size for both APF and SSSL is set to 500. To showcase the robustness of SSSL against the initial prior distribution, we intentionally set the initial distribution of both SSSL and APF away from the ground truth initial prior. See Appendix I for more details on training parameters.

Metrics for assimilation. To quantitatively measure the performance of SSSL and study the impact of ensemble size on the assimilation performance, we focus on four metrics as Spantini et al. (2022), including

- (i) RMSE: the root mean squared error,

- (ii) spread: the root mean trace of the ensemble covariance matrix,
- (iii) coverage probability: the coverage probability of the intervals given by the empirical 2.5% and 97.5% quantiles of each marginal of the ensemble, and
- (iv) CRPS: the continuous ranked probability score (Gneiting et al., 2007, Bröcker, 2012).

The RMSE quantifies the discrepancy between estimated states and reference states, while the spread indicates the concentration of the ensemble particles. The coverage probability assesses the likelihood that a marginal confidence interval includes the reference states. The CRPS is a statistical metric used to assess the accuracy of the estimated posterior by comparing it to the observed data. It measures the discrepancy between the cumulative distribution function of the estimated posterior and the cumulative distribution function of the observations. A lower CRPS value indicates a better alignment between the estimated posterior and observed distributions, indicating a more accurate estimate.

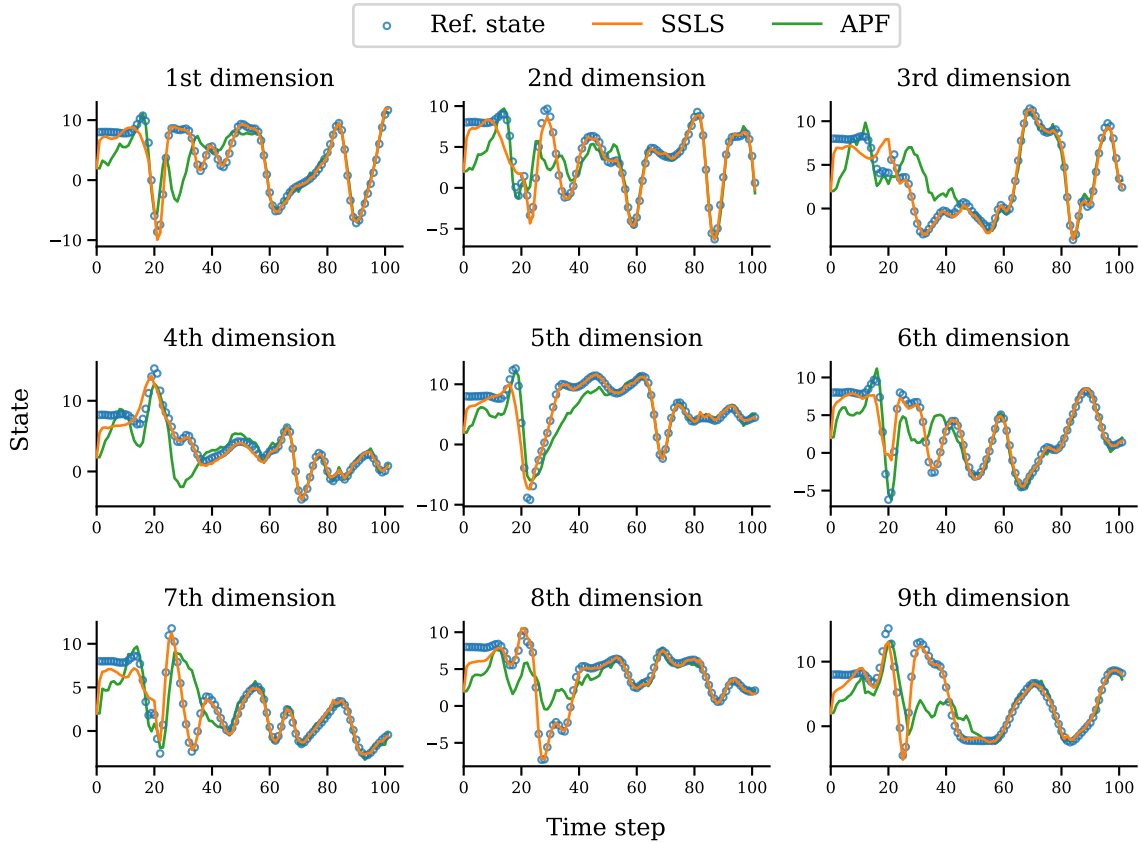


FIGURE 6. Evolution of the reference states, the SSSL ensemble mean, and the APF ensemble mean for Lorenz-96 (4.6).

Experimental results. Figure 6 demonstrates the evolution of the first nine elements of the states estimated by SSSL and APF, respectively. Despite an initial prior distribution shift, SSSL effectively corrects this error within a few subsequent assimilation steps, whereas APF requires a significantly longer assimilation time to compensate for the initial prior distribution shift. These empirical observations are consistent with those of the previous experiment. Figure 7 presents four metrics for both SSSL and APF with different ensemble size.

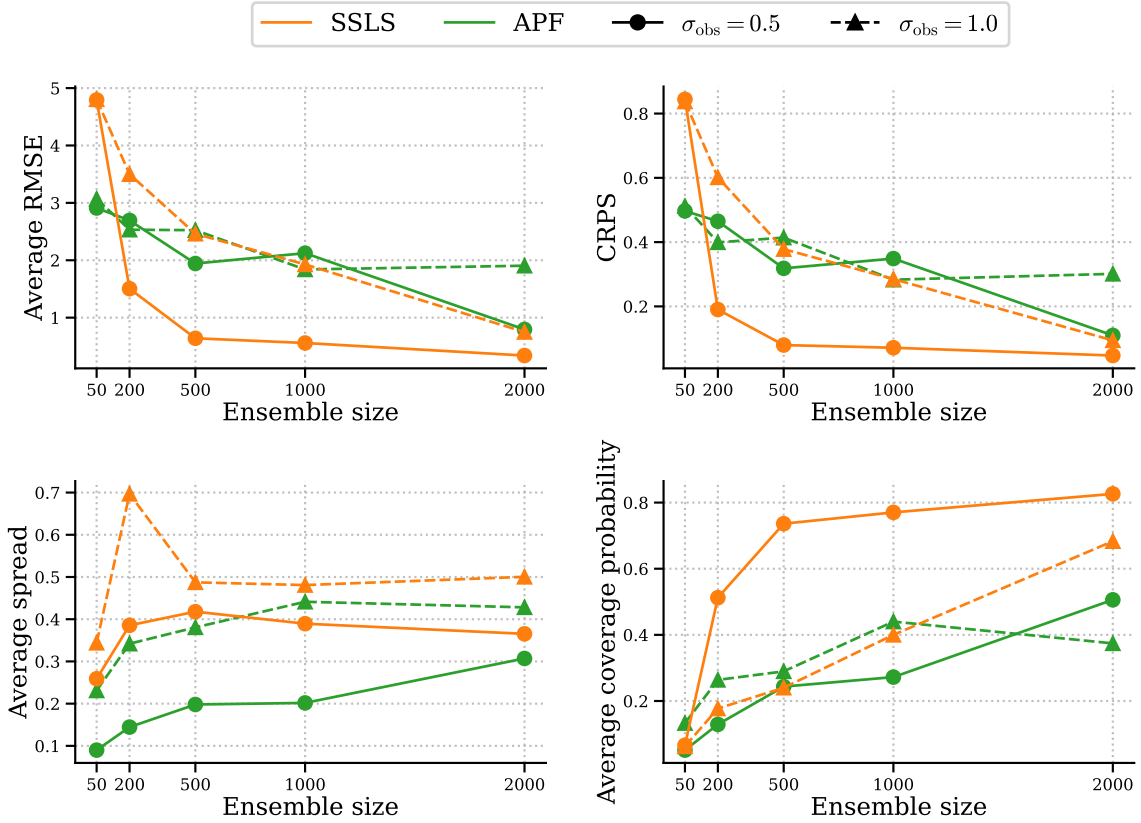


FIGURE 7. Performance metrics of SSSL and APF for Lorenz-96 (4.6). For each ensemble size, metrics are averaged over elements of the estimated states and time steps.

- (i) **RMSE:** The average RMSE of both SSSL and APF decreases as the ensemble size increases, which is consistent with our theoretical findings. Specifically, Remark 3.2 indicates that the score matching error in SSSL approaches zero as the ensemble size increases towards infinity. Consequently, the assimilation error decreases as the ensemble size increases, as evidenced by the results in Theorem 3.5. Additionally, Figure 7 illustrates that SSSL performs better than APF for ensemble sizes exceeding 200.
- (ii) **CRPS:** As depicted in the upper right portion of Figure 7, the average CRPS of SSSL decreases significantly as the ensemble size increases. This trend suggests an enhanced alignment between the estimated posterior distribution and the observation data. Furthermore, for ensemble sizes exceeding 500, SSSL demonstrates lower CRPS values compared to the APF, underscoring the superior effectiveness of SSSL in posterior estimation.
- (iii) **Spread and coverage probability:** The bottom row of Figure 7 demonstrates that the coverage probability of SSSL noticeably grows with the increase in ensemble size, while the spread remains relatively stable. Moreover, Figure 7 indicates that at a low noise level of $\sigma_{\text{obs}} = 0.5$, SSSL exhibits a much higher coverage probability compared to APF, despite having a larger average spread. This disparity can be attributed to particle degeneracy in APF.

For further discussion on this experiment, please refer to Appendix I.

4.4. Kolmogorov flow. In this example, we consider the assimilation of a Kolmogorov flow, which arises in atmospheric sciences and fluid dynamics (Cotter et al., 2009, Rozet and Louppe, 2023a). Kolmogorov flow is a viscous and incompressible fluid flow governed by the Navier-Stokes (NS) equation on the two-dimensional torus $[0, 2\pi]^2$,

$$(4.8) \quad \begin{cases} \partial_t \mathbf{u} = -(\mathbf{u} \cdot \nabla) \mathbf{u} + \frac{1}{\text{Re}} \nabla^2 \mathbf{u} - \frac{1}{\rho} \nabla p + \mathbf{F}, \\ 0 = \nabla \cdot \mathbf{u}, \end{cases}$$

where \mathbf{u} represents the velocity field, Re is the Reynolds number, ρ denotes the fluid density, p is the pressure field, and \mathbf{F} is the external forcing. This example uses the periodic boundary conditions, a large Reynolds number $\text{Re} = 10^3$, a constant density $\rho \equiv 1$ and an external forcing \mathbf{F} corresponding to Kolmogorov forcing with linear damping. Our objective is to track a velocity field describing the solutions to the NS equation (4.8) with unknown initial condition.

Reference states generation. Let \mathbf{u}_0 be a initial random state sampled from a Gaussian random field. The NS equation (4.8) is evolved from this initial state \mathbf{u}_0 . Following a warm-up period of $T_0 = 10$, reference states are downsampled from the trajectory between $T_0 = 10$ and $T = 20$ with a spatial resolution of 128×128 and a temporal resolution of $\Delta t = 0.2$. Here the NS equation (4.8) is solved using the `jax-cfd` package (Kochkov et al., 2021).

Initial prior distribution shift. In SSSL, the assimilation begins with a set of independent random copies of \mathbf{u}_0 . It is important to note that the initial reference state is \mathbf{u}_{T_0} , which has a distribution distinct from the initial distribution used in SSSL. This initial distributional shift is common in practical applications, as the exact distribution of the initial state is typically unknown. Consequently, assimilation under an initial distributional shift is a crucial yet challenging task.

4.4.1. Assimilation with sparse or partial observation data. In this subsection, we adopt three tasks to show the efficiency of SSSL with sparse or partial observation data:

- (i) super-resolution: low-resolution observation,
- (ii) sparse reconstruction: uniform sparse observation, and
- (iii) box reconstruction: partial observation.

In the super-resolution task, observation data are obtained by coarsening the reference states through average pooling and then introducing pointwise Gaussian noise. The measurement model in the sparse reconstruction task invokes the Gaussian perturbation and subsampling with uniform stride. In the box reconstruction task, measurements within a specific domain is not accessible, while those outside of the domain are perturbed by Gaussian noise.

Experimental results of SSSL with various measurement models are illustrated in Figure 8, showcasing the vorticity field $\omega = \nabla \times \mathbf{u}$ for visualization purposes. The outcomes indicate remarkable performance of SSSL in tasks such as super-resolution, sparse reconstruction, and box reconstruction.

- (i) In the super-resolution task, as shown in the second row of Figure 8, the observation data loses nearly all of the micro-structures of the reference vorticity field. However, the states estimated by SSSL are able to reconstruct a majority of the intricate details.
- (ii) In the task of sparse reconstruction, SSSL exhibits remarkable performance even when masking out a substantial 88.72% of all points, as illustrated in the fourth and fifth

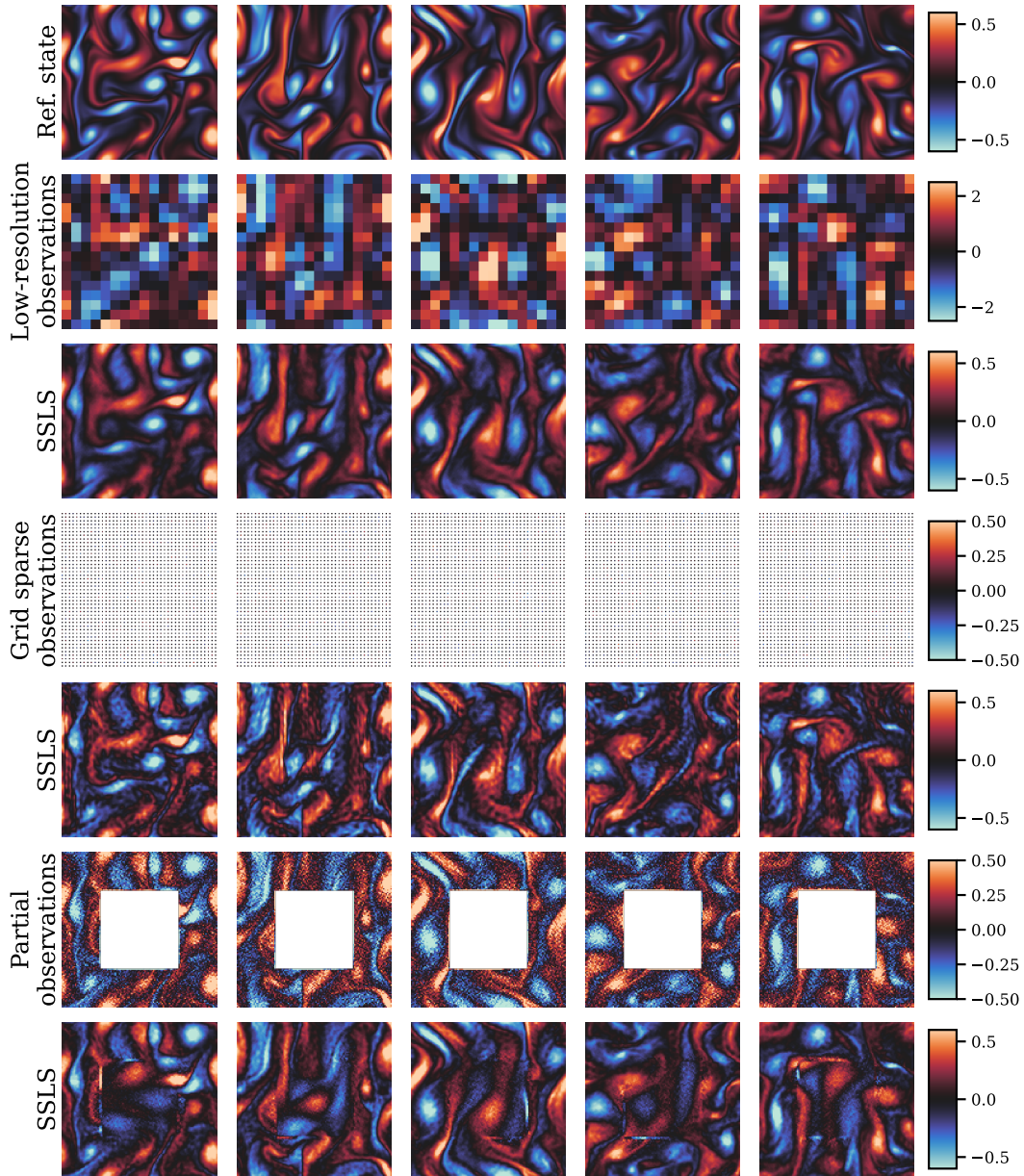


FIGURE 8. Results of assimilation for Kolmogorov flow (4.8) with different measurement model. Each column corresponds to distinct time steps (states are plotted for every 10 time steps). The first row displays the reference state. (i) Super-resolution: The 2nd and 3rd rows display the noisy observations with 8x average pooling and the corresponding SSLS estimations, respectively. (ii) Sparse reconstruction: The 4th and 5th rows show the noisy observations with a uniform mask and the corresponding SSLS estimations, respectively. (iii) Box reconstruction: The 6th and 7th rows demonstrate the noisy observations with a centering square mask and the corresponding SSLS estimations, respectively.

rows of Figure 8. This underscores the robustness of SSLS in handling observation sparsity, which is crucial in application scenarios where observation costs are high and the number of measurements is limited.

- (iii) It is worth noting that in the challenging task of box reconstruction, the observations within the masked box are completely obscured. However, SSLS exhibits impressive performance even within the masked domain, as depicted in the last row of Figure 8.

In the aforementioned tasks, there is a notable discrepancy between the estimated states and the observation data, suggesting that the prior information have a substantial impact on the assimilation. The efficiency of the prior in the assimilation will be investigated further through an ablation study in subsequent experiments.

4.4.2. Uncertainty quantification in assimilation. The previous experiments demonstrate that the states estimated by the SSLS closely match the reference states, even when significant occlusion and noise are present. However, mere point estimation is insufficient, particularly in situations where the reliability of the estimations is of utmost importance. In such high-stakes scenarios, quantifying uncertainties associated with the estimations becomes crucial for making decisions (Sullivan, 2015, Adler and Öktem, 2025).

In this experiment, we will demonstrate how to quantify the uncertainties associated with the states estimated by SSLS. To this end, we consider the random reconstruction task as an example, where the observation data are obtained by masking 95% of grid points randomly and perturbing with Gaussian noise. The experimental results are shown in Figure 9.

Standard deviation and uncertainty. It is worth noting that SSLS is able to generate multiple ensemble samples from the posterior distribution, enabling the computation of the standard deviation that provide insights into the quality of the estimated states (Patel and Oberai, 2021, Adler and Öktem, 2025). The estimated pointwise standard deviations are shown in the last row of Figure 9.

The first and last rows of Figure 9 illustrate that the standard deviation is concentrated on regions where the magnitude of the reference vorticity is large. This empirical observation is comprehensible. Vorticity, defined as the curl of the velocity field, measures the local rotation of the fluid. High vorticity indicates strong rotation and swirling motion in the fluid. The uniformly distributed measurement positions are insufficient for capturing high-frequency information in these high-vorticity regions. Therefore, the estimated states have more uncertainty in such regions.

Well-calibrated uncertainty estimation. One way to assess the quality of the estimated uncertainty is to determine whether it is calibrated. A well-calibrated uncertainty estimation means that the estimated uncertainty, i.e., standard deviation, aligns with the pointwise error (Raad et al., 2022, Antoran et al., 2023, Raad et al., 2024).

The last two rows of Figure 9 highlights that the standard deviation estimated by SSLS correlates with the pointwise error. To delve deeper into this correlation, we plot the standard deviation versus the error for pixels down-sampled using max-pooling with a kernel size of 16 in Figure 10. We examine the correlation at three equally separated time points from left to right. Figure 10 reveals a positive correlation between the standard deviation and the error at all three time points.

Both Figures 9 and 10 demonstrate that the standard deviation of SSLS provides a well-calibrated uncertainty estimation. Specifically, the standard deviation calculated by SSLS can serve as an indicator of the error in the states estimated by SSLS. Consequently, uncertainty quantification using SSLS is crucial for assessing the reliability of the estimated states. Further,

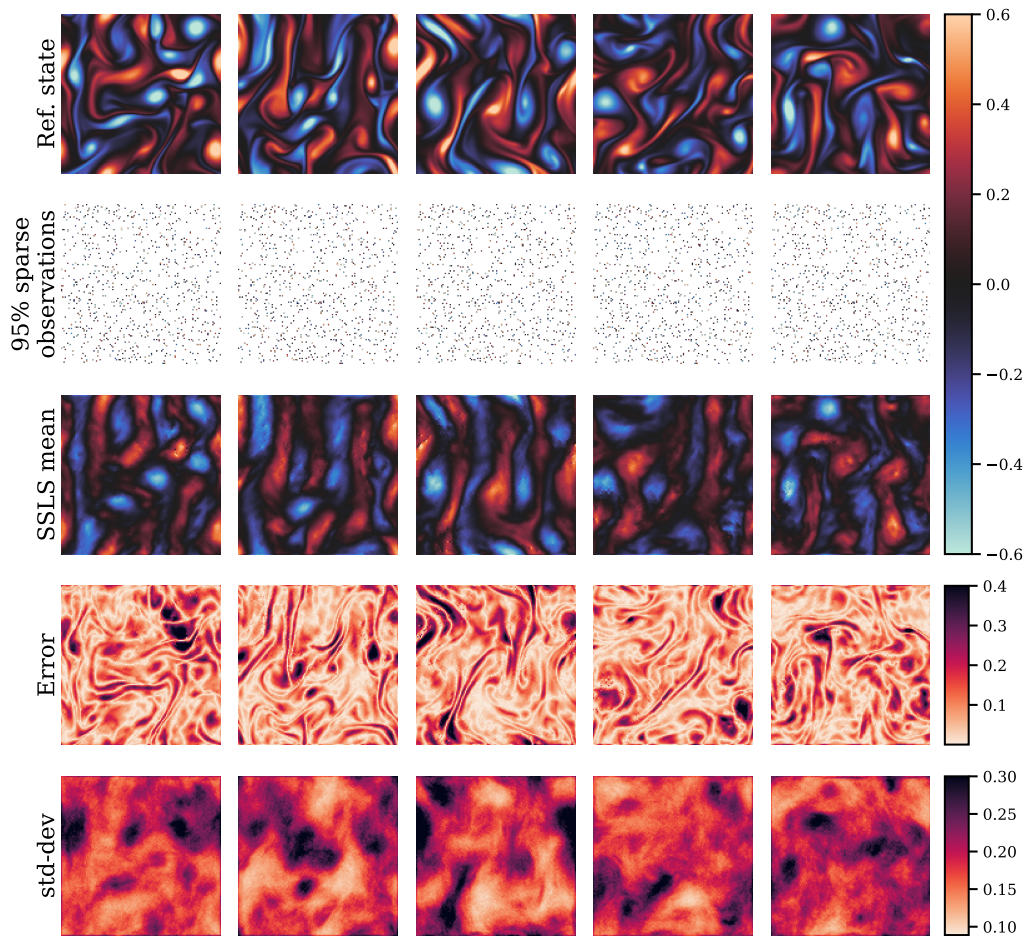


FIGURE 9. Quantify the uncertainty associated with states estimated by SLS. From top to bottom: the reference states, observations (95% random mask), the SLS assimilated states, point-wise error (in absolute value) and standard deviation. The noise level is set as $\sigma_{\text{obs}} = 0.4$.

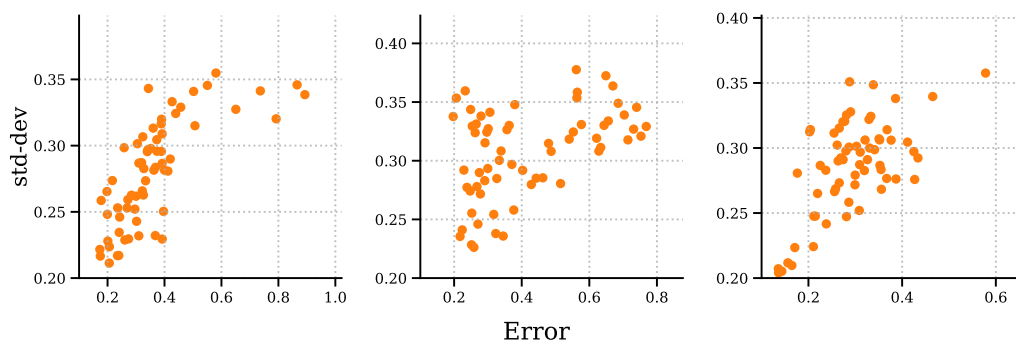


FIGURE 10. The correlation between the standard deviation and estimation error of the SLS. The standard deviation and error are down-sampled by max pooling for clearer visualization. From left to right: the results at three equally separated time points of the assimilation process.

estimating the uncertainty can provide valuable insights in improving the observational positions and refining the model.

4.4.3. *Ablation study: influence of the prior score.* Previous experiments highlight that the estimated states are close to the reference states, even in the presence of significant occlusion and noise in observation data. This reveals the crucial role of the prior information. In this experiment, we aim to delve deeper into the impact of the prior score in the SSSL method through a detailed comparison with score-free methods.

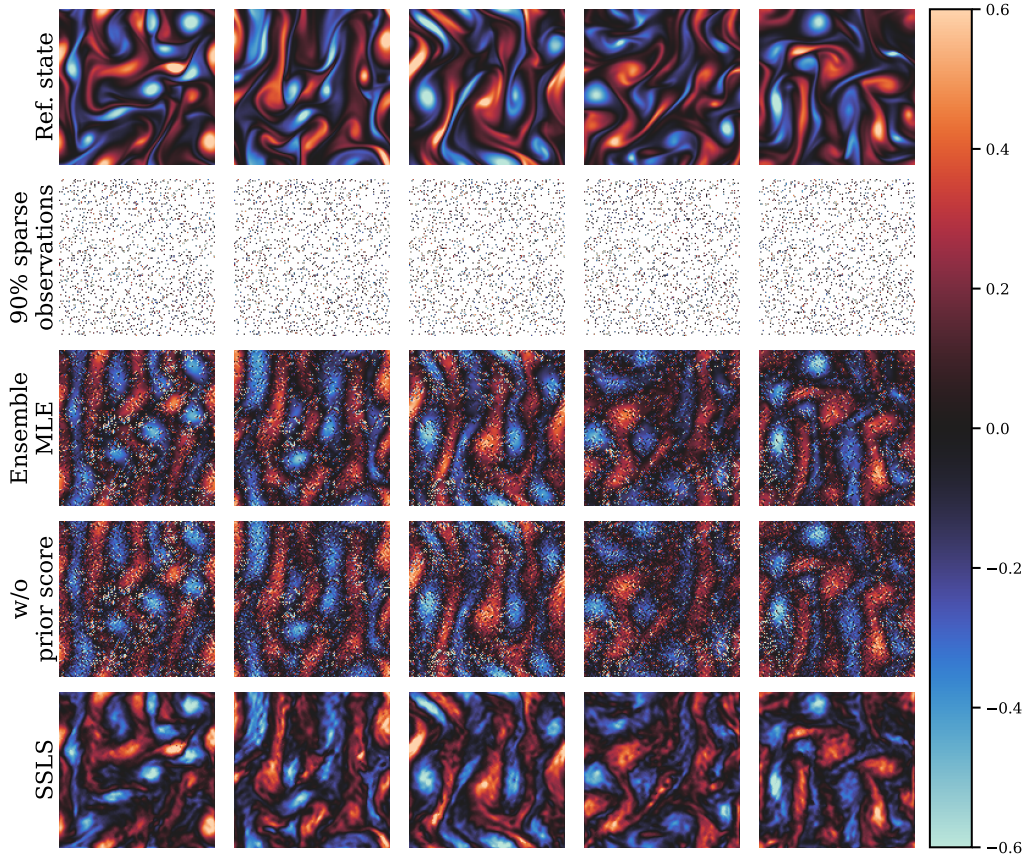


FIGURE 11. Comparison of results of SSSL and methods without prior score. From top to bottom: the reference state, observations, estimations of the ensemble MLE, estimations of Langevin sampling without the prior score, and estimations of SSSL. Here the noise level is set as $\sigma_{\text{obs}} = 0.3$ and let 90% points be randomly masked.

Baseline. To demonstrate the impact of the prior score in the SSSL, we introduce two comparison methods:

- (i) Langevin sampling without the prior score, and
- (ii) ensemble maximum likelihood estimation (MLE).

In method (i), we exclude the prior score from the drift term of the Langevin Monte Carlo (2.12), which reads

$$(4.9) \quad \widehat{\mathbf{Z}}_{(\ell+1)h} = \widehat{\mathbf{Z}}_{\ell h} + h \nabla_{\mathbf{x}} \log g_{k+1}(\mathbf{y}_{k+1} | \widehat{\mathbf{Z}}_{\ell h}) + \sqrt{2h} \boldsymbol{\xi}_{\ell}, \quad \widehat{\mathbf{Z}}_0 \sim \widehat{q}_{k+1}(\cdot | \mathbf{y}_{[k]}),$$

for each $0 \leq \ell \leq K - 1$. It is worth noting that (4.10) can be viewed as a noised gradient method for maximum likelihood estimation. In contrast, the pure gradient method for MLE is given as

$$(4.10) \quad \widehat{\mathbf{Z}}_{(\ell+1)h} = \widehat{\mathbf{Z}}_{\ell h} + h \nabla_{\mathbf{x}} \log g_{k+1}(\mathbf{y}_{k+1} | \widehat{\mathbf{Z}}_{\ell h}), \quad \widehat{\mathbf{Z}}_0 \sim \widehat{q}_{k+1}(\cdot | \mathbf{y}_{[k]}),$$

for each $0 \leq \ell \leq K - 1$. In the ensemble MLE, we iterate the gradient method (4.10) initialized by a set of particles drawn from an initial distribution. The estimation of states is defined as the mean of the terminal particles.

To ensure a fair comparison, we set the initial distribution of (4.9) and (4.10) as the approximated prediction distribution (2.7), which aligns with the SSLS setting. Consequently, the states estimated by (4.9) or (4.10) are still influenced by historical observations through the initial distribution, even though these methods do not rely on the prior score.

Influence of the prior score. As illustrated in Figure 11, it is evident that both Langevin sampling without the prior score and the ensemble MLE result in state estimations with a high level of noise. In contrast, the states estimated by the SSLS closely match the reference states. This experimental finding highlights the crucial role played by the prior score in the SSLS.

5. RELATED WORK

5.1. Diffusion models for Bayesian inverse problems. Bayesian inverse problems are closely linked to data assimilation, as demonstrated in Section 2.4. In recent years, diffusion methods have gained prominence as an effective technique for posterior sampling in Bayesian inverse problems, such as Chung et al. (2023), Song et al. (2023), Purohit et al. (2024). This section provides a comprehensive review of the existing literature on diffusion-based approaches for posterior sampling.

We first introduce the setup of Bayesian inverse problems. Suppose the forward model is defined as

$$\mathbf{U} = \mathcal{G}(\mathbf{Z}, \mathbf{W}), \quad \mathbf{Z} \sim p_{\mathbf{Z}},$$

where \mathcal{G} represents a given measurement model, $p_{\mathbf{Z}}$ is a known prior distribution, and \mathbf{W} is a random variable with a known distribution. As a result, the measurement likelihood $p_{\mathbf{U}|\mathbf{Z}}(\mathbf{u}|\mathbf{z})$ can be obtained from the measurement model \mathcal{G} and the distribution of \mathbf{W} .

Bayesian inverse problems aim to estimate the posterior distribution $p_{\mathbf{Z}|\mathbf{U}}(\mathbf{z}|\mathbf{u})$ given the observation \mathbf{u} , the prior $p_{\mathbf{Z}}$, and the measurement likelihood $p_{\mathbf{U}|\mathbf{Z}}$. It is evident that the update step (Section 2.4) within the recursive Bayesian framework exactly corresponds to solving a Bayesian inverse problem.

Diffusion model with guidance. The mainstream technique in diffusion models for conditional or posterior sampling is guidance (Guo et al., 2024b). As an illustrative example, we consider the diffusion model with the following forward process

$$d\mathbf{Z}_s = -\mathbf{Z}_s ds + \sqrt{2} d\mathbf{B}_s, \quad \mathbf{Z}_0 \sim p_{\mathbf{Z}}, \quad s \in (0, T),$$

where $(\mathbf{B}_s)_{s \geq 0}$ is a standard Brownian motion. Denote by $p_{\mathbf{Z}_s}$ the law of \mathbf{Z}_s for each $s \in (0, T)$. Following Bayes' rule, the time-reversal process for sampling from the posterior distribution $p_{\mathbf{Z}|\mathbf{U}}(\cdot|\mathbf{u})$ reads (Chung et al., 2023)

$$(5.1) \quad d\bar{\mathbf{Z}}_s = \left\{ \bar{\mathbf{Z}}_s - 2 \overbrace{\nabla_{\mathbf{z}} \log p_{\mathbf{U}|\mathbf{Z}_{T-s}}(\mathbf{u}|\bar{\mathbf{Z}}_s)}^{\text{intractable}} - 2 \overbrace{\nabla_{\mathbf{z}} \log p_{\mathbf{Z}_{T-s}}(\bar{\mathbf{Z}}_s)}^{\text{score}} \right\} ds + \sqrt{2} d\mathbf{B}_s, \\ \bar{\mathbf{Z}}_0 \sim N(0, 1), \quad s \in (0, T),$$

where $p_{\mathbf{U}|\mathbf{Z}_s}(\mathbf{u}|\mathbf{z})$ is the time-dependent likelihood, and $p_{\mathbf{Z}_s}(\mathbf{z})$ is the time-dependent prior. It worth noting that the score in (5.1) can be estimated by denoising score matching (Vincent, 2011, Song et al., 2021), while the gradient of log-likelihood is typically intractable.

Linear Gaussian inverse problems. When the measurement model \mathcal{G} is linear, and both the prior and the likelihood are Gaussian, that is,

$$\mathcal{G}(\mathbf{Z}, \mathbf{W}) := \mathbf{G}\mathbf{Z} + \sigma_{\text{obs}}\mathbf{W}, \quad \mathbf{Z} \sim p_{\mathbf{Z}} = N(\mu, \Sigma), \quad \mathbf{W} \sim N(0, \mathbf{I}_d),$$

the gradient of time-dependent log-likelihood in (5.1) can be estimated without bias. For a detailed derivation, please refer to Guo et al. (2024b, Lemma 1). However, this linear scenario corresponds to the assimilation with linear state-space model. The solution to the linear assimilation can be obtained using the ensemble Kalman filter (Särkkä and Svensson, 2023). Therefore, there is no necessity to utilize diffusion models for the linear assimilation.

Nonlinear inverse problems. Researchers' interests lie in nonlinear inverse problems, which corresponds to the nonlinear assimilation. One of the most widely-used diffusion-based approaches for nonlinear inverse problem is the diffusion posterior sampling (DPS) (Chung et al., 2023), which estimates the gradient of time-dependent log-likelihood in (5.1) by exchanging the expectation with likelihood, that is,

$$\begin{aligned} p_{\mathbf{U}|\mathbf{Z}_s}(\mathbf{u}|\mathbf{z}) &= \int p_{\mathbf{U}|\mathbf{Z}_0}(\mathbf{u}|\mathbf{z}_0)p_{\mathbf{Z}_0|\mathbf{Z}_s}(\mathbf{z}_0|\mathbf{z}) d\mathbf{z}_0 \\ (5.2) \quad &= \mathbb{E}[p_{\mathbf{U}|\mathbf{Z}_0}(\mathbf{u}|\mathbf{Z}_0)|\mathbf{Z}_s = \mathbf{z}] \approx p_{\mathbf{U}|\mathbf{Z}_0}(\mathbf{u}|\mathbb{E}[\mathbf{Z}_0|\mathbf{Z}_s = \mathbf{z}]). \end{aligned}$$

However, it is important to note that this approximation introduces a bias term known as Jensen's gap, as pointed out by Chung et al. (2023). Therefore, DPS can not yield a consistent estimation in nonlinear Bayesian inverse problems. In contrast, the score-based LMC proposed by this work is consistent in nonlinear scenarios, as shown in Theorem 3.3.

5.2. Diffusion-based methods for assimilation. In the preceding subsection, we discussed diffusion-based methods for Bayesian inverse problems. Building upon these methods, a variety of diffusion-based approaches have been developed for data assimilation, which can be broadly classified into data-driven methods and filtering methods. A comparison of these techniques, along with commonly used classical methods, is presented in Table 1.

TABLE 1. A comparison of methods for nonlinear assimilation.

Method	Consistent	Approximation or assumption
3D-Var/4D-Var	✗	(i) Linearization (ii) Gaussian prior and likelihood
SDA (Rozet and Louppe, 2023a)	✗	Jensen's gap (Chung et al., 2023)
SOAD (Li et al., 2024)	✓	Gaussian prior and likelihood
EnKF	✗	(i) Linearization (ii) Gaussian prior and likelihood
PF	✓	None
SF (Bao et al., 2024)	✗	Damping function
SSLS (ours)	✓	None

Data-driven methods for assimilation. Data-driven methods focus on estimating the posterior distribution of all latent states $\mathbf{Z} := \mathbf{X}_{[k]}$ given all available observation data

$\mathbf{U} := \mathbf{Y}_{[k]}$. By substituting \mathbf{Z} and \mathbf{U} into the time-reversal process (5.1), this line of methods reformulate the assimilation as a single Bayesian inverse problem (Rozet and Louppe, 2023a,b, Li et al., 2024).

The prior score in (5.1) can be approximated by utilizing random copies of $\mathbf{Z} = \mathbf{X}_{[k+1]}$ through denoising score matching, as discussed in (Rozet and Louppe, 2023a, Li et al., 2024). This characteristic makes these methods data-driven, as they rely on empirical data rather than explicit knowledge of the underlying physical models, i.e., the states transition dynamics. In these data-driven approaches, the physical mechanism is implicitly incorporated into the prior score.

Then it remains to estimate the gradient of time-dependent log-likelihood in (5.1). For example, the score-based data assimilation (SDA) (Rozet and Louppe, 2023a,b) estimates the gradient of time-dependent log-likelihood in a similar manner as DPS (5.2). In Li et al. (2024), the authors propose the state-observation augmented diffusion (SOAD) method, which involves converting a nonlinear state-space model into a linear one through variable augmentation. The gradient of time-dependent log-likelihood of augmented linear state-space model can be estimated without bias, as discussed in the previous section.

Computing the joint distribution of the states across all time steps is computationally inefficient due to the increasing dimensionality of the diffusion model as the number of time steps increases. This limitation of the data-driven methods hinders the application of these methods to high-dimensional data assimilation tasks. Additionally, data-driven methods are unable to fully leverage the underlying physical mechanisms. In contrast, the dimensionality of SSLS proposed in this study remains constant, regardless of the assimilation time. Moreover, SSLS effectively integrates physical principles with observation data.

Filtering methods for assimilation. Another category of diffusion-based assimilation methods are developed within the Bayesian filtering framework (Section 2.2), with examples including the score-based filter (SF) (Bao et al., 2024). In the update at the $(k+1)$ -th time step, SF sets $\mathbf{U} := \mathbf{Y}_{k+1}$, $\mathbf{u} := \mathbf{y}_{k+1}$, and $\mathbf{Z}_0 \sim \hat{q}_{k+1}(\cdot | \mathbf{y}[k])$. SF estimates the prior score in (5.1) using sliced score matching (Song et al., 2020), while approximating the gradient of the time-dependent log-likelihood through a separation of variables:

$$\nabla_{\mathbf{z}} \log p_{\mathbf{U}|\mathbf{Z}_s}(\mathbf{u}|\mathbf{z}) = h(s) \nabla_{\mathbf{z}} \log p_{\mathbf{U}|\mathbf{Z}_0}(\mathbf{u}|\mathbf{z}), \quad s \in (0, T),$$

Here, the damping function h is a monotonically decreasing function in the interval $[0, T]$, with $h(0) = 1$ and $h(T) = 0$. However, this separation of variable approximation is often inconsistent, and the optimal choice of the damping function remains unresolved. In contrast, our method is consistent and does not rely on such heuristic approximations.

6. CONCLUSIONS

In conclusion, this paper introduces a novel approach for nonlinear assimilation known as score-based sequential Langevin sampling (SSLS) within a recursive Bayesian framework. The convergence of SSLS in TV-distance is examined under mild conditions, offering insights into error behavior related to hyper-parameters. Numerical examples showcase the exceptional performance of SSLS in high-dimensional and nonlinear scenarios, as well as situations with sparse or partial measurements. Additionally, SSLS effectively quantifies the uncertainty of estimated states, highlighting its potential for error calibration.

Moving forward, there are several avenues for improvement and extension of our method. While our current work assumes knowledge of the state-space model, there may be unknown

parameters in the dynamics or measurement models. Future research will focus on extending SSLs to simultaneously estimate latent states and unknown parameters within the state-space model. Additionally, the computational cost of training a score network in each time step can be significant. Our future work aims to reduce this cost through techniques such as in-context learning. Furthermore, we are interested in expanding our method to assimilation with time sparsity.

REFERENCES

- Jonas Adler and Ozan Öktem. Deep Bayesian inversion. In Tatiana A. Bubba, editor, *Data-driven Models in Inverse Problems*, volume 31 of *Radon Series on Computational and Applied Mathematics*, pages 359–412. Berlin, Boston: De Gruyter, 2025.
- Jeffrey L. Anderson. Spatially and temporally varying adaptive covariance inflation for ensemble filters. *Tellus A*, 61(1):72–83, 2009.
- Jeffrey L. Anderson and Stephen L. Anderson. A Monte Carlo implementation of the nonlinear filtering problem to produce ensemble assimilations and forecasts. *Monthly Weather Review*, 121:2741–2758, 1999.
- Javier Antoran, Riccardo Barbano, Johannes Leuschner, José Miguel Hernández-Lobato, and Bangti Jin. Uncertainty estimation for computed tomography with a linearised deep image prior. *Transactions on Machine Learning Research*, 2023. ISSN 2835–8856.
- Dominique Bakr, Ivan Gentil, and Michel Ledoux. *Analysis and Geometry of Markov Diffusion Operators*, volume 348 of *Grundlehren der mathematischen Wissenschaften (GL)*. Springer Cham, first edition, 2014.
- Feng Bao, Zezhong Zhang, and Guannan Zhang. A score-based filter for nonlinear data assimilation. *Journal of Computational Physics*, 514:113207, 2024. ISSN 0021-9991.
- Thomas Bengtsson, Peter Bickel, and Bo Li. Curse-of-dimensionality revisited: Collapse of the particle filter in very large scale systems. In Deborah Nolan and Terry Speed, editors, *Institute of Mathematical Statistics Collections, Probability and Statistics: Essays in Honor of David A. Freedman*, pages 316–334. Institute of Mathematical Statistics, 2008.
- Alexandros Beskos, Ajay Jasra, Ege A. Muzaffer, and Andrew M. Stuart. Sequential Monte Carlo methods for Bayesian elliptic inverse problems. *Statistics and Computing*, 25:727–737, 2015.
- Ramaprasad Bhar. *Stochastic Filtering with Applications in Finance*. World Scientific, 2010.
- Peter Bickel, Bo Li, and Thomas Bengtsson. Sharp failure rates for the bootstrap particle filter in high dimensions. In Bertrand Clarke and Subhashis Ghosal, editors, *Institute of Mathematical Statistics Collections, Pushing the Limits of Contemporary Statistics: Contributions in Honor of Jayanta K. Ghosh*, pages 318–329. Institute of Mathematical Statistics, 2008.
- Jochen Bröcker. Evaluating raw ensembles with the continuous ranked probability score. *Quarterly Journal of the Royal Meteorological Society*, 138(667):1611–1617, 2012.
- Nicolas Brosse, Alain Durmus, and Éric Moulines. Normalizing constants of log-concave densities. *Electronic Journal of Statistics*, 12(1):851 – 889, 2018.
- Minshuo Chen, Song Mei, Jianqing Fan, and Mengdi Wang. Opportunities and challenges of diffusion models for generative AI. *National Science Review*, 11(12):nwae348, 2024.
- Sitan Chen, Sinho Chewi, Jerry Li, Yuanzhi Li, Adil Salim, and Anru Zhang. Sampling is as easy as learning the score: theory for diffusion models with minimal data assumptions. In *The Eleventh International Conference on Learning Representations*, 2023.

- Sinho Chewi. Log-concave sampling, 2024. URL <https://chewisinho.github.io/main.pdf>. unfinished draft.
- Sinho Chewi, Murat A. Erdogdu, Mufan Li, Ruoqi Shen, and Matthew S. Zhang. Analysis of Langevin Monte Carlo from Poincaré to log-Sobolev. *Foundations of Computational Mathematics*, 2024.
- Hyungjin Chung and Jong Chul Ye. Score-based diffusion models for accelerated MRI. *Medical Image Analysis*, 80:102479, 2022. ISSN 1361–8415.
- Hyungjin Chung, Jeongsol Kim, Michael Thompson Mccann, Marc Louis Klasky, and Jong Chul Ye. Diffusion posterior sampling for general noisy inverse problems. In *The Eleventh International Conference on Learning Representations*, 2023.
- S L Cotter, M Dashti, J C Robinson, and A M Stuart. Bayesian inverse problems for functions and applications to fluid mechanics. *Inverse Problems*, 25(11):115008, 2009.
- Florinel-Alin Croitoru, Vlad Hondru, Radu Tudor Ionescu, and Mubarak Shah. Diffusion models in vision: A survey. *IEEE Transactions on Pattern Analysis and Machine Intelligence*, 45(9):10850–10869, 2023.
- Pierre Del Moral, Arnaud Doucet, and Ajay Jasra. Sequential Monte Carlo samplers. *Journal of the Royal Statistical Society Series B: Statistical Methodology*, 68(3):411–436, 05 2006.
- Arnaud Doucet, Nando Freitas, and Neil Gordon, editors. *Sequential Monte Carlo Methods in Practice*. Information Science and Statistics (ISS). Springer New York, NY, first edition, 2001.
- John C. Duchi. Information theory and statistics, 2024. URL <http://web.stanford.edu/class/stats311/lecture-notes.pdf>. unfinished draft.
- Robert J. Elliott and Tak Kuen Siu. Option pricing and filtering with hidden Markov-modulated pure-jump processes. *Applied Mathematical Finance*, 20(1):1–25, 2013.
- Geir Evensen, Femke C. Vossepoel, and Peter Jan van Leeuwen. *Data Assimilation Fundamentals: A Unified Formulation of the State and Parameter Estimation Problem*. Springer Textbooks in Earth Sciences, Geography and Environment (STEGE). Springer Cham, first edition, 2022.
- Rüdiger Frey and Thorsten Schmidt. Pricing and hedging of credit derivatives via the innovations approach to nonlinear filtering. *Finance and Stochastics*, 16:105–133, 2012.
- Rong Ge, Holden Lee, and Jianfeng Lu. Estimating normalizing constants for log-concave distributions: algorithms and lower bounds. In *Proceedings of the 52nd Annual ACM SIGACT Symposium on Theory of Computing, STOC 2020*, pages 579–586. Association for Computing Machinery, 2020.
- Tilmann Gneiting, Fadoua Balabdaoui, and Adrian E. Raftery. Probabilistic forecasts, calibration and sharpness. *Journal of the Royal Statistical Society: Series B (Statistical Methodology)*, 69(2):243–268, 2007.
- N.J. Gordon, D.J. Salmond, and A.F.M. Smith. Novel approach to nonlinear/non-Gaussian Bayesian state estimation. *IEE Proceedings on Radar and Signal Processing*, 140:107–113, 1993.
- Wei Guo, Molei Tao, and Yongxin Chen. Provable benefit of annealed Langevin Monte Carlo for non-log-concave sampling, 2024a. arXiv:2407.16936.
- Yingqing Guo, Hui Yuan, Yukang Yang, Minshuo Chen, and Mengdi Wang. Gradient guidance for diffusion models: An optimization perspective, 2024b. arXiv:2404.14743.
- Zhiye Guo, Jian Liu, Yanli Wang, Mengrui Chen, Duolin Wang, Dong Xu, and Jianlin Cheng. Diffusion models in bioinformatics and computational biology. *Nature Reviews Bioengineering*, 2:136–154, 2024c.
- Jonathan Ho, Ajay Jain, and Pieter Abbeel. Denoising diffusion probabilistic models. In H. Larochelle, M. Ranzato, R. Hadsell, M.F. Balcan, and H. Lin, editors, *Advances in Neural*

- Information Processing Systems*, volume 33, pages 6840–6851. Curran Associates, Inc., 2020.
- Peter L Houtekamer and Herschel L Mitchell. Data assimilation using an ensemble kalman filter technique. *Monthly weather review*, 126(3):796–811, 1998.
- Aapo Hyvärinen. Estimation of non-normalized statistical models by score matching. *Journal of Machine Learning Research*, 6(24):695–709, 2005.
- Ajil Jalal, Marius Arvinte, Giannis Daras, Eric Price, Alexandros G Dimakis, and Jon Tamir. Robust compressed sensing MRI with deep generative priors. In M. Ranzato, A. Beygelzimer, Y. Dauphin, P.S. Liang, and J. Wortman Vaughan, editors, *Advances in Neural Information Processing Systems*, volume 34, pages 14938–14954. Curran Associates, Inc., 2021.
- Yuling Jiao, Guohao Shen, Yuanyuan Lin, and Jian Huang. Deep nonparametric regression on approximate manifolds: Nonasymptotic error bounds with polynomial prefactors. *The Annals of Statistics*, 51(2):691 – 716, 2023.
- Nikolas Kantas, Alexandros Beskos, and Ajay Jasra. Sequential Monte Carlo methods for high-dimensional inverse problems: A case study for the Navier-Stokes equations. *SIAM/ASA Journal on Uncertainty Quantification*, 2(1):464–489, 2014.
- Petros Katsafados, Elias Mavromatidis, and Christos Spyrou. *Numerical Weather Prediction and Data Assimilation*. John Wiley & Sons, Ltd, 2020.
- Genshiro Kitagawa. Monte Carlo filter and smoother for non-Gaussian nonlinear state space models. *Journal of Computational and Graphical Statistics*, 5(1):1–25, 1996.
- Peter E. Kloeden and Eckhard Platen. *Numerical Solution of Stochastic Differential Equations*, volume 23 of *Stochastic Modelling and Applied Probability (SMAP)*. Springer Berlin, Heidelberg, first edition, 1992.
- Dmitrii Kochkov, Jamie A. Smith, Ayya Alieva, Qing Wang, Michael P. Brenner, and Stephan Hoyer. Machine learning-accelerated computational fluid dynamics. *Proceedings of the National Academy of Sciences*, 118(21):e2101784118, 2021.
- Michael Kohler and Sophie Langer. On the rate of convergence of fully connected deep neural network regression estimates. *The Annals of Statistics*, 49(4):2231–2249, 2021.
- Kody Law, Andrew Stuart, and Konstantinos Zygalakis. *Data Assimilation: A Mathematical Introduction*, volume 62 of *Texts in Applied Mathematics (TAM)*. Springer Cham, first edition, 2015.
- François-Xavier Le Dimet and Olivier Talagrand. Variational algorithms for analysis and assimilation of meteorological observations: theoretical aspects. *Tellus A*, 38A(2):97–110, 1986.
- Holden Lee, Jianfeng Lu, and Yixin Tan. Convergence for score-based generative modeling with polynomial complexity. In S. Koyejo, S. Mohamed, A. Agarwal, D. Belgrave, K. Cho, and A. Oh, editors, *Advances in Neural Information Processing Systems*, volume 35, pages 22870–22882. Curran Associates, Inc., 2022.
- Zhuoyuan Li, Bin Dong, and Pingwen Zhang. State-observation augmented diffusion model for nonlinear assimilation, 2024. arXiv:2407.21314.
- Andrew J. Majda and John Harlim. *Filtering Complex Turbulent Systems*. Cambridge University Press, 2012.
- Jan Mandel, Loren Cobb, and Jonathan D. Beezley. On the convergence of the ensemble kalman filter. *Applications of Mathematics*, 56:533–541, 2012.
- Richard Nickl and Sven Wang. On polynomial-time computation of high-dimensional posterior measures by Langevin-type algorithms. *Journal of the European Mathematical*

- Society*, 26(3):1031–1112, 2024.
- Dhruv V. Patel and Assad A. Oberai. GAN-based priors for quantifying uncertainty in supervised learning. *SIAM/ASA Journal on Uncertainty Quantification*, 9(3):1314–1343, 2021.
- Grigorios A. Pavliotis. *Stochastic Processes and Applications: Diffusion Processes, the Fokker-Planck and Langevin Equations*, volume 60 of *Texts in Applied Mathematics (TAM)*. Springer New York, NY, 2014.
- Michael K Pitt and Neil Shephard. Filtering via simulation: Auxiliary particle filters. *Journal of the American statistical association*, 94(446):590–599, 1999.
- Vishal Purohit, Matthew Repasky, Jianfeng Lu, Qiang Qiu, Yao Xie, and Xiuyuan Cheng. Posterior sampling via Langevin dynamics based on generative priors, 2024. arXiv:2410.02078.
- Ragheb Raad, Dhruv Patel, Chiao-Chih Hsu, Vijay Kothapalli, Deep Ray, Bino Varghese, Darryl Hwang, Inderbir Gill, Vinay Duddalwar, and Assad A. Oberai. Probabilistic medical image imputation via deep adversarial learning. *Engineering with Computers*, 38:3975–3986, 2022.
- Ragheb Raad, Deep Ray, Bino Varghese, Darryl Hwang, Inderbir Gill, Vinay Duddalwar, and Assad A. Oberai. Conditional generative learning for medical image imputation. *Scientific Reports*, 14(171), 2024.
- Firas Rassoul-Agha and Timo Seppäläinen. *A Course on Large Deviations with an Introduction to Gibbs Measures*, volume 162 of *Graduate Studies in Mathematics*. American Mathematical Society (AMS), 2015.
- Sebastian Reich. Data assimilation: The Schrödinger perspective. *Acta Numerica*, 28:635–711, 2019.
- Sebastian Reich and Colin Cotter. *Probabilistic Forecasting and Bayesian Data Assimilation*. Cambridge University Press, 2015.
- Gareth O. Roberts and Richard L. Tweedie. Exponential convergence of Langevin distributions and their discrete approximations. *Bernoulli*, 2(4):341 – 363, 1996.
- François Rozet and Gilles Louppe. Score-based data assimilation. In A. Oh, T. Naumann, A. Globerson, K. Saenko, M. Hardt, and S. Levine, editors, *Advances in Neural Information Processing Systems*, volume 36, pages 40521–40541. Curran Associates, Inc., 2023a.
- François Rozet and Gilles Louppe. Score-based data assimilation for a two-layer quasi-geostrophic model, 2023b. arXiv:2310.01853.
- William Sacher and Peter Bartello. Sampling errors in ensemble Kalman filtering. Part I: Theory. *Monthly Weather Review*, 136:3035–3049, 2008.
- Simo Särkkä and Lennart Svensson. *Bayesian filtering and smoothing*. Institute of Mathematical Statistics Textbooks. Cambridge University Press, second edition, 2023.
- Johannes Schmidt-Hieber. Nonparametric regression using deep neural networks with relu activation function. *The Annals of Statistics*, 48(4):1875–1897, 2020.
- Phillip Si and Peng Chen. Latent-EnSF: A latent ensemble score filter for high-dimensional data assimilation with sparse observation data, 2024. arXiv:2409.00127.
- Chris Snyder, Thomas Bengtsson, Peter Bickel, and Jeff Anderson. Obstacles to high-dimensional particle filtering. *Monthly weather review*, 136:4629–4640, 2008.
- Jiaming Song, Arash Vahdat, Morteza Mardani, and Jan Kautz. Pseudoinverse-guided diffusion models for inverse problems. In *International Conference on Learning Representations*, 2023.
- Yang Song and Stefano Ermon. Generative modeling by estimating gradients of the data distribution. In H. Wallach, H. Larochelle, A. Beygelzimer, F. d'Alché-Buc, E. Fox, and

- R. Garnett, editors, *Advances in Neural Information Processing Systems*, volume 32. Curran Associates, Inc., 2019.
- Yang Song and Stefano Ermon. Improved techniques for training score-based generative models. In H. Larochelle, M. Ranzato, R. Hadsell, M.F. Balcan, and H. Lin, editors, *Advances in Neural Information Processing Systems*, volume 33, pages 12438–12448. Curran Associates, Inc., 2020.
- Yang Song, Sahaj Garg, Jiaxin Shi, and Stefano Ermon. Sliced score matching: A scalable approach to density and score estimation. In Ryan P. Adams and Vibhav Gogate, editors, *Proceedings of The 35th Uncertainty in Artificial Intelligence Conference*, volume 115 of *Proceedings of Machine Learning Research*, pages 574–584. PMLR, 22–25 Jul 2020.
- Yang Song, Jascha Sohl-Dickstein, Diederik P Kingma, Abhishek Kumar, Stefano Ermon, and Ben Poole. Score-based generative modeling through stochastic differential equations. In *International Conference on Learning Representations*, 2021.
- Yang Song, Liyue Shen, Lei Xing, and Stefano Ermon. Solving inverse problems in medical imaging with score-based generative models. In *International Conference on Learning Representations*, 2022.
- Alessio Spantini, Ricardo Baptista, and Youssef Marzouk. Coupling techniques for nonlinear ensemble filtering. *SIAM Review*, 64(4):921–953, 2022.
- T.J. Sullivan. *Introduction to Uncertainty Quantification*, volume 63 of *Texts in Applied Mathematics (TAM)*. Springer Cham, first edition, 2015.
- Rong Tang and Yun Yang. Adaptivity of diffusion models to manifold structures. In Sanjoy Dasgupta, Stephan Mandt, and Yingzhen Li, editors, *Proceedings of The 27th International Conference on Artificial Intelligence and Statistics*, volume 238 of *Proceedings of Machine Learning Research*, pages 1648–1656. PMLR, 02–04 May 2024.
- Adam Thelen, Xiaoge Zhang, Olga Fink, Yan Lu, Sayan Ghosh, D. Byeng Youn, Michael D. Todd, Sankaran Mahadevan, Chao Hu, and Zhen Hu. A comprehensive review of digital twin – part 1: modeling and twinning enabling technologies. *Structural and Multidisciplinary Optimization*, 65(354), 2022.
- Adam Thelen, Xiaoge Zhang, Olga Fink, Yan Lu, Sayan Ghosh, D. Byeng Youn, Michael D. Todd, Sankaran Mahadevan, Chao Hu, and Zhen Hu. A comprehensive review of digital twin – part 2: roles of uncertainty quantification and optimization, a battery digital twin, and perspectives. *Structural and Multidisciplinary Optimization*, 66(1), 2023.
- Alexandre B. Tsybakov. *Introduction to Nonparametric Estimation*. Springer Series in Statistics (SSS). Springer New York, NY, first edition, 2009.
- Santosh Vempala and Andre Wibisono. Rapid convergence of the unadjusted Langevin algorithm: Isoperimetry suffices. In H. Wallach, H. Larochelle, A. Beygelzimer, F. d'Alché-Buc, E. Fox, and R. Garnett, editors, *Advances in Neural Information Processing Systems*, volume 32. Curran Associates, Inc., 2019.
- Pascal Vincent. A connection between score matching and denoising autoencoders. *Neural Computation*, 23(7):1661–1674, 2011.
- Martin J. Wainwright. *High-Dimensional Statistics: A Non-Asymptotic Viewpoint*. Cambridge Series in Statistical and Probabilistic Mathematics. Cambridge University Press, 2019.
- Joseph L. Watson, David Juergens, Nathaniel R. Bennett, Brian L. Trippe, Jason Yim, Helen E. Eisenach, Woody Ahern, Andrew J. Borst, Robert J. Ragotte, Lukas F. Milles, Basile I. M. Wicky, Nikita Hanikel, Samuel J. Pellock, Alexis Courbet, William Sheffler, Jue Wang, Preetham Venkatesh, Isaac Sappington, Susana Vázquez Torres, Anna Lauko, Valentin De

- Bortoli, Emile Mathieu, Sergey Ovchinnikov, Regina Barzilay, Tommi S. Jaakkola, Frank DiMaio, Minkyung Baek, and David Baker. De novo design of protein structure and function with RFDiffusion. *Nature*, 620:1089–1100, 2023.
- Tomer Weiss, Eduardo Mayo Yanes, Sabyasachi Chakraborty, Luca Cosmo, Alex M. Bronstein, and Renana Gershoni-Poranne. Guided diffusion for inverse molecular design. *Nature Computational Science*, 3:873–882, 2023.
- Dongze Wu and Yao Xie. Annealing flow generative model towards sampling high-dimensional and multi-modal distributions, 2024. arXiv:2409.20547.
- Ling Yang, Zhilong Zhang, Yang Song, Shenda Hong, Runsheng Xu, Yue Zhao, Wentao Zhang, Bin Cui, and Ming-Hsuan Yang. Diffusion models: A comprehensive survey of methods and applications. *ACM Computing Surveys*, 56(4):1–39, 2023.
- Chenshuang Zhang, Chaoning Zhang, Sheng Zheng, Mengchun Zhang, Maryam Qamar, Sung-Ho Bae, and In So Kweon. A survey on audio diffusion models: Text to speech synthesis and enhancement in generative AI, 2023. arXiv:2303.13336.

OUTLINE OF APPENDICES

We include several appendices with a summary of notations, additional derivations, proofs of theoretical results, and experimental details.

- (i) A summary of notations is shown in Appendix [A](#).
- (ii) Our approach follows the recursive Bayesian framework, for which we provide detailed derivations in Appendix [B](#). We also give the derivations of denoising score matching in Appendix [B](#).
- (iii) The convergence of the score-based sequential Langevin Monte Carlo (Section [3](#)) is proven in Appendix [C](#). Specifically, Appendix [C](#) decomposes the error of the assimilation into three terms: the convergence of Langevin Monte Carlo, the prior error, and the error of the score matching. The detailed analysis for these three errors are presented in Appendices [D](#), [E](#) and [F](#), respectively.
- (iv) Some auxiliary definitions and lemmas used in this work are introduced in Appendix [H](#).
- (v) The experimental details are summarized in Appendix [I](#).

APPENDIX A. A SUMMARY OF NOTATIONS

Table [2](#) summarizes the notations used in Sections [2](#) and [3](#) for easy reference and cross-checking.

TABLE 2. The list of notations defined in Sections 2 and 3.

Symbols	Description
\mathcal{F}_k	The dynamics model at the k -th time step, defined as (2.1).
\mathcal{G}_k	The measurement model at the k -th time step, defined as (2.2).
\mathbf{X}_k	The state at the k -th time step.
\mathbf{Y}_k	The observation of \mathbf{X}_k .
$\widehat{\mathbf{X}}_k$	The estimated state at the k -th time step using SSSL.
$\underline{\mathbf{X}}_k$	The predicted state at the k -th time step using the dynamics model, defined as (2.8).
ρ_k	The state transition density at the k -th time step, specified by (2.1).
g_k	The measurement likelihood at the k -th time step, specified by (2.2).
π_k	The posterior at the k -th time step, defined as (2.3).
$\widehat{\pi}_k$ or $\widehat{\pi}_k^T$	The estimated posterior at the k -th time step using SSSL with terminal time T , which is the law of $\widehat{\mathbf{X}}_k$.
q_k	The prediction distribution at the k -th time step, defined as (2.5), serving as the prior in the posterior π_k .
\widehat{q}_k	The approximated prediction distribution at the k -th time step, defined as (2.7), which is the law of $\underline{\mathbf{X}}_k$.
\mathbf{Z}_t	The stochastic process specified by the Langevin diffusion (2.11).
$\widehat{\mathbf{Z}}_t$	The stochastic process specified by the Langevin Monte Carlo (2.12).
$\widehat{\mathbf{b}}_k$	The drift term in the score-based Langevin Monte Carlo (2.13).
$(\beta_m)_{m=1}^M$	A sequence of inverse temperatures for annealing.
$\widehat{\mathbf{Z}}_t^m$	The stochastic process specified by the annealed Langevin Monte Carlo (2.14) with a inverse temperature β_m .
$\widehat{\mathbf{b}}_k^m$	The drift term in the score-based annealed Langevin Monte Carlo (2.15) with a inverse temperature β_m .

APPENDIX B. PROOFS IN SECTION 2

In this section, we provide proofs in Section 2. The derivation of the recursive Bayesian framework is shown in Appendix B.1, and the proof of the denoising score matching is demonstrated in Appendix B.2.

B.1. Recursive Bayesian framework. This section verifies the recursion (2.6). Indeed,

$$\begin{aligned}
& \pi_{k+1}(\mathbf{x}_{k+1} | \mathbf{Y}_{[k+1]}) \\
&= \frac{p_{\mathbf{Y}_{k+1} | \mathbf{x}_{k+1}, \mathbf{Y}_{[k]}}(\mathbf{y}_{k+1} | \mathbf{x}_{k+1}, \mathbf{Y}_{[k]})}{p_{\mathbf{Y}_{k+1} | \mathbf{Y}_{[k]}}(\mathbf{y}_{k+1} | \mathbf{Y}_{[k]})} p_{\mathbf{x}_{k+1} | \mathbf{Y}_{[k]}}(\mathbf{x}_{k+1} | \mathbf{Y}_{[k]}) \\
&= \frac{g_{k+1}(\mathbf{y}_{k+1} | \mathbf{x}_{k+1})}{p_{\mathbf{Y}_{k+1} | \mathbf{Y}_{[k]}}(\mathbf{y}_{k+1} | \mathbf{Y}_{[k]})} \int p_{\mathbf{x}_{k+1} | \mathbf{x}_k, \mathbf{Y}_{[k]}}(\mathbf{x}_{k+1} | \mathbf{x}_k, \mathbf{Y}_{[k]}) \pi_k(\mathbf{x}_k | \mathbf{Y}_{[k]}) d\mathbf{x}_k \\
&= \frac{g_{k+1}(\mathbf{y}_{k+1} | \mathbf{x}_{k+1})}{p_{\mathbf{Y}_{k+1} | \mathbf{Y}_{[k]}}(\mathbf{y}_{k+1} | \mathbf{Y}_{[k]})} \int \rho_k(\mathbf{x}_{k+1} | \mathbf{x}_k) \pi_k(\mathbf{x}_k | \mathbf{Y}_{[k]}) d\mathbf{x}_k,
\end{aligned}$$

where the first equality follows from Bayes's rule. The second equality invokes Chapman-Kolmogorov identity and the fact that \mathbf{Y}_{k+1} is independent of \mathbf{Y}_k given \mathbf{X}_{k+1} . The last equality is owing to the fact that \mathbf{X}_{k+1} is independent of $\mathbf{Y}_{[k]}$ given \mathbf{X}_k .

B.2. Denoising score matching. In this section, we provide the derivations of the denoising score matching, which has been proven by Vincent (2011), Ho et al. (2020), Song and Ermon (2019).

Let $\underline{\mathbf{X}}_{k+1}$ be a random variable drawn from the prediction distribution $\hat{q}_{k+1}(\cdot|\mathbf{y}_{[k]})$, and let ε be a standard Gaussian noise independent of $\underline{\mathbf{X}}_{k+1}$. For each fixed noise level $\sigma > 0$, define

$$(B.1) \quad \underline{\mathbf{X}}_{k+1}^\sigma = \underline{\mathbf{X}}_{k+1} + \sigma\varepsilon.$$

It is evident that $\underline{\mathbf{X}}_{k+1}^\sigma$ obeys the Gaussian smoothed prediction distribution, that is,

$$\begin{aligned} q_{k+1}^\sigma(\mathbf{x}^\sigma|\mathbf{y}_{[k]}) &:= \int p_{\underline{\mathbf{X}}_{k+1}^\sigma|\underline{\mathbf{X}}_{k+1}}(\mathbf{x}^\sigma|\mathbf{x})\hat{q}_{k+1}(\mathbf{x}|\mathbf{y}_{[k]})d\mathbf{x} \\ &= \int \underbrace{N(\mathbf{x}^\sigma; \mathbf{x}, \sigma^2\mathbf{I}_d)}_{\text{Gaussian kernel}}\hat{q}_{k+1}(\mathbf{x}|\mathbf{y}_{[k]})d\mathbf{x}. \end{aligned}$$

Observe that the score of the Gaussian kernel is given as

$$(B.2) \quad \nabla_{\mathbf{x}^\sigma} \log p_{\underline{\mathbf{X}}_{k+1}^\sigma|\underline{\mathbf{X}}_{k+1}}(\mathbf{x}^\sigma|\mathbf{x}) = -\frac{\mathbf{x}^\sigma - \mathbf{x}}{\sigma^2}.$$

Step (I). We first show that for each function \mathbf{s} ,

$$(B.3) \quad \begin{aligned} &\mathbb{E}_{\underline{\mathbf{X}}_{k+1}^\sigma \sim p_{\underline{\mathbf{X}}_{k+1}^\sigma|\mathbf{Y}_{[k]}}(\cdot|\mathbf{y}_{[k]})} [\|\mathbf{s}(\underline{\mathbf{X}}_{k+1}^\sigma, \mathbf{y}_{[k]}) - \nabla_{\mathbf{x}^\sigma} \log p_{\underline{\mathbf{X}}_{k+1}^\sigma|\mathbf{Y}_{[k]}}(\underline{\mathbf{X}}_{k+1}^\sigma|\mathbf{y}_{[k]})\|_2^2] \\ &= \mathbb{E}_{\underline{\mathbf{X}}_{k+1} \sim \hat{q}_{k+1}(\cdot|\mathbf{y}_{[k]})} \mathbb{E}_{\underline{\mathbf{X}}_{k+1}^\sigma \sim p_{\underline{\mathbf{X}}_{k+1}^\sigma|\underline{\mathbf{X}}_{k+1}} [\|\mathbf{s}(\underline{\mathbf{X}}_{k+1}^\sigma, \mathbf{y}_{[k]}) \\ &\quad - \nabla_{\mathbf{x}^\sigma} \log p_{\underline{\mathbf{X}}_{k+1}^\sigma|\underline{\mathbf{X}}_{k+1}}(\underline{\mathbf{X}}_{k+1}^\sigma|\underline{\mathbf{X}}_{k+1})\|_2^2] + c, \end{aligned}$$

where c is a constant independent of \mathbf{s} . Indeed,

$$(B.4) \quad \begin{aligned} &\mathbb{E}_{\underline{\mathbf{X}}_{k+1}^\sigma \sim p_{\underline{\mathbf{X}}_{k+1}^\sigma|\mathbf{Y}_{[k]}}(\cdot|\mathbf{y}_{[k]})} [\|\mathbf{s}(\underline{\mathbf{X}}_{k+1}^\sigma, \mathbf{y}_{[k]}) - \nabla_{\mathbf{x}^\sigma} \log p_{\underline{\mathbf{X}}_{k+1}^\sigma|\mathbf{Y}_{[k]}}(\underline{\mathbf{X}}_{k+1}^\sigma|\mathbf{y}_{[k]})\|_2^2] \\ &= \underbrace{\mathbb{E}_{\underline{\mathbf{X}}_{k+1}^\sigma \sim p_{\underline{\mathbf{X}}_{k+1}^\sigma|\mathbf{Y}_{[k]}}(\cdot|\mathbf{y}_{[k]})} [\|\mathbf{s}(\underline{\mathbf{X}}_{k+1}^\sigma, \mathbf{y}_{[k]})\|_2^2]}_{(i)} \\ &\quad - \underbrace{2 \mathbb{E}_{\underline{\mathbf{X}}_{k+1}^\sigma \sim p_{\underline{\mathbf{X}}_{k+1}^\sigma|\mathbf{Y}_{[k]}}(\cdot|\mathbf{y}_{[k]})} [\mathbf{s}(\underline{\mathbf{X}}_{k+1}^\sigma, \mathbf{y}_{[k]}) \cdot \nabla_{\mathbf{x}^\sigma} \log p_{\underline{\mathbf{X}}_{k+1}^\sigma|\mathbf{Y}_{[k]}}(\underline{\mathbf{X}}_{k+1}^\sigma|\mathbf{y}_{[k]})]}_{(i)} + c_1, \end{aligned}$$

where c_1 is a constant independent of \mathbf{s} . For the term (i) in (B.4), we have

$$(B.5) \quad \begin{aligned} &\mathbb{E}_{\underline{\mathbf{X}}_{k+1}^\sigma \sim p_{\underline{\mathbf{X}}_{k+1}^\sigma|\mathbf{Y}_{[k]}}(\cdot|\mathbf{y}_{[k]})} [\|\mathbf{s}(\underline{\mathbf{X}}_{k+1}^\sigma, \mathbf{y}_{[k]})\|_2^2] \\ &= \int \|\mathbf{s}(\mathbf{x}_\sigma, \mathbf{y}_{[k]})\|_2^2 p_{\underline{\mathbf{X}}_{k+1}^\sigma|\mathbf{Y}_{[k]}}(\mathbf{x}_\sigma|\mathbf{y}_{[k]})d\mathbf{x}_\sigma \\ &= \int \|\mathbf{s}(\mathbf{x}_\sigma, \mathbf{y}_{[k]})\|_2^2 \left(\int p_{\underline{\mathbf{X}}_{k+1}^\sigma|\underline{\mathbf{X}}_{k+1}, \mathbf{Y}_{[k]}}(\mathbf{x}_\sigma|\mathbf{x}, \mathbf{y}_{[k]})q_{k+1}(\mathbf{x}|\mathbf{y}_{[k]})d\mathbf{x} \right) d\mathbf{x}_\sigma \\ &= \int \|\mathbf{s}(\mathbf{x}_\sigma, \mathbf{y}_{[k]})\|_2^2 \left(\int p_{\underline{\mathbf{X}}_{k+1}^\sigma|\underline{\mathbf{X}}_{k+1}}(\mathbf{x}_\sigma|\mathbf{x})q_{k+1}(\mathbf{x}|\mathbf{y}_{[k]})d\mathbf{x} \right) d\mathbf{x}_\sigma \\ &= \int \left(\int \|\mathbf{s}(\mathbf{x}_\sigma, \mathbf{y}_{[k]})\|_2^2 p_{\underline{\mathbf{X}}_{k+1}^\sigma|\underline{\mathbf{X}}_{k+1}}(\mathbf{x}_\sigma|\mathbf{x})d\mathbf{x}_\sigma \right) q_{k+1}(\mathbf{x}|\mathbf{y}_{[k]})d\mathbf{x} \\ &= \mathbb{E}_{\underline{\mathbf{X}}_{k+1} \sim \hat{q}_{k+1}(\cdot|\mathbf{y}_{[k]})} \mathbb{E}_{\underline{\mathbf{X}}_{k+1}^\sigma \sim p_{\underline{\mathbf{X}}_{k+1}^\sigma|\underline{\mathbf{X}}_{k+1}} [\|\mathbf{s}(\underline{\mathbf{X}}_{k+1}^\sigma, \mathbf{y}_{[k]})\|_2^2], \end{aligned}$$

where the second equality follows from Chapman-Kolmogorov identity, the third equality is due to the fact that $\underline{\mathbf{X}}_{k+1}^\sigma$ is conditionally independent of $\mathbf{Y}^{[k]}$ given $\underline{\mathbf{X}}_{k+1}$. For the term (ii) in (B.4), by the same argument,

$$\begin{aligned}
& \mathbb{E}_{\underline{\mathbf{X}}_{k+1}^\sigma \sim p_{\underline{\mathbf{X}}_{k+1}^\sigma | \mathbf{Y}^{[k]}}(\cdot | \mathbf{y}^{[k]})} \left[\mathbf{s}(\underline{\mathbf{X}}_{k+1}^\sigma, \mathbf{y}^{[k]}) \cdot \nabla_{\mathbf{x}_\sigma} \log p_{\underline{\mathbf{X}}_{k+1}^\sigma | \mathbf{Y}^{[k]}}(\underline{\mathbf{X}}_{k+1}^\sigma | \mathbf{y}^{[k]}) \right] \\
&= \int \mathbf{s}(\mathbf{x}_\sigma, \mathbf{y}^{[k]}) \cdot \nabla_{\mathbf{x}_\sigma} p_{\underline{\mathbf{X}}_{k+1}^\sigma | \mathbf{Y}^{[k]}}(\mathbf{x}_\sigma | \mathbf{y}^{[k]}) d\mathbf{x}_\sigma \\
&= \int \mathbf{s}(\mathbf{x}_\sigma, \mathbf{y}^{[k]}) \cdot \nabla_{\mathbf{x}_\sigma} \left(\int p_{\underline{\mathbf{X}}_{k+1}^\sigma | \underline{\mathbf{X}}_{k+1}}(\mathbf{x}_\sigma | \mathbf{x}) q_{k+1}(\mathbf{x} | \mathbf{y}^{[k]}) d\mathbf{x} \right) d\mathbf{x}_\sigma \\
&= \int \mathbf{s}(\mathbf{x}_\sigma, \mathbf{y}^{[k]}) \cdot \left(\int \nabla_{\mathbf{x}_\sigma} p_{\underline{\mathbf{X}}_{k+1}^\sigma | \underline{\mathbf{X}}_{k+1}}(\mathbf{x}_\sigma | \mathbf{x}) q_{k+1}(\mathbf{x} | \mathbf{y}^{[k]}) d\mathbf{x} \right) d\mathbf{x}_\sigma \\
&= \int \left(\int \mathbf{s}(\mathbf{x}_\sigma, \mathbf{y}^{[k]}) \cdot \nabla_{\mathbf{x}_\sigma} p_{\underline{\mathbf{X}}_{k+1}^\sigma | \underline{\mathbf{X}}_{k+1}}(\mathbf{x}_\sigma | \mathbf{x}) d\mathbf{x}_\sigma \right) q_{k+1}(\mathbf{x} | \mathbf{y}^{[k]}) d\mathbf{x} \\
\text{(B.6)} \quad &= \mathbb{E}_{\underline{\mathbf{X}}_{k+1} \sim \hat{q}_{k+1}(\cdot | \mathbf{y}^{[k]})} \mathbb{E}_{\underline{\mathbf{X}}_{k+1}^\sigma \sim p_{\underline{\mathbf{X}}_{k+1}^\sigma | \underline{\mathbf{X}}_{k+1}}(\cdot | \underline{\mathbf{X}}_{k+1})} \left[\mathbf{s}(\underline{\mathbf{X}}_{k+1}^\sigma, \mathbf{y}^{[k]}) \cdot \nabla \log p_{\underline{\mathbf{X}}_{k+1}^\sigma | \underline{\mathbf{X}}_{k+1}}(\underline{\mathbf{X}}_{k+1}^\sigma | \underline{\mathbf{X}}_{k+1}) \right].
\end{aligned}$$

Plugging (B.5) and (B.6) into (B.4) completes the proof of (B.3).

Step (II). We next reformulate the right-hand side of (B.3) as

$$\begin{aligned}
& \mathbb{E}_{\underline{\mathbf{X}}_{k+1} \sim \hat{q}_{k+1}(\cdot | \mathbf{y}^{[k]})} \mathbb{E}_{\underline{\mathbf{X}}_{k+1}^\sigma \sim p_{\underline{\mathbf{X}}_{k+1}^\sigma | \underline{\mathbf{X}}_{k+1}}(\cdot | \underline{\mathbf{X}}_{k+1})} \left[\|\mathbf{s}(\underline{\mathbf{X}}_{k+1}^\sigma, \mathbf{y}^{[k]}) - \nabla_{\mathbf{x}} \log p_{\underline{\mathbf{X}}_{k+1}^\sigma | \underline{\mathbf{X}}_{k+1}}(\underline{\mathbf{X}}_{k+1}^\sigma | \underline{\mathbf{X}}_{k+1})\|_2^2 \right] \\
&= \mathbb{E}_{\underline{\mathbf{X}}_{k+1} \sim \hat{q}_{k+1}(\cdot | \mathbf{y}^{[k]})} \mathbb{E}_{\underline{\mathbf{X}}_{k+1}^\sigma \sim p_{\underline{\mathbf{X}}_{k+1}^\sigma | \underline{\mathbf{X}}_{k+1}}(\cdot | \underline{\mathbf{X}}_{k+1})} \left[\|\mathbf{s}(\underline{\mathbf{X}}_{k+1}^\sigma, \mathbf{y}^{[k]}) + \frac{1}{\sigma^2}(\underline{\mathbf{X}}_{k+1}^\sigma - \underline{\mathbf{X}}_{k+1})\|_2^2 \right] \\
&= \frac{1}{\sigma^2} \mathbb{E}_{\underline{\mathbf{X}}_{k+1} \sim \hat{q}_{k+1}(\cdot | \mathbf{y}^{[k]})} \mathbb{E}_{\boldsymbol{\varepsilon} \sim N(0, \mathbf{I}_d)} \left[\|\sigma \mathbf{s}(\underline{\mathbf{X}}_{k+1} + \sigma \boldsymbol{\varepsilon}, \mathbf{y}^{[k]}) + \boldsymbol{\varepsilon}\|_2^2 \right],
\end{aligned}$$

where the first equality is due to (B.2), and the second equality used (B.1). Combining this with (B.3) yields

$$\begin{aligned}
& \mathbb{E}_{\underline{\mathbf{X}}_{k+1}^\sigma \sim p_{\underline{\mathbf{X}}_{k+1}^\sigma | \mathbf{Y}^{[k]}}(\cdot | \mathbf{y}^{[k]})} \left[\|\mathbf{s}(\underline{\mathbf{X}}_{k+1}^\sigma, \mathbf{y}^{[k]}) - \nabla \log p_{\underline{\mathbf{X}}_{k+1}^\sigma | \mathbf{Y}^{[k]}}(\underline{\mathbf{X}}_{k+1}^\sigma | \mathbf{y}^{[k]})\|_2^2 \right] \\
&= \frac{1}{\sigma^2} \mathbb{E}_{\underline{\mathbf{X}}_{k+1} \sim \hat{q}_{k+1}(\cdot | \mathbf{y}^{[k]})} \mathbb{E}_{\boldsymbol{\varepsilon} \sim N(0, \mathbf{I}_d)} \left[\|\sigma \mathbf{s}(\underline{\mathbf{X}}_{k+1} + \sigma \boldsymbol{\varepsilon}, \mathbf{y}^{[k]}) + \boldsymbol{\varepsilon}\|_2^2 \right] + c,
\end{aligned}$$

which achieves the population risk of the denoising score matching. Consequently,

$$\nabla_{\mathbf{x}_\sigma} \log q_{k+1}^\sigma(\cdot | \mathbf{y}^{[k+1]}) = \arg \min_{\mathbf{s}} \mathbb{E}_{\underline{\mathbf{X}}_{k+1} \sim \hat{q}_{k+1}(\cdot | \mathbf{y}^{[k]})} \mathbb{E}_{\boldsymbol{\varepsilon} \sim N(0, \mathbf{I}_d)} \left[\|\sigma \mathbf{s}(\underline{\mathbf{X}}_{k+1} + \sigma \boldsymbol{\varepsilon}, \mathbf{y}^{[k]}) + \boldsymbol{\varepsilon}\|_2^2 \right].$$

Finally, approximate the above population risk by its empirical counterpart yields (2.10).

APPENDIX C. PROOFS IN SECTION 3

In this section, we provide proofs of Theorems 3.3 and 3.5. We first decompose the error of the posterior distribution in Appendix C.1. The error analysis for the posterior sampling (Theorem 3.3), and the convergence of assimilation (Theorem 3.5) are proven in Appendix C.2.

C.1. Error Decomposition. Recall the Langevin diffusion for the $(k+1)$ -th time step of the data assimilation

$$\text{(C.1)} \quad d\mathbf{Z}_t = \nabla_{\mathbf{x}} \log \pi_{k+1}(\mathbf{Z}_t | \mathbf{y}^{[k+1]}) dt + \sqrt{2} d\mathbf{B}_t, \quad \mathbf{Z}_0 \sim \pi_{k+1}^0(\cdot | \mathbf{y}^{[k+1]}), \quad t \geq 0.$$

Denote by π_{k+1}^t the law of \mathbf{Z}_t for each $t \geq 0$. The Langevin Monte Carlo is defined as the Euler-Maruyama discretization of the Langevin diffusion. The interpolation of the Langevin Monte Carlo is given as, for each $0 \leq \ell \leq K-1$,

$$\text{(C.2)} \quad d\bar{\mathbf{Z}}_t = \nabla_{\mathbf{x}} \log \pi_{k+1}(\bar{\mathbf{Z}}_{\ell h} | \mathbf{y}^{[k+1]}) dt + \sqrt{2} d\mathbf{B}_t, \quad \ell h \leq t \leq (\ell+1)h,$$

where $\bar{\mathbf{Z}}_0 \sim \pi_{k+1}^0(\cdot|\mathbf{y}_{[k+1]})$. Denote by $\bar{\pi}_{k+1}^t$ the law of $\bar{\mathbf{Z}}_t$ for each $0 \leq t \leq Kh = T$. We next introduce the interpolation of the score-based Langevin Monte Carlo

$$(C.3) \quad d\hat{\mathbf{Z}}_t = \hat{\mathbf{b}}_{k+1}(\hat{\mathbf{Z}}_{\ell h}|\mathbf{y}_{[k+1]}) dt + \sqrt{2} d\mathbf{B}_t, \quad \ell h \leq t \leq (\ell+1)h,$$

where $\hat{\mathbf{Z}}_0 \sim \pi_{k+1}^0(\cdot|\mathbf{y}_{[k+1]})$, and the estimator of posterior score function is given as

$$\hat{\mathbf{b}}_{k+1}(\mathbf{x}|\mathbf{y}_{[k+1]}) = \nabla_{\mathbf{x}} \log g_{k+1}(\mathbf{y}_{k+1}|\mathbf{x}) + \hat{\mathbf{s}}_{k+1}(\mathbf{x}, \mathbf{y}_{[k]}).$$

Here the prediction score $\hat{\mathbf{s}}_{k+1}$ is defined as (2.10). Denote by $\hat{\pi}_{k+1}^t$ the law of $\hat{\mathbf{Z}}_t$ for each $0 \leq t \leq Kh = T$. Recall the prediction distribution (2.5)

$$q_{k+1}(\mathbf{x}|\mathbf{y}_{[k]}) = \int \rho_k(\mathbf{x}|\mathbf{x}_k) \pi_k(\mathbf{x}_k|\mathbf{y}_{[k]}) d\mathbf{x}_k,$$

which serves as the prior in the Bayesian recursive framework. Recall the approximated prediction distribution (2.7)

$$\hat{q}_{k+1}(\mathbf{x}|\mathbf{y}_{[k]}) := \int \rho_k(\mathbf{x}|\mathbf{x}_k) \hat{\pi}_k^T(\mathbf{x}_k|\mathbf{y}_{[k]}) d\mathbf{x}_k.$$

The following lemma decomposes the TV distance between π_{k+1} and $\hat{\pi}_{k+1}^T$ into three parts: the convergence of the Langevin Monte Carlo, the prior error, and the error of score matching.

Lemma C.1 (Error decomposition). *Let π_{k+1} be the stationary distribution of the Langevin diffusion (C.1), and let $\hat{\pi}_{k+1}^T$ be the law of the score-based Langevin Monte Carlo (C.3). Then for each $k \in \mathbb{N}$,*

$$\begin{aligned} & \text{TV}^2(\pi_{k+1}(\cdot|\mathbf{y}_{[k+1]}), \hat{\pi}_{k+1}^T(\cdot|\mathbf{y}_{[k+1]})) \\ & \leq 2 \underbrace{\text{TV}^2(\pi_{k+1}(\cdot|\mathbf{y}_{[k+1]}), \bar{\pi}_{k+1}^T(\cdot|\mathbf{y}_{[k+1]}))}_{\text{convergence of Langevin Monte Carlo}} \\ & \quad + 4T \underbrace{\|\nabla_{\mathbf{x}} \log q_{k+1}(\cdot|\mathbf{y}_{[k]}) - \nabla_{\mathbf{x}} \log \hat{q}_{k+1}(\cdot|\mathbf{y}_{[k]})\|_{L^\infty(\mathbb{R}^d)}^2}_{\text{prior error}} \\ & \quad + 4 \underbrace{\sum_{\ell=0}^{K-1} h \mathbb{E}_{\bar{\mathbf{Z}}_{\ell h}} \left[\|\nabla_{\mathbf{x}} \log \hat{q}_{k+1}(\bar{\mathbf{Z}}_{\ell h}|\mathbf{y}_{[k]}) - \hat{\mathbf{s}}_{k+1}(\bar{\mathbf{Z}}_{\ell h}, \mathbf{y}_{[k]})\|_2^2 \right]}_{\text{score estimation error}}, \end{aligned}$$

where the expectation $\mathbb{E}_{\bar{\mathbf{Z}}_{\ell h}}[\cdot]$ is taken with respect to $\bar{\mathbf{Z}}_{\ell h} \sim \bar{\pi}_{k+1}^{\ell h}(\cdot|\mathbf{y}_{[k+1]})$.

Remark C.2. The convergence of the Langevin Monte Carlo will be analyzed in Appendix D. The prior error characterizes the error of the approximated prediction distribution \hat{q}_{k+1} , which is induced by the error of the posterior distribution $\hat{\pi}_k^T$ in the previous time step. The detailed analysis will be shown in Appendix E. Finally, we will investigate the score estimation error in Appendix F.

Proof of Lemma C.1. According to the triangular inequality of TV distance, we have

$$\begin{aligned} & \text{TV}^2(\pi_{k+1}(\cdot|\mathbf{y}_{[k+1]}), \hat{\pi}_{k+1}^T(\cdot|\mathbf{y}_{[k+1]})) \\ & \leq 2 \text{TV}^2(\pi_{k+1}(\cdot|\mathbf{y}_{[k+1]}), \bar{\pi}_{k+1}^T(\cdot|\mathbf{y}_{[k+1]})) + 2 \text{TV}^2(\bar{\pi}_{k+1}^T(\cdot|\mathbf{y}_{[k+1]}), \hat{\pi}_{k+1}^T(\cdot|\mathbf{y}_{[k+1]})). \end{aligned}$$

For the second term, we invoke Girsanov theorem (Chen et al., 2023) to show that

$$\begin{aligned}
& \text{TV}^2(\widehat{\pi}_{k+1}^T(\cdot|\mathbf{y}_{[k+1]}), \widehat{\pi}_{k+1}^T(\cdot|\mathbf{y}_{[k+1]})) \\
& \leq 2 \text{KL}(\widehat{\pi}_{k+1}^T(\cdot|\mathbf{y}_{[k+1]}), \widehat{\pi}_{k+1}^T(\cdot|\mathbf{y}_{[k+1]})) \\
& \leq \sum_{\ell=0}^{K-1} h \mathbb{E}_{\bar{\mathbf{Z}}_{\ell h}} [\|\nabla_{\mathbf{x}} \log \pi_{k+1}(\bar{\mathbf{Z}}_{\ell h}|\mathbf{y}_{[k+1]}) - \widehat{\mathbf{b}}_{k+1}(\bar{\mathbf{Z}}_{\ell h}, \mathbf{y}_{[k+1]})\|_2^2] \\
& = \sum_{\ell=0}^{K-1} h \mathbb{E}_{\bar{\mathbf{Z}}_{\ell h}} [\|\nabla_{\mathbf{x}} \log q_{k+1}(\bar{\mathbf{Z}}_{\ell h}|\mathbf{y}_{[k]}) - \widehat{\mathbf{s}}_{k+1}(\bar{\mathbf{Z}}_{\ell h}, \mathbf{y}_{[k]})\|_2^2] \\
& \leq 2 \sum_{\ell=0}^{K-1} h \mathbb{E}_{\bar{\mathbf{Z}}_{\ell h}} [\|\nabla_{\mathbf{x}} \log q_{k+1}(\bar{\mathbf{Z}}_{\ell h}|\mathbf{y}_{[k]}) - \nabla_{\mathbf{x}} \log \widehat{q}_{k+1}(\bar{\mathbf{Z}}_{\ell h}|\mathbf{y}_{[k]})\|_2^2] \\
& \quad + 2 \sum_{\ell=0}^{K-1} h \mathbb{E}_{\bar{\mathbf{Z}}_{\ell h}} [\|\nabla_{\mathbf{x}} \log \widehat{q}_{k+1}(\bar{\mathbf{Z}}_{\ell h}|\mathbf{y}_{[k]}) - \widehat{\mathbf{s}}_{k+1}(\bar{\mathbf{Z}}_{\ell h}, \mathbf{y}_{[k]})\|_2^2] \\
& \leq 2T \|\nabla_{\mathbf{x}} \log q_{k+1}(\cdot|\mathbf{y}_{[k]}) - \nabla_{\mathbf{x}} \log \widehat{q}_{k+1}(\cdot|\mathbf{y}_{[k]})\|_{L^\infty(\mathbb{R}^d)}^2 \\
& \quad + 2 \sum_{\ell=0}^{K-1} h \mathbb{E}_{\bar{\mathbf{Z}}_{\ell h}} [\|\nabla_{\mathbf{x}} \log \widehat{q}_{k+1}(\bar{\mathbf{Z}}_{\ell h}|\mathbf{y}_{[k]}) - \widehat{\mathbf{s}}_{k+1}(\bar{\mathbf{Z}}_{\ell h}, \mathbf{y}_{[k]})\|_2^2],
\end{aligned}$$

where the first inequality follows from Pinsker's inequality (Lemma H.5), the second inequality invokes Girsanov theorem (Chen et al., 2023), and the third inequality is due to the triangular inequality. This completes the proof. \square

C.2. Error of the posterior sampling and assimilation.

Proof of Theorem 3.3. Substituting Lemmas D.1, E.1, and F.1 into Lemma C.1

$$\begin{aligned}
(\varepsilon_{\text{TV}}^{k+1})^2 & \leq \frac{1}{2} \exp\left(-\frac{T}{5C_{\text{LSI}}}\right) \eta_{\chi}^2 + 70dC_{\text{LSI}}\lambda^2h + 64B^4D^4T(\varepsilon_{\text{TV}}^k)^2 \\
& \quad + 112C_{\text{LSI}}\sqrt{GB^3D^3}\eta_{\chi}\Delta + 32\sqrt{GB^3D^3}T\Delta,
\end{aligned}$$

where we used Lemma H.4. This completes the proof. \square

Proof of Corollary 3.4. A direct conclusion of Theorem 3.3. \square

Proof of Theorem 3.5. According to Corollary 3.4, we have that for each $k \in \mathbb{N}$,

$$(\text{C.4}) \quad (\varepsilon_{\text{TV}}^{k+1})^2 \leq C_{\text{LSI}}^k (CB^4D^4)^k \log^k\left(\frac{\eta_{\chi}^2}{\varepsilon^2}\right) \{(\varepsilon_{\text{TV}}^1)^2 + (k-1)\varepsilon^2\}.$$

On the other hand, if the terminal time T , the step size h , and the score matching error Δ are set, respectively, as

$$T = \Theta\left(C_{\text{LSI}} \log\left(\frac{\eta_{\chi}^2}{\varepsilon^2}\right)\right), \quad h = \Theta\left(\frac{\varepsilon^2}{dC_{\text{LSI}}\lambda^2}\right), \quad \Delta = \Theta\left(\frac{\varepsilon^2}{\sqrt{GB^3D^3}(T + C_{\text{LSI}}\eta_{\chi})}\right),$$

it follows from Lemma G.1 that

$$(\text{C.5}) \quad (\varepsilon_{\text{TV}}^1)^2 \lesssim C_{\text{LSI}} \log\left(\frac{\eta_{\chi}^2}{\varepsilon^2}\right) \|\nabla_{\mathbf{x}} \log q_1 - \nabla_{\mathbf{x}} \log \widehat{q}_1\|_{L^\infty(\mathbb{R}^d)}^2 + \varepsilon^2.$$

Combining (C.4) and (C.5) completes the proof. \square

APPENDIX D. CONVERGENCE OF LANGEVIN MONTE CARLO

In this section, we aim to analyze the convergence of the Langevin Monte Carlo

$$\text{TV}^2(\pi_{k+1}(\cdot|\mathbf{y}_{[k+1]}), \bar{\pi}_{k+1}^T(\cdot|\mathbf{y}_{[k+1]})).$$

Indeed, we provide a stronger convergence result in χ^2 -divergence rather than the TV distance, since bounding the error of the score matching (Appendix F) also requires the convergence results in χ^2 -divergence.

Lemma D.1. *Suppose Assumptions 1 and 2 hold. Then*

$$\chi^2(\bar{\pi}_{k+1}^T(\cdot|\mathbf{y}_{[k+1]})\|\pi_{k+1}(\cdot|\mathbf{y}_{[k+1]})) \leq \exp\left(-\frac{T}{5C_{\text{LSI}}}\right)\eta_\chi^2 + 140dC_{\text{LSI}}\lambda^2h,$$

where $T = Kh$, and the step size $h > 0$ satisfies $400dC_{\text{LSI}}\lambda^2h \leq 1$.

Remark D.2. The proof of Lemma D.1 is inspired by Lee et al. (2022, Theorem 2.1), and Chewi et al. (2024, Theorem 4). We show the proof in this section for the sake of completeness. The first term in Lemma D.1 converges to zero exponentially as the time T increases, which corresponds to the convergence of the Langevin diffusion (C.1). The second term is linear with respect to the step size h , induced by the Euler-Maruyama approximation.

Recall the Langevin Monte Carlo (C.2). For each $0 \leq \ell \leq K-1$ and $\ell h \leq t \leq (\ell+1)h$,

$$\begin{aligned} \bar{\mathbf{Z}}_t &= \bar{\mathbf{Z}}_{\ell h} + \int_{\ell h}^t \nabla_{\mathbf{x}} \log \pi_{k+1}(\bar{\mathbf{Z}}_{\ell h}|\mathbf{y}_{[k+1]}) ds + \sqrt{2} \int_{\ell h}^t d\mathbf{B}_s \\ (D.1) \quad &= \bar{\mathbf{Z}}_{\ell h} + (t - \ell h) \nabla_{\mathbf{x}} \log \pi_{k+1}(\bar{\mathbf{Z}}_{\ell h}|\mathbf{y}_{[k+1]}) + \sqrt{2}(\mathbf{B}_t - \mathbf{B}_{\ell h}), \end{aligned}$$

where $\mathbf{B}_t - \mathbf{B}_{\ell h} \sim N(0, (t - \ell h)\mathbf{I}_d)$ is independent of $\bar{\mathbf{Z}}_{\ell h}$.

D.1. Differential inequality for the chi-squared divergence. The most crucial recipe in the proof of Lemma D.1 is the following differential inequality for the χ^2 -divergence, which is inspired by Chewi et al. (2024, Theorem 4) and Lee et al. (2022, Theorem 4.2).

Before proceeding, we introduce some notations and properties. Define the Radon-Nikodym derivative of $\bar{\pi}_{k+1}^t$ with respect to π_{k+1}

$$(D.2) \quad \phi_{k+1}^t(\mathbf{x}|\mathbf{y}_{[k+1]}) := \frac{\bar{\pi}_{k+1}^t(\mathbf{x}|\mathbf{y}_{[k+1]})}{\pi_{k+1}(\mathbf{x}|\mathbf{y}_{[k+1]})}, \quad \mathbf{x} \in \mathbb{R}^d.$$

Apparently, we find

$$(D.3) \quad \mathbb{E}_{\mathbf{Z}}[\phi_{k+1}^t(\mathbf{Z}|\mathbf{y}_{[k+1]})^2] = \mathbb{E}_{\bar{\mathbf{Z}}_t}[\phi_{k+1}^t(\bar{\mathbf{Z}}_t|\mathbf{y}_{[k+1]})].$$

Further, we define

$$(D.4) \quad \psi_{k+1}^t(\mathbf{x}|\mathbf{y}_{[k+1]}) := \frac{\phi_{k+1}^t(\mathbf{x}|\mathbf{y}_{[k+1]})}{\mathbb{E}_{\mathbf{Z}}[\phi_{k+1}^t(\mathbf{Z}|\mathbf{y}_{[k+1]})^2]}, \quad \mathbf{x} \in \mathbb{R}^d.$$

Then it is straightforward that

$$\begin{aligned} \mathbb{E}_{\bar{\mathbf{Z}}_t}[\psi_{k+1}^t(\bar{\mathbf{Z}}_t|\mathbf{y}_{[k+1]})] &= \int \psi_{k+1}^t(\mathbf{x}|\mathbf{y}_{[k+1]}) \phi_{k+1}^t(\mathbf{x}|\mathbf{y}_{[k+1]}) \pi_{k+1}(\mathbf{x}|\mathbf{y}_{[k+1]}) d\mathbf{x} \\ (D.5) \quad &= \int \frac{\phi_{k+1}^t(\mathbf{x}|\mathbf{y}_{[k+1]})^2}{\mathbb{E}_{\mathbf{Z}}[\phi_{k+1}^t(\mathbf{Z}|\mathbf{y}_{[k+1]})^2]} \pi_{k+1}(\mathbf{x}|\mathbf{y}_{[k+1]}) d\mathbf{x} = 1. \end{aligned}$$

The following lemmas shows that the derivative of the χ^2 -divergence can be bounded by two parts: Dirichlet energy and the discretization error.

Lemma D.3. For each $\ell h \leq t \leq (\ell + 1)h$, it holds that

$$\begin{aligned} & \frac{d}{dt} \chi^2(\bar{\pi}_{k+1}^t(\cdot|\mathbf{y}_{[k+1]})\|\pi_{k+1}(\cdot|\mathbf{y}_{[k+1]})) \\ & \leq - \underbrace{\mathbb{E}_{\mathbf{Z}}[\|\nabla_{\mathbf{x}}\phi_{k+1}^t(\mathbf{Z}|\mathbf{y}_{[k+1]})\|_2^2]}_{\text{Dirichlet energy}} \\ & \quad + \underbrace{\mathbb{E}_{\mathbf{Z}}[\phi_{k+1}^t(\mathbf{Z}|\mathbf{y}_{[k+1]})^2]\mathbb{E}_{(\bar{\mathbf{Z}}_{\ell h}, \bar{\mathbf{Z}}_t)}[\|\mathbf{e}_{k+1}(\bar{\mathbf{Z}}_{\ell h}, \bar{\mathbf{Z}}_t|\mathbf{y}_{[k+1]})\|_2^2\psi_{k+1}^t(\bar{\mathbf{Z}}_t|\mathbf{y}_{[k+1]})]}_{\text{discretization error}} \end{aligned}$$

where the pointwise discretization error is defined as

$$\mathbf{e}_{k+1}(\mathbf{x}_{\ell h}, \mathbf{x}|\mathbf{y}_{[k+1]}) := \nabla_{\mathbf{x}} \log \pi_{k+1}(\mathbf{x}_{\ell h}|\mathbf{y}_{[k+1]}) - \nabla_{\mathbf{x}} \log \pi_{k+1}(\mathbf{x}|\mathbf{y}_{[k+1]}).$$

Here the expectation $\mathbb{E}_{\mathbf{Z}}[\cdot]$ is taken with respect to $\mathbf{Z} \sim \pi_{k+1}(\cdot|\mathbf{y}_{[k+1]})$, and the expectation $\mathbb{E}_{(\bar{\mathbf{Z}}_{\ell h}, \bar{\mathbf{Z}}_t)}[\cdot]$ is taken with respect to $(\bar{\mathbf{Z}}_{\ell h}, \bar{\mathbf{Z}}_t) \sim \bar{\pi}_{k+1}^{\ell h, t}(\cdot|\mathbf{y}_{[k+1]})$.

Remark D.4. According to [Vempala and Wibisono \(2019, Lemma 6\)](#), the law of the Langevin diffusion [\(C.1\)](#) $\pi_{k+1}^t(\cdot|\mathbf{y}_{[k+1]})$ satisfies

$$\frac{d}{dt} \chi^2(\pi_{k+1}^t(\cdot|\mathbf{y}_{[k+1]})\|\pi_{k+1}(\cdot|\mathbf{y}_{[k+1]})) \leq -2\mathbb{E}_{\mathbf{Z}}[\|\nabla_{\mathbf{x}}\phi_{k+1}^t(\mathbf{Z}|\mathbf{y}_{[k+1]})\|_2^2],$$

which can also be derived from [\(D.8\)](#). Compared with this inequality, the differential inequality of the Langevin Monte Carlo in [Lemma D.3](#) has an additional term known as the discretization error.

We first introduce the Fokker-Planck equation associated to the Langevin Monte Carlo [\(C.2\)](#), which has appeared in [Chewi et al. \(2024, Proposition 17\)](#).

Lemma D.5. For each $\ell h \leq t \leq (\ell + 1)h$, the law of Langevin Monte Carlo [\(C.2\)](#) satisfies the Fokker-Planck equation

$$\frac{\partial}{\partial t} \bar{\pi}_{k+1}^t(\mathbf{x}|\mathbf{y}_{[k+1]}) = -\nabla_{\mathbf{x}} \cdot (\bar{\pi}_{k+1}^t(\mathbf{x}|\mathbf{y}_{[k+1]})\bar{\mathbf{b}}_{k+1}^t(\mathbf{x}|\mathbf{y}_{[k+1]})) + \Delta_{\mathbf{x}} \bar{\pi}_{k+1}^t(\mathbf{x}|\mathbf{y}_{[k+1]}),$$

where the drift term is given as

$$(D.6) \quad \bar{\mathbf{b}}_{k+1}^t(\mathbf{x}|\mathbf{y}_{[k+1]}) = \mathbb{E}[\nabla_{\mathbf{x}} \log \pi_{k+1}(\bar{\mathbf{Z}}_{\ell h}|\mathbf{y}_{[k+1]})|\bar{\mathbf{Z}}_t = \mathbf{x}, \mathbf{Y}^{[k+1]} = \mathbf{y}_{[k+1]}].$$

Proof of Lemma D.5. Let $\bar{\pi}_{k+1}^{t|\ell h}(\cdot|\mathbf{x}_{\ell h}, \mathbf{y}_{[k+1]})$ denote the conditional distribution of $\bar{\mathbf{Z}}_t$ given $\bar{\mathbf{Z}}_{\ell h} = \mathbf{x}_{\ell h}$ and $\mathbf{Y}^{[k+1]} = \mathbf{y}_{[k+1]}$, which satisfies the Fokker-Planck equation ([Pavliotis, 2014, Theorem 2.2](#))

$$(D.7) \quad \begin{aligned} & \frac{\partial}{\partial t} \bar{\pi}_{k+1}^{t|\ell h}(\mathbf{x}|\mathbf{x}_{\ell h}, \mathbf{y}_{[k+1]}) \\ & = \nabla_{\mathbf{x}} \cdot \left(-\bar{\pi}_{k+1}^{t|\ell h}(\mathbf{x}|\mathbf{x}_{\ell h}, \mathbf{y}_{[k+1]})\nabla_{\mathbf{x}} \log \pi_{k+1}(\mathbf{x}_{\ell h}|\mathbf{y}_{[k+1]}) \right) + \Delta_{\mathbf{x}} \bar{\pi}_{k+1}^{t|\ell h}(\mathbf{x}|\mathbf{x}_{\ell h}, \mathbf{y}_{[k+1]}). \end{aligned}$$

Multiplying both sides of the equality by $\bar{\pi}_{k+1}^{\ell h}(\mathbf{x}_{\ell h}|\mathbf{y}_{[k+1]})$ and then integrating with respect to $\mathbf{x}_{\ell h} \in \mathbb{R}^d$ deduces

$$\begin{aligned}
& \frac{\partial}{\partial t} \bar{\pi}_{k+1}^t(\mathbf{x}|\mathbf{y}_{[k+1]}) \\
&= \frac{\partial}{\partial t} \int \bar{\pi}_{k+1}^{t|\ell h}(\mathbf{x}|\mathbf{x}_{\ell h}, \mathbf{y}_{[k+1]}) \bar{\pi}_{k+1}^{\ell h}(\mathbf{x}_{\ell h}|\mathbf{y}_{[k+1]}) d\mathbf{x}_{\ell h} \\
&= \int \frac{\partial}{\partial t} \bar{\pi}_{k+1}^{t|\ell h}(\mathbf{x}|\mathbf{x}_{\ell h}, \mathbf{y}_{[k+1]}) \bar{\pi}_{k+1}^{\ell h}(\mathbf{x}_{\ell h}|\mathbf{y}_{[k+1]}) d\mathbf{x}_{\ell h} \\
&= - \int \nabla_{\mathbf{x}} \cdot \left(\bar{\pi}_{k+1}^{t|\ell h}(\mathbf{x}|\mathbf{x}_{\ell h}, \mathbf{y}_{[k+1]}) \nabla_{\mathbf{x}} \log \pi_{k+1}(\mathbf{x}_{\ell h}|\mathbf{y}_{[k+1]}) \right) \bar{\pi}_{k+1}^{\ell h}(\mathbf{x}_{\ell h}|\mathbf{y}_{[k+1]}) d\mathbf{x}_{\ell h} \\
&\quad + \int \Delta_{\mathbf{x}} \bar{\pi}_{k+1}^{t|\ell h}(\mathbf{x}|\mathbf{x}_{\ell h}, \mathbf{y}_{[k+1]}) \bar{\pi}_{k+1}^{\ell h}(\mathbf{x}_{\ell h}|\mathbf{y}_{[k+1]}) d\mathbf{x}_{\ell h} \\
&= - \int \nabla_{\mathbf{x}} \cdot \left(\bar{\pi}_{k+1}^{t,\ell h}(\mathbf{x}, \mathbf{x}_{\ell h}|\mathbf{y}_{[k+1]}) \nabla_{\mathbf{x}} \log \pi_{k+1}(\mathbf{x}_{\ell h}|\mathbf{y}_{[k+1]}) \right) d\mathbf{x}_{\ell h} \\
&\quad + \int \Delta_{\mathbf{x}} \bar{\pi}_{k+1}^{t,\ell h}(\mathbf{x}, \mathbf{x}_{\ell h}|\mathbf{y}_{[k+1]}) d\mathbf{x}_{\ell h} \\
&= - \nabla_{\mathbf{x}} \cdot \left(\bar{\pi}_{k+1}^t(\mathbf{x}|\mathbf{y}_{[k+1]}) \int \bar{\pi}_{k+1}^{\ell h|t}(\mathbf{x}_{\ell h}|\mathbf{x}, \mathbf{y}_{[k+1]}) \nabla_{\mathbf{x}} \log \pi_{k+1}(\mathbf{x}_{\ell h}|\mathbf{y}_{[k+1]}) d\mathbf{x}_{\ell h} \right) \\
&\quad + \Delta_{\mathbf{x}} \bar{\pi}_{k+1}^t(\mathbf{x}|\mathbf{y}_{[k+1]}) \int \bar{\pi}_{k+1}^{\ell h|t}(\mathbf{x}_{\ell h}|\mathbf{x}, \mathbf{y}_{[k+1]}) d\mathbf{x}_{\ell h} \\
&= - \nabla_{\mathbf{x}} \cdot \left(\bar{\pi}_{k+1}^t(\mathbf{x}|\mathbf{y}_{[k+1]}) \bar{\mathbf{b}}_{k+1}^t(\mathbf{x}|\mathbf{y}_{[k+1]}) \right) + \Delta_{\mathbf{x}} \bar{\pi}_{k+1}^t(\mathbf{x}|\mathbf{y}_{[k+1]}),
\end{aligned}$$

where the first equality holds from Chapman-Kolmogorov identity, the third equality follows from (D.7), and the last equality invokes (D.6). This completes the proof. \square

Now we are ready to prove Lemma D.3.

Proof of Lemma D.3. According to the definition of the χ^2 -divergence, we have

$$\begin{aligned}
& \frac{d}{dt} \chi^2(\bar{\pi}_{k+1}^t(\cdot|\mathbf{y}_{[k+1]}) || \pi_{k+1}(\cdot|\mathbf{y}_{[k+1]})) \\
&= 2 \int \frac{\partial \bar{\pi}_{k+1}^t}{\partial t}(\mathbf{x}|\mathbf{y}_{[k+1]}) \frac{\bar{\pi}_{k+1}^t(\mathbf{x}|\mathbf{y}_{[k+1]})}{\pi_{k+1}(\mathbf{x}|\mathbf{y}_{[k+1]})} d\mathbf{x} \\
&= 2 \int \nabla_{\mathbf{x}} \cdot \left(- \bar{\pi}_{k+1}^t(\mathbf{x}|\mathbf{y}_{[k+1]}) \bar{\mathbf{b}}_{k+1}^t(\mathbf{x}|\mathbf{y}_{[k+1]}) \right) \phi_{k+1}^t(\mathbf{x}|\mathbf{y}_{[k+1]}) d\mathbf{x} \\
&\quad + 2 \int \Delta_{\mathbf{x}} \bar{\pi}_{k+1}^t(\mathbf{x}|\mathbf{y}_{[k+1]}) \phi_{k+1}^t(\mathbf{x}|\mathbf{y}_{[k+1]}) d\mathbf{x} \\
&= 2 \underbrace{\mathbb{E}_{\bar{\mathbf{Z}}_t} \left[\left(\bar{\mathbf{b}}_{k+1}^t - \nabla_{\mathbf{x}} \log \pi_{k+1} \right) (\bar{\mathbf{Z}}_t|\mathbf{y}_{[k+1]}) \cdot \nabla_{\mathbf{x}} \phi_{k+1}^t(\bar{\mathbf{Z}}_t|\mathbf{y}_{[k+1]}) \right]}_{(*)} \\
(D.8) \quad & - 2 \mathbb{E}_{\mathbf{Z}} \left[\|\nabla_{\mathbf{x}} \phi_{k+1}^t(\mathbf{Z}|\mathbf{y}_{[k+1]})\|_2^2 \right],
\end{aligned}$$

where the first inequality invokes the chain rule, the second equality holds from Fokker-Planck equation (Lemma D.5) and (D.2), and the last equation used the Green's formula and Lemma H.9. Here the expectation $\mathbb{E}_{\bar{\mathbf{Z}}_t}[\cdot]$ is taken with respect to $\bar{\mathbf{Z}}_t \sim \bar{\pi}_{k+1}^t(\cdot|\mathbf{y}_{[k+1]})$, while the expectation $\mathbb{E}_{\mathbf{Z}}[\cdot]$ is taken with respect to $\mathbf{Z} \sim \pi_{k+1}(\cdot|\mathbf{y}_{[k+1]})$. Now it remains to estimate

the term (\star) in (D.8). Notice that

$$\begin{aligned}
& \mathbb{E}_{\bar{\mathbf{Z}}_t} [\bar{\mathbf{b}}_{k+1}^t(\bar{\mathbf{Z}}_t | \mathbf{y}_{[k+1]}) \cdot \nabla_{\mathbf{x}} \phi_{k+1}^t(\bar{\mathbf{Z}}_t | \mathbf{y}_{[k+1]})] \\
&= \int \bar{\pi}_{k+1}^t(\mathbf{x} | \mathbf{y}_{[k+1]}) \bar{\mathbf{b}}_{k+1}^t(\mathbf{x} | \mathbf{y}_{[k+1]}) \cdot \nabla_{\mathbf{x}} \phi_{k+1}^t(\mathbf{x} | \mathbf{y}_{[k+1]}) \, d\mathbf{x} \\
&= \iint \bar{\pi}_{k+1}^{\ell h, t}(\mathbf{x}_{\ell h}, \mathbf{x} | \mathbf{y}_{[k+1]}) \nabla_{\mathbf{x}} \log \pi_{k+1}(\mathbf{x}_{\ell h} | \mathbf{y}_{[k+1]}) \cdot \nabla_{\mathbf{x}} \phi_{k+1}^t(\mathbf{x} | \mathbf{y}_{[k+1]}) \, d\mathbf{x}_{\ell h} \, d\mathbf{x} \\
&= \mathbb{E}_{(\bar{\mathbf{Z}}_{\ell h}, \bar{\mathbf{Z}}_t)} [\nabla_{\mathbf{x}} \log \pi_{k+1}(\bar{\mathbf{Z}}_{\ell h} | \mathbf{y}_{[k+1]}) \cdot \nabla_{\mathbf{x}} \phi_{k+1}^t(\bar{\mathbf{Z}}_t | \mathbf{y}_{[k+1]})],
\end{aligned}$$

where we used the definition of $\bar{\mathbf{b}}_{k+1}^t(\mathbf{x} | \mathbf{y}_{[k+1]})$ as (D.6). As a consequence,

$$\begin{aligned}
(\star) &= \mathbb{E}_{\bar{\mathbf{Z}}_t} [(\bar{\mathbf{b}}_{k+1}^t - \nabla_{\mathbf{x}} \log \pi_{k+1})(\bar{\mathbf{Z}}_t | \mathbf{y}_{[k+1]}) \cdot \nabla_{\mathbf{x}} \phi_{k+1}^t(\bar{\mathbf{Z}}_t | \mathbf{y}_{[k+1]})] \\
&= \mathbb{E}_{(\bar{\mathbf{Z}}_{\ell h}, \bar{\mathbf{Z}}_t)} [\mathbf{e}_{k+1}(\bar{\mathbf{Z}}_{\ell h}, \bar{\mathbf{Z}}_t | \mathbf{y}_{[k+1]}) \cdot \nabla_{\mathbf{x}} \phi_{k+1}^t(\bar{\mathbf{Z}}_t | \mathbf{y}_{[k+1]})] \\
&= \mathbb{E}_{(\bar{\mathbf{Z}}_{\ell h}, \bar{\mathbf{Z}}_t)} \left[\mathbf{e}_{k+1}(\bar{\mathbf{Z}}_{\ell h}, \bar{\mathbf{Z}}_t | \mathbf{y}_{[k+1]}) \sqrt{\phi_{k+1}^t(\bar{\mathbf{Z}}_t | \mathbf{y}_{[k+1]})} \cdot \frac{\nabla_{\mathbf{x}} \phi_{k+1}^t(\bar{\mathbf{Z}}_t | \mathbf{y}_{[k+1]})}{\sqrt{\phi_{k+1}^t(\bar{\mathbf{Z}}_t | \mathbf{y}_{[k+1]})}} \right] \\
&\leq \mathbb{E}_{(\bar{\mathbf{Z}}_{\ell h}, \bar{\mathbf{Z}}_t)}^{\frac{1}{2}} [\|\mathbf{e}_{k+1}(\bar{\mathbf{Z}}_{\ell h}, \bar{\mathbf{Z}}_t | \mathbf{y}_{[k+1]})\|_2^2 \phi_{k+1}^t(\bar{\mathbf{Z}}_t | \mathbf{y}_{[k+1]})] \mathbb{E}_{\mathbf{Z}}^{\frac{1}{2}} [\|\nabla_{\mathbf{x}} \phi_{k+1}^t(\mathbf{Z} | \mathbf{y}_{[k+1]})\|_2^2] \\
&\leq \frac{1}{2} \mathbb{E}_{(\bar{\mathbf{Z}}_{\ell h}, \bar{\mathbf{Z}}_t)} [\|\mathbf{e}_{k+1}(\bar{\mathbf{Z}}_{\ell h}, \bar{\mathbf{Z}}_t | \mathbf{y}_{[k+1]})\|_2^2 \phi_{k+1}^t(\bar{\mathbf{Z}}_t | \mathbf{y}_{[k+1]})] \\
&\quad + \frac{1}{2} \mathbb{E}_{\mathbf{Z}} [\|\nabla_{\mathbf{x}} \phi_{k+1}^t(\mathbf{Z} | \mathbf{y}_{[k+1]})\|_2^2] \\
&= \frac{1}{2} \mathbb{E}_{\mathbf{Z}} [\phi_{k+1}^t(\mathbf{Z} | \mathbf{y}_{[k+1]})^2] \mathbb{E}_{(\bar{\mathbf{Z}}_{\ell h}, \bar{\mathbf{Z}}_t)} [\|\mathbf{e}_{k+1}(\bar{\mathbf{Z}}_{\ell h}, \bar{\mathbf{Z}}_t | \mathbf{y}_{[k+1]})\|_2^2 \psi_{k+1}^t(\bar{\mathbf{Z}}_t | \mathbf{y}_{[k+1]})] \\
\text{(D.9)} \quad &+ \frac{1}{2} \mathbb{E}_{\mathbf{Z}} [\|\nabla_{\mathbf{x}} \phi_{k+1}^t(\mathbf{Z} | \mathbf{y}_{[k+1]})\|_2^2],
\end{aligned}$$

where the first inequality invokes the Cauchy-Schwarz inequality, the second inequality follows from $ab \leq (a^2 + b^2)/2$. Substituting (D.9) into (D.8) completes the proof. \square

D.2. Dirichlet energy and chi-squared divergence. We relate the Dirichlet energy to χ^2 -divergence by the following lemma.

Lemma D.6. *Suppose Assumption 2 holds. Then*

$$\frac{1}{2C_{\text{LSI}}} \chi^2(\bar{\pi}_{k+1}^t(\cdot | \mathbf{y}_{[k+1]}) \| \pi_{k+1}(\cdot | \mathbf{y}_{[k+1]})) \leq \mathbb{E}_{\mathbf{Z}} [\|\nabla_{\mathbf{x}} \phi_{k+1}^t(\mathbf{Z} | \mathbf{y}_{[k+1]})\|_2^2].$$

Proof of Lemma D.6. A direct conclusion of Lemma H.10. \square

D.3. Discretization error. The main results for the discretization error is stated as follows.

Lemma D.7. *Suppose Assumptions 1 and 2 hold. Then for each $\ell h \leq t \leq (\ell + 1)h$,*

$$\begin{aligned}
& \mathbb{E}_{\mathbf{Z}} [\phi_{k+1}^t(\mathbf{Z} | \mathbf{y}_{[k+1]})^2] \mathbb{E}_{(\bar{\mathbf{Z}}_{\ell h}, \bar{\mathbf{Z}}_t)} [\|\mathbf{e}_{k+1}(\bar{\mathbf{Z}}_{\ell h}, \bar{\mathbf{Z}}_t | \mathbf{y}_{[k+1]})\|_2^2 \psi_{k+1}^t(\bar{\mathbf{Z}}_t | \mathbf{y}_{[k+1]})] \\
& \leq 80C_{\text{LSI}} \lambda^2 (t - \ell h) \mathbb{E}_{\mathbf{Z}} [\|\nabla_{\mathbf{x}} \phi_{k+1}^t(\mathbf{Z} | \mathbf{y}_{[k+1]})\|_2^2] + 20d\lambda^2 (t - \ell h) \mathbb{E}_{\mathbf{Z}} [\phi_{k+1}^t(\mathbf{Z} | \mathbf{y}_{[k+1]})^2],
\end{aligned}$$

where the step size $h > 0$ satisfies $4\lambda h \leq 1$.

To verify Lemma D.7, we provide some auxiliary lemmas.

Lemma D.8. *Suppose Assumption 1 holds. Then for each $\ell h \leq t \leq (\ell + 1)h$,*

$$\begin{aligned} & \mathbb{E}_{(\bar{\mathbf{Z}}_{\ell h}, \bar{\mathbf{Z}}_t)} \left[\|\mathbf{e}_{k+1}(\bar{\mathbf{Z}}_{\ell h}, \bar{\mathbf{Z}}_t | \mathbf{y}_{[k+1]})\|_2^2 \psi_{k+1}^t(\bar{\mathbf{Z}}_t | \mathbf{y}_{[k+1]}) \right] \\ & \leq 8\lambda^2 (t - \ell h)^2 \mathbb{E}_{\bar{\mathbf{Z}}_t} \left[\|\nabla_{\mathbf{x}} \log \pi_{k+1}(\bar{\mathbf{Z}}_t | \mathbf{y}_{[k+1]})\|_2^2 \psi_{k+1}^t(\bar{\mathbf{Z}}_t | \mathbf{y}_{[k+1]}) \right] \\ & \quad + 6\lambda^2 \mathbb{E}_{(\mathbf{B}_{\ell h}, \mathbf{B}_t, \bar{\mathbf{Z}}_t)} \left[\|\mathbf{B}_t - \mathbf{B}_{\ell h}\|_2^2 \psi_{k+1}^t(\bar{\mathbf{Z}}_t | \mathbf{y}_{[k+1]}) \right], \end{aligned}$$

where the step size $h > 0$ satisfies $4\lambda h \leq 1$.

Proof of Lemma D.8. Recall the solution to the Langevin Monte Carlo (D.1), which implies

$$(D.10) \quad \|\bar{\mathbf{Z}}_t - \bar{\mathbf{Z}}_{\ell h}\|_2^2 \leq 2(t - \ell h)^2 \|\nabla_{\mathbf{x}} \log \pi_{k+1}(\bar{\mathbf{Z}}_{\ell h} | \mathbf{y}_{[k+1]})\|_2^2 + 4\|\mathbf{B}_t - \mathbf{B}_{\ell h}\|_2^2,$$

where the first inequality invokes the triangular inequality, and last inequality holds from the fact $\ell h \leq t \leq (\ell + 1)h$. According to Assumption 1, we have

$$\begin{aligned} & \|\nabla_{\mathbf{x}} \log \pi_{k+1}(\bar{\mathbf{Z}}_t | \mathbf{y}_{[k+1]}) - \nabla_{\mathbf{x}} \log \pi_{k+1}(\bar{\mathbf{Z}}_{\ell h} | \mathbf{y}_{[k+1]})\|_2^2 \\ & \leq \lambda^2 \|\bar{\mathbf{Z}}_t - \bar{\mathbf{Z}}_{\ell h}\|_2^2 \\ (D.11) \quad & \leq 2\lambda^2 (t - \ell h)^2 \|\nabla_{\mathbf{x}} \log \pi_{k+1}(\bar{\mathbf{Z}}_{\ell h} | \mathbf{y}_{[k+1]})\|_2^2 + 4\lambda^2 \|\mathbf{B}_t - \mathbf{B}_{\ell h}\|_2^2, \end{aligned}$$

where the last inequality used (D.1). As a consequence, for each step size h with $4\lambda h \leq 1$,

$$\begin{aligned} & \|\nabla_{\mathbf{x}} \log \pi_{k+1}(\bar{\mathbf{Z}}_{\ell h} | \mathbf{y}_{[k+1]})\|_2^2 \\ & \leq 2\|\nabla_{\mathbf{x}} \log \pi_{k+1}(\bar{\mathbf{Z}}_t | \mathbf{y}_{[k+1]}) - \nabla_{\mathbf{x}} \log \pi_{k+1}(\bar{\mathbf{Z}}_{\ell h} | \mathbf{y}_{[k+1]})\|_2^2 + 2\|\nabla_{\mathbf{x}} \log \pi_{k+1}(\bar{\mathbf{Z}}_t | \mathbf{y}_{[k+1]})\|_2^2 \\ & \leq 4\lambda^2 (t - \ell h)^2 \|\nabla_{\mathbf{x}} \log \pi_{k+1}(\bar{\mathbf{Z}}_{\ell h} | \mathbf{y}_{[k+1]})\|_2^2 + 8\lambda^2 \|\mathbf{B}_t - \mathbf{B}_{\ell h}\|_2^2 + 2\|\nabla_{\mathbf{x}} \log \pi_{k+1}(\bar{\mathbf{Z}}_t | \mathbf{y}_{[k+1]})\|_2^2 \\ & \leq \frac{1}{4} \|\nabla_{\mathbf{x}} \log \pi_{k+1}(\bar{\mathbf{Z}}_{\ell h} | \mathbf{y}_{[k+1]})\|_2^2 + 8\lambda^2 \|\mathbf{B}_t - \mathbf{B}_{\ell h}\|_2^2 + 2\|\nabla_{\mathbf{x}} \log \pi_{k+1}(\bar{\mathbf{Z}}_t | \mathbf{y}_{[k+1]})\|_2^2, \end{aligned}$$

where the first inequality follows from the triangular inequality. Rearranging this inequality yields

$$(D.12) \quad \begin{aligned} & \|\nabla_{\mathbf{x}} \log \pi_{k+1}(\bar{\mathbf{Z}}_{\ell h} | \mathbf{y}_{[k+1]})\|_2^2 \\ & \leq 16\lambda^2 \|\mathbf{B}_t - \mathbf{B}_{\ell h}\|_2^2 + 4\|\nabla_{\mathbf{x}} \log \pi_{k+1}(\bar{\mathbf{Z}}_t | \mathbf{y}_{[k+1]})\|_2^2. \end{aligned}$$

Then substituting (D.12) into (D.11) yields

$$(D.13) \quad \begin{aligned} & \|\nabla_{\mathbf{x}} \log \pi_{k+1}(\bar{\mathbf{Z}}_t | \mathbf{y}_{[k+1]}) - \nabla_{\mathbf{x}} \log \pi_{k+1}(\bar{\mathbf{Z}}_{\ell h} | \mathbf{y}_{[k+1]})\|_2^2 \\ & \leq 8\lambda^2 (t - \ell h)^2 \|\nabla_{\mathbf{x}} \log \pi_{k+1}(\bar{\mathbf{Z}}_t | \mathbf{y}_{[k+1]})\|_2^2 + \{32\lambda^4 h^2 + 4\lambda^2\} \|\mathbf{B}_t - \mathbf{B}_{\ell h}\|_2^2 \\ & \leq 8\lambda^2 (t - \ell h)^2 \|\nabla_{\mathbf{x}} \log \pi_{k+1}(\bar{\mathbf{Z}}_t | \mathbf{y}_{[k+1]})\|_2^2 + 6\lambda^2 \|\mathbf{B}_t - \mathbf{B}_{\ell h}\|_2^2, \end{aligned}$$

where we used the inequality $4\lambda h \leq 1$. Multiplying both sides of (D.13) by ψ_{k+1}^t and taking expectation complete the proof. \square

We bound the first term in Lemma D.7 by the following lemma, which is based on Chewi et al. (2024, Lemma 20).

Lemma D.9. *Suppose Assumption 1 holds. Then for each $\ell h \leq t \leq (\ell + 1)h$,*

$$\begin{aligned} & \mathbb{E}_{\bar{\mathbf{Z}}_t} \left[\|\nabla_{\mathbf{x}} \log \pi_{k+1}(\bar{\mathbf{Z}}_t | \mathbf{y}_{[k+1]})\|_2^2 \psi_{k+1}^t(\bar{\mathbf{Z}}_t | \mathbf{y}_{[k+1]}) \right] \\ & \leq \frac{4\mathbb{E}_{\mathbf{Z}} [\|\nabla_{\mathbf{x}} \phi_{k+1}^t(\mathbf{Z} | \mathbf{y}_{[k+1]})\|_2^2]}{\mathbb{E}_{\mathbf{Z}} [\phi_{k+1}^t(\mathbf{Z} | \mathbf{y}_{[k+1]})^2]} + 2d\lambda, \end{aligned}$$

where the expectation $\mathbb{E}_{\mathbf{Z}}[\cdot]$ is taken with respect to $\mathbf{Z} \sim \pi_{k+1}(\cdot | \mathbf{y}_{[k+1]})$.

Proof of Lemma D.9. According to (D.5), we define a change of measure

$$\mu_{k+1}^t(\mathbf{x}|\mathbf{y}_{[k+1]}) := \psi_{k+1}^t(\mathbf{x}|\mathbf{y}_{[k+1]})\bar{\pi}_{k+1}^t(\mathbf{x}|\mathbf{y}_{[k+1]}).$$

Then it suffices to consider the expectation under this change of measures

$$\begin{aligned} & \mathbb{E}_{\tilde{\mathbf{Z}}_t} [\|\nabla_{\mathbf{x}} \log \pi_{k+1}(\tilde{\mathbf{Z}}_t|\mathbf{y}_{[k+1]})\|_2^2] \\ &= \mathbb{E}_{\tilde{\mathbf{Z}}_t} [\|\nabla_{\mathbf{x}} \log \pi_{k+1}(\tilde{\mathbf{Z}}_t|\mathbf{y}_{[k+1]})\|_2^2 \psi_{k+1}^t(\tilde{\mathbf{Z}}_t|\mathbf{y}_{[k+1]})], \end{aligned}$$

where $\tilde{\mathbf{Z}}_t$ is a random variable with probability density $\mu_{k+1}^t(\cdot|\mathbf{y}_{[k+1]})$. We first verify that

$$\begin{aligned} & \mathbb{E}_{\tilde{\mathbf{Z}}_t} [\|\nabla_{\mathbf{x}} \log \pi_{k+1}(\tilde{\mathbf{Z}}_t|\mathbf{y}_{[k+1]})\|_2^2] \\ (D.14) \quad & \leq \underbrace{\mathbb{E}_{\tilde{\mathbf{Z}}_t} [\Delta_{\mathbf{x}} \log \pi_{k+1}(\tilde{\mathbf{Z}}_t|\mathbf{y}_{[k+1]})]}_{(i)} + \underbrace{\mathbb{E}_{\mathbf{Z}} \left[\nabla_{\mathbf{x}} \log \pi_{k+1}(\mathbf{Z}|\mathbf{y}_{[k+1]}) \cdot \nabla_{\mathbf{x}} \frac{\mu_{k+1}^t(\mathbf{Z}|\mathbf{y}_{[k+1]})}{\pi_{k+1}(\mathbf{Z}|\mathbf{y}_{[k+1]})} \right]}_{(ii)}. \end{aligned}$$

Indeed, according to the Green's formula, we obtain

$$\begin{aligned} & \mathbb{E}_{\tilde{\mathbf{Z}}_t} [\Delta_{\mathbf{x}} \log \pi_{k+1}(\tilde{\mathbf{Z}}_t|\mathbf{y}_{[k+1]})] \\ &= \int \Delta_{\mathbf{x}} \log \pi_{k+1}(\mathbf{x}|\mathbf{y}_{[k+1]}) \frac{\mu_{k+1}^t(\mathbf{x}|\mathbf{y}_{[k+1]})}{\pi_{k+1}(\mathbf{x}|\mathbf{y}_{[k+1]})} \pi_{k+1}(\mathbf{x}|\mathbf{y}_{[k+1]}) \, d\mathbf{x} \\ &= - \int \nabla_{\mathbf{x}} \log \pi_{k+1}(\mathbf{x}|\mathbf{y}_{[k+1]}) \cdot \nabla_{\mathbf{x}} \left(\frac{\mu_{k+1}^t(\mathbf{x}|\mathbf{y}_{[k+1]})}{\pi_{k+1}(\mathbf{x}|\mathbf{y}_{[k+1]})} \pi_{k+1}(\mathbf{x}|\mathbf{y}_{[k+1]}) \right) \, d\mathbf{x} \\ &= - \mathbb{E}_{\mathbf{Z}} \left[\nabla_{\mathbf{x}} \log \pi_{k+1}(\mathbf{Z}|\mathbf{y}_{[k+1]}) \cdot \nabla_{\mathbf{x}} \frac{\mu_{k+1}^t(\mathbf{Z}|\mathbf{y}_{[k+1]})}{\pi_{k+1}(\mathbf{Z}|\mathbf{y}_{[k+1]})} \right] + \mathbb{E}_{\tilde{\mathbf{Z}}_t} [\|\nabla_{\mathbf{x}} \log \pi_{k+1}(\tilde{\mathbf{Z}}_t|\mathbf{y}_{[k+1]})\|_2^2]. \end{aligned}$$

For the term (i) in (D.15), it follows from Assumption 1 that

$$(D.15) \quad \mathbb{E}_{\tilde{\mathbf{Z}}_t} [\Delta_{\mathbf{x}} \log \pi_{k+1}(\tilde{\mathbf{Z}}_t|\mathbf{y}_{[k+1]})] \leq d\lambda.$$

For the term (ii) in (D.15), we find

$$\begin{aligned} & \mathbb{E}_{\mathbf{Z}} \left[\nabla_{\mathbf{x}} \log \pi_{k+1}(\mathbf{Z}|\mathbf{y}_{[k+1]}) \cdot \nabla_{\mathbf{x}} \frac{\mu_{k+1}^t(\mathbf{Z}|\mathbf{y}_{[k+1]})}{\pi_{k+1}(\mathbf{Z}|\mathbf{y}_{[k+1]})} \right] \\ &= 2\mathbb{E}_{\mathbf{Z}} \left[\nabla_{\mathbf{x}} \log \pi_{k+1}(\mathbf{Z}|\mathbf{y}_{[k+1]}) \sqrt{\frac{\mu_{k+1}^t(\mathbf{Z}|\mathbf{y}_{[k+1]})}{\pi_{k+1}(\mathbf{Z}|\mathbf{y}_{[k+1]})}} \cdot \nabla_{\mathbf{x}} \sqrt{\frac{\mu_{k+1}^t(\mathbf{Z}|\mathbf{y}_{[k+1]})}{\pi_{k+1}(\mathbf{Z}|\mathbf{y}_{[k+1]})}} \right] \\ &\leq \frac{1}{2} \mathbb{E}_{\mathbf{Z}} \left[\|\nabla_{\mathbf{x}} \log \pi_{k+1}(\mathbf{Z}|\mathbf{y}_{[k+1]})\|_2^2 \frac{\mu_{k+1}^t(\mathbf{Z}|\mathbf{y}_{[k+1]})}{\pi_{k+1}(\mathbf{Z}|\mathbf{y}_{[k+1]})} \right] + 2\mathbb{E}_{\mathbf{Z}} \left[\|\nabla_{\mathbf{x}} \sqrt{\frac{\mu_{k+1}^t(\mathbf{Z}|\mathbf{y}_{[k+1]})}{\pi_{k+1}(\mathbf{Z}|\mathbf{y}_{[k+1]})}}\|_2^2 \right] \\ (D.16) \quad &= \frac{1}{2} \mathbb{E}_{\tilde{\mathbf{Z}}_t} [\|\nabla_{\mathbf{x}} \log \pi_{k+1}(\tilde{\mathbf{Z}}_t|\mathbf{y}_{[k+1]})\|_2^2] + 2\mathbb{E}_{\mathbf{Z}} \left[\|\nabla_{\mathbf{x}} \sqrt{\frac{\mu_{k+1}^t(\mathbf{Z}|\mathbf{y}_{[k+1]})}{\pi_{k+1}(\mathbf{Z}|\mathbf{y}_{[k+1]})}}\|_2^2 \right], \end{aligned}$$

where the second equality holds from the chain rule, and the inequality follows from Young's inequality. Substituting (D.15) and (D.16) into (D.14) implies

$$(D.17) \quad \mathbb{E}_{\tilde{\mathbf{Z}}_t} [\|\nabla_{\mathbf{x}} \log \pi_{k+1}(\tilde{\mathbf{Z}}_t|\mathbf{y}_{[k+1]})\|_2^2] \leq 4\mathbb{E}_{\mathbf{Z}} \left[\|\nabla_{\mathbf{x}} \sqrt{\frac{\mu_{k+1}^t(\mathbf{Z}|\mathbf{y}_{[k+1]})}{\pi_{k+1}(\mathbf{Z}|\mathbf{y}_{[k+1]})}}\|_2^2 \right] + 2d\lambda.$$

Applying Lemma H.14 to (D.17) yields

$$\begin{aligned}
& \mathbb{E}_{\tilde{\mathbf{Z}}_t} \left[\|\nabla_{\mathbf{x}} \log \pi_{k+1}(\tilde{\mathbf{Z}}_t | \mathbf{y}_{[k+1]})\|_2^2 \right] \\
& \leq \mathbb{E}_{\tilde{\mathbf{Z}}_t} \left[\left\| \nabla_{\mathbf{x}} \log \frac{\mu_{k+1}^t(\tilde{\mathbf{Z}}_t | \mathbf{y}_{[k+1]})}{\pi_{k+1}(\tilde{\mathbf{Z}}_t | \mathbf{y}_{[k+1]})} \right\|_2^2 \right] + 2d\lambda \\
& = \mathbb{E}_{\tilde{\mathbf{Z}}_t} \left[\left\| \nabla_{\mathbf{x}} \log \frac{\mu_{k+1}^t(\tilde{\mathbf{Z}}_t | \mathbf{y}_{[k+1]})}{\pi_{k+1}(\tilde{\mathbf{Z}}_t | \mathbf{y}_{[k+1]})} \right\|_2^2 \psi_{k+1}^t(\tilde{\mathbf{Z}}_t | \mathbf{y}_{[k+1]}) \right] + 2d\lambda.
\end{aligned}$$

Finally, using Lemma H.15 completes the proof. \square

For the second term in Lemma D.7, we have the following result by a similar argument as Chewi et al. (2024, Lemma 19).

Lemma D.10. *Suppose Assumptions 1 and 2 hold. Then for each $\ell h \leq t \leq (\ell + 1)h$,*

$$\begin{aligned}
& \mathbb{E} \left[\|\mathbf{B}_t - \mathbf{B}_{\ell h}\|_2^2 \psi_{k+1}^t(\tilde{\mathbf{Z}}_t | \mathbf{y}_{[k+1]}) \right] \\
& \leq 3d(t - \ell h) + 8C_{\text{LSI}}(t - \ell h) \frac{\mathbb{E}_{\mathbf{Z}} \left[\|\nabla_{\mathbf{x}} \phi_{k+1}^t(\mathbf{Z} | \mathbf{y}_{[k+1]})\|_2^2 \right]}{\mathbb{E}_{\mathbf{Z}} \left[\phi_{k+1}^t(\mathbf{Z} | \mathbf{y}_{[k+1]})^2 \right]},
\end{aligned}$$

where the expectation $\mathbb{E}_{\mathbf{Z}}[\cdot]$ is taken with respect to $\mathbf{Z} \sim \pi_{k+1}(\cdot | \mathbf{y}_{[k+1]})$.

Proof of Lemma D.10. According to Donsker-Varadhan variational principle (Lemma H.11), for each $s > 0$, we have

$$\begin{aligned}
& \mathbb{E} \left[\|\mathbf{B}_t - \mathbf{B}_{\ell h}\|_2^2 \psi_{k+1}^t(\tilde{\mathbf{Z}}_t | \mathbf{y}_{[k+1]}) \right] - \mathbb{E} \left[\|\mathbf{B}_t - \mathbf{B}_{\ell h}\|_2^2 \right] \\
& = \frac{1}{s} \mathbb{E} \left[s \left(\|\mathbf{B}_t - \mathbf{B}_{\ell h}\|_2^2 - \mathbb{E} \left[\|\mathbf{B}_t - \mathbf{B}_{\ell h}\|_2^2 \right] \right) \psi_{k+1}^t(\tilde{\mathbf{Z}}_t | \mathbf{y}_{[k+1]}) \right] \\
& \leq \frac{1}{s} \text{KL} \left(\mu_{k+1}^t(\cdot | \mathbf{y}_{[k+1]}) \parallel \bar{\pi}_{k+1}^t(\cdot | \mathbf{y}_{[k+1]}) \right) \\
& \quad + \frac{1}{s} \log \mathbb{E} \left[\exp \left\{ s \left(\|\mathbf{B}_t - \mathbf{B}_{\ell h}\|_2^2 - \mathbb{E} \left[\|\mathbf{B}_t - \mathbf{B}_{\ell h}\|_2^2 \right] \right) \right\} \right].
\end{aligned}$$

Rearranging the above inequality yields

$$\begin{aligned}
& \mathbb{E} \left[\|\mathbf{B}_t - \mathbf{B}_{\ell h}\|_2^2 \psi_{k+1}^t(\tilde{\mathbf{Z}}_t | \mathbf{y}_{[k+1]}) \right] \\
& \leq \underbrace{\mathbb{E} \left[\|\mathbf{B}_t - \mathbf{B}_{\ell h}\|_2^2 \right]}_{\text{(i)}} + \frac{1}{s} \underbrace{\text{KL} \left(\mu_{k+1}^t(\cdot | \mathbf{y}_{[k+1]}) \parallel \bar{\pi}_{k+1}^t(\cdot | \mathbf{y}_{[k+1]}) \right)}_{\text{(ii)}} \\
\text{(D.18)} \quad & \quad + \frac{1}{s} \underbrace{\log \mathbb{E} \left[\exp \left\{ s \left(\|\mathbf{B}_t - \mathbf{B}_{\ell h}\|_2^2 - \mathbb{E} \left[\|\mathbf{B}_t - \mathbf{B}_{\ell h}\|_2^2 \right] \right) \right\} \right]}_{\text{(iii)}}.
\end{aligned}$$

For the term (i) in (D.18), it holds that

$$\text{(D.19)} \quad \mathbb{E} \left[\|\mathbf{B}_t - \mathbf{B}_{\ell h}\|_2^2 \right] = d(t - \ell h).$$

For the term (ii) in (D.18), we find

$$\begin{aligned}
& \text{KL}(\mu_{k+1}^t(\cdot|\mathbf{y}_{[k+1]})\|\bar{\pi}_{k+1}^t(\cdot|\mathbf{y}_{[k+1]})) \\
&= \int \mu_{k+1}^t(\mathbf{x}|\mathbf{y}_{[k+1]}) \log \psi_{k+1}^t(\mathbf{x}|\mathbf{y}_{[k+1]}) \, d\mathbf{x} \\
&= \frac{1}{2} \int \mu_{k+1}^t(\mathbf{x}|\mathbf{y}_{[k+1]}) \log \frac{\phi_{k+1}^t(\mathbf{x}|\mathbf{y}_{[k+1]})^2}{\mathbb{E}_{\bar{\mathbf{Z}}_t}[\phi_{k+1}^t(\bar{\mathbf{Z}}_t|\mathbf{y}_{[k+1]})]^2} \, d\mathbf{x} \\
&= \frac{1}{2} \int \mu_{k+1}^t(\mathbf{x}|\mathbf{y}_{[k+1]}) \left\{ \log \frac{\phi_{k+1}^t(\mathbf{x}|\mathbf{y}_{[k+1]})^2}{\mathbb{E}_{\bar{\mathbf{Z}}_t}[\phi_{k+1}^t(\bar{\mathbf{Z}}_t|\mathbf{y}_{[k+1]})]} - \log \mathbb{E}_{\bar{\mathbf{Z}}_t}[\phi_{k+1}^t(\bar{\mathbf{Z}}_t|\mathbf{y}_{[k+1]})] \right\} \, d\mathbf{x} \\
&\leq \frac{1}{2} \int \mu_{k+1}^t(\mathbf{x}|\mathbf{y}_{[k+1]}) \log \frac{\phi_{k+1}^t(\mathbf{x}|\mathbf{y}_{[k+1]})^2}{\mathbb{E}_{\bar{\mathbf{Z}}_t}[\phi_{k+1}^t(\bar{\mathbf{Z}}_t|\mathbf{y}_{[k+1]})]} \, d\mathbf{x} \\
&= \frac{1}{2} \int \mu_{k+1}^t(\mathbf{x}|\mathbf{y}_{[k+1]}) \log \{ \psi_{k+1}^t(\mathbf{x}|\mathbf{y}_{[k+1]}) \phi_{k+1}^t(\mathbf{x}|\mathbf{y}_{[k+1]}) \} \, d\mathbf{x} \\
&= \frac{1}{2} \text{KL}(\mu_{k+1}^t(\cdot|\mathbf{y}_{[k+1]})\|\pi_{k+1}(\cdot|\mathbf{y}_{[k+1]})) \\
&\leq \frac{C_{\text{LSI}}}{4} \mathbb{E}_{\bar{\mathbf{Z}}_t} \left[\left\| \nabla \log \{ \psi_{k+1}^t(\bar{\mathbf{Z}}_t|\mathbf{y}_{[k+1]}) \phi_{k+1}^t(\bar{\mathbf{Z}}_t|\mathbf{y}_{[k+1]}) \} \right\|_2^2 \right] \\
\text{(D.20)} \quad &= C_{\text{LSI}} \frac{\mathbb{E}_{\mathbf{Z}}[\|\nabla_{\mathbf{x}} \phi_{k+1}^t(\mathbf{Z}|\mathbf{y}_{[k+1]})\|_2^2]}{\mathbb{E}_{\mathbf{Z}}[\phi_{k+1}^t(\mathbf{Z}|\mathbf{y}_{[k+1]})^2]},
\end{aligned}$$

where the second equality holds from (D.3) and (D.4), the second inequality invokes Lemmas H.13 and H.14, and the last equality is due to Lemma H.15. Finally, we consider the term (iii) in (D.18). Applying Lemma H.12 deduces

$$\text{(D.21)} \quad \log \mathbb{E} \left[\exp \{ s \|\mathbf{B}_t - \mathbf{B}_{\ell h}\|_2^2 - \mathbb{E}[\|\mathbf{B}_t - \mathbf{B}_{\ell h}\|_2^2] \} \right] \leq 2ds(t - \ell h),$$

provided that $4s(t - \ell h) \leq 1$. Substituting (D.19), (D.20), and (D.21) into (D.18) implies

$$\begin{aligned}
& \mathbb{E}[\|\mathbf{B}_t - \mathbf{B}_{\ell h}\|_2^2 \psi_{k+1}^t(\bar{\mathbf{Z}}_t|\mathbf{y}_{[k+1]})] \\
&\leq d(t - \ell h) + \frac{C_{\text{LSI}}}{s} \frac{\mathbb{E}_{\mathbf{Z}}[\|\nabla_{\mathbf{x}} \phi_{k+1}^t(\mathbf{Z}|\mathbf{y}_{[k+1]})\|_2^2]}{\mathbb{E}_{\mathbf{Z}}[\phi_{k+1}^t(\mathbf{Z}|\mathbf{y}_{[k+1]})^2]} + 2d(t - \ell h),
\end{aligned}$$

for each $s > 0$ such that $4s(t - \ell h) \leq 1$. Letting $8s(t - \ell h) = 1$ completes the proof. \square

With the help of the preceding three lemmas, we can now prove Lemma D.7.

Proof of Lemma D.7. Applying Lemmas D.9 and D.10 into Lemma D.8 implies

$$\begin{aligned}
& \mathbb{E}_{(\bar{\mathbf{Z}}_{\ell h}, \bar{\mathbf{Z}}_t)} \left[\|\mathbf{e}_{k+1}(\bar{\mathbf{Z}}_{\ell h}, \bar{\mathbf{Z}}_t|\mathbf{y}_{[k+1]})\|_2^2 \psi_{k+1}^t(\bar{\mathbf{Z}}_t|\mathbf{y}_{[k+1]}) \right] \\
&\leq 8\lambda^2(t - \ell h)^2 \left\{ \frac{4\mathbb{E}_{\mathbf{Z}}[\|\nabla_{\mathbf{x}} \phi_{k+1}^t(\mathbf{Z}|\mathbf{y}_{[k+1]})\|_2^2]}{\mathbb{E}_{\mathbf{Z}}[\phi_{k+1}^t(\mathbf{Z}|\mathbf{y}_{[k+1]})^2]} + 2d\lambda \right\} \\
&\quad + 6\lambda^2 \left\{ 3d(t - \ell h) + 8C_{\text{LSI}}(t - \ell h) \frac{\mathbb{E}_{\mathbf{Z}}[\|\nabla_{\mathbf{x}} \phi_{k+1}^t(\mathbf{Z}|\mathbf{y}_{[k+1]})\|_2^2]}{\mathbb{E}_{\mathbf{Z}}[\phi_{k+1}^t(\mathbf{Z}|\mathbf{y}_{[k+1]})^2]} \right\} \\
&= \{32\lambda^2(t - \ell h)^2 + 48C_{\text{LSI}}\lambda^2(t - \ell h)\} \frac{\mathbb{E}_{\mathbf{Z}}[\|\nabla_{\mathbf{x}} \phi_{k+1}^t(\mathbf{Z}|\mathbf{y}_{[k+1]})\|_2^2]}{\mathbb{E}_{\mathbf{Z}}[\phi_{k+1}^t(\mathbf{Z}|\mathbf{y}_{[k+1]})^2]} \\
&\quad + 16d\lambda^3(t - \ell h)^2 + 16d\lambda^2(t - \ell h) \\
&\leq 80C_{\text{LSI}}\lambda^2(t - \ell h) \frac{\mathbb{E}_{\mathbf{Z}}[\|\nabla_{\mathbf{x}} \phi_{k+1}^t(\mathbf{Z}|\mathbf{y}_{[k+1]})\|_2^2]}{\mathbb{E}_{\mathbf{Z}}[\phi_{k+1}^t(\mathbf{Z}|\mathbf{y}_{[k+1]})^2]} + 20d\lambda^2(t - \ell h),
\end{aligned}$$

where the last inequality holds from $4\lambda h \leq 1$. This completes the proof. \square

D.4. Proof of the convergence of Langevin Monte Carlo. Combining Lemmas D.3, D.6, and D.7 achieves the following recursion of χ^2 -divergence.

Lemma D.11. *Suppose Assumptions 1 and 2 hold. Then for each $0 \leq \ell \leq K - 1$,*

$$\begin{aligned} & \chi^2(\bar{\pi}_{k+1}^{(\ell+1)h}(\cdot|\mathbf{y}_{[k+1]})\|\pi_{k+1}(\cdot|\mathbf{y}_{[k+1]})) \\ & \leq \exp\left(-\frac{h}{5C_{\text{LSI}}}\right)\chi^2(\bar{\pi}_{k+1}^{\ell h}(\cdot|\mathbf{y}_{[k+1]})\|\pi_{k+1}(\cdot|\mathbf{y}_{[k+1]})) + 20d\lambda^2h^2, \end{aligned}$$

where the step size $h > 0$ satisfies $400dC_{\text{LSI}}\lambda^2h \leq 1$.

Proof of Lemma D.11. Plugging Lemma D.7 into Lemma D.3 implies

$$\begin{aligned} & \frac{d}{dt}\chi^2(\bar{\pi}_{k+1}^t(\cdot|\mathbf{y}_{[k+1]})\|\pi_{k+1}(\cdot|\mathbf{y}_{[k+1]})) \\ & \leq -\mathbb{E}_{\mathbf{Z}}\left[\|\nabla_{\mathbf{x}}\phi_{k+1}^t(\mathbf{Z}|\mathbf{y}_{[k+1]})\|_2^2\right] + 80C_{\text{LSI}}\lambda^2h\mathbb{E}_{\mathbf{Z}}\left[\|\nabla_{\mathbf{x}}\phi_{k+1}^t(\mathbf{Z}|\mathbf{y}_{[k+1]})\|_2^2\right] \\ & \quad + 20d\lambda^2(t-\ell h)\mathbb{E}_{\mathbf{Z}}[\phi_{k+1}^t(\mathbf{Z}|\mathbf{y}_{[k+1]})^2] \\ (D.22) \quad & \leq -\frac{4}{5}\underbrace{\mathbb{E}_{\mathbf{Z}}\left[\|\nabla_{\mathbf{x}}\phi_{k+1}^t(\mathbf{Z}|\mathbf{y}_{[k+1]})\|_2^2\right]}_{(i)} + 20d\lambda^2(t-\ell h)\underbrace{\mathbb{E}_{\mathbf{Z}}[\phi_{k+1}^t(\mathbf{Z}|\mathbf{y}_{[k+1]})^2]}_{(ii)}, \end{aligned}$$

where the second inequality invokes $400C_{\text{LSI}}\lambda^2h \leq 1$. For the term (i) in (D.22), it follows from Lemma D.6 that

$$(D.23) \quad \frac{1}{2C_{\text{LSI}}}\chi^2(\bar{\pi}_{k+1}^t(\cdot|\mathbf{y}_{[k+1]})\|\pi_{k+1}(\cdot|\mathbf{y}_{[k+1]})) \leq \mathbb{E}_{\mathbf{Z}}\left[\|\nabla_{\mathbf{x}}\phi_{k+1}^t(\mathbf{Z}|\mathbf{y}_{[k+1]})\|_2^2\right].$$

For the term (ii) in (D.22), using the definition of χ^2 -divergence and (D.2),

$$(D.24) \quad \mathbb{E}_{\mathbf{Z}}[\phi_{k+1}^t(\mathbf{Z}|\mathbf{y}_{[k+1]})^2] \leq \chi^2(\bar{\pi}_{k+1}^t(\cdot|\mathbf{y}_{[k+1]})\|\pi_{k+1}(\cdot|\mathbf{y}_{[k+1]})) + 1.$$

Substituting (D.23) and (D.24) into (D.22) yields that for h satisfying $100dC_{\text{LSI}}\lambda^2h \leq 1$,

$$\begin{aligned} & \frac{d}{dt}\chi^2(\bar{\pi}_{k+1}^t(\cdot|\mathbf{y}_{[k+1]})\|\pi_{k+1}(\cdot|\mathbf{y}_{[k+1]})) \\ (D.25) \quad & \leq -\frac{1}{5C_{\text{LSI}}}\chi^2(\bar{\pi}_{k+1}^t(\cdot|\mathbf{y}_{[k+1]})\|\pi_{k+1}(\cdot|\mathbf{y}_{[k+1]})) + 20d\lambda^2h. \end{aligned}$$

Multiplying both sides of (D.25) by $\exp(\frac{t}{5C_{\text{LSI}}})$ deduces

$$(D.26) \quad \frac{d}{dt}\left(\exp\left(\frac{t}{5C_{\text{LSI}}}\right)\chi^2(\bar{\pi}_{k+1}^t(\cdot|\mathbf{y}_{[k+1]})\|\pi_{k+1}(\cdot|\mathbf{y}_{[k+1]}))\right) \leq 20d\lambda^2h\exp\left(\frac{t}{5C_{\text{LSI}}}\right).$$

Before proceeding, we verify a useful inequality

$$(D.27) \quad \exp\left(\frac{h}{5C_{\text{LSI}}}\right) - 1 \leq \frac{h}{5C_{\text{LSI}}}.$$

In fact, since that $400C_{\text{LSI}}\lambda^2h \leq 1$ and $C_{\text{LSI}}\lambda \geq 1$ (Lemma H.8), it holds that

$$0 < \frac{h}{5C_{\text{LSI}}} \leq \frac{h}{5C_{\text{LSI}}}\frac{1}{400C_{\text{LSI}}\lambda^2h} < 1,$$

which implies (D.27) directly. Then integrating both sides of (D.26) from ℓh to $(\ell + 1)h$ yields

$$\begin{aligned} & \chi^2(\bar{\pi}_{k+1}^{(\ell+1)h}(\cdot|\mathbf{y}_{[k+1]})\|\pi_{k+1}(\cdot|\mathbf{y}_{[k+1]})) \\ & \leq \exp\left(-\frac{h}{5C_{\text{LSI}}}\right)\chi^2(\bar{\pi}_{k+1}^{\ell h}(\cdot|\mathbf{y}_{[k+1]})\|\pi_{k+1}(\cdot|\mathbf{y}_{[k+1]})) \\ & \quad + 100dC_{\text{LSI}}\lambda^2h\exp\left(-\frac{h}{5C_{\text{LSI}}}\right)\left\{\exp\left(\frac{h}{5C_{\text{LSI}}}\right)-1\right\} \\ & \leq \exp\left(-\frac{h}{5C_{\text{LSI}}}\right)\chi^2(\bar{\pi}_{k+1}^{\ell h}(\cdot|\mathbf{y}_{[k+1]})\|\pi_{k+1}(\cdot|\mathbf{y}_{[k+1]})) + 20d\lambda^2h^2, \end{aligned}$$

where the last inequality invokes (D.27). This completes the proof. \square

Proof of Lemma D.1. It is straightforward from Lemma D.11 that

$$\begin{aligned} & \chi^2(\bar{\pi}_{k+1}^{\ell h}(\cdot|\mathbf{y}_{[k+1]})\|\pi_{k+1}(\cdot|\mathbf{y}_{[k+1]})) \\ & \leq \exp\left(-\frac{\ell h}{5C_{\text{LSI}}}\right)\chi^2(\pi_{k+1}^0(\cdot|\mathbf{y}_{[k+1]})\|\pi_{k+1}(\cdot|\mathbf{y}_{[k+1]})) + \frac{20d\lambda^2h^2}{1-\exp(-\frac{h}{5C_{\text{LSI}}})} \\ & \leq \exp\left(-\frac{\ell h}{5C_{\text{LSI}}}\right)\chi^2(\pi_{k+1}^0(\cdot|\mathbf{y}_{[k+1]})\|\pi_{k+1}(\cdot|\mathbf{y}_{[k+1]})) + 140dC_{\text{LSI}}\lambda^2h, \end{aligned}$$

where the last inequality used $1 - \exp(-\frac{h}{5C_{\text{LSI}}}) \geq \frac{3h}{20C_{\text{LSI}}}$ for $0 < \frac{h}{5C_{\text{LSI}}} \leq \frac{1}{4}$. Indeed, combining the condition $400dC_{\text{LSI}}\lambda^2h \leq 1$ and Lemma H.8 implies $4h\lambda \leq 1$, which deduces that $\frac{h}{5C_{\text{LSI}}} \leq \frac{1}{20C_{\text{LSI}}\lambda} \leq \frac{1}{4}$. This completes the proof. \square

APPENDIX E. PRIOR ERROR

In this section, we bound the prior error

$$\|\nabla_{\mathbf{x}} \log q_{k+1}(\cdot|\mathbf{y}_{[k]}) - \nabla_{\mathbf{x}} \log \hat{q}_{k+1}(\cdot|\mathbf{y}_{[k]})\|_{L^\infty(\mathbb{R}^d)},$$

where \hat{q}_{k+1} is defined as (2.7)

$$\hat{q}_{k+1}(\mathbf{x}|\mathbf{y}_{[k]}) := \int \rho_k(\mathbf{x}|\mathbf{x}_k)\hat{\pi}_k^T(\mathbf{x}_k|\mathbf{y}_{[k]}) d\mathbf{x}_k.$$

The main result is stated as follows.

Lemma E.1. *Suppose Assumption 3 holds. Then for each $\mathbf{x} \in \mathbb{R}^d$,*

$$\|\nabla_{\mathbf{x}} \log q_{k+1}(\mathbf{x}|\mathbf{y}_{[k]}) - \nabla_{\mathbf{x}} \log \hat{q}_{k+1}(\mathbf{x}|\mathbf{y}_{[k]})\|_\infty \leq 4B^2D^2\varepsilon_{\text{TV}}^k.$$

Before proceeding, we introduce two auxiliary lemmas.

Lemma E.2. *Suppose Assumption 3 holds. Then for each $\mathbf{x} \in \mathbb{R}^d$,*

$$|q_{k+1}(\mathbf{x}|\mathbf{y}_{[k]}) - \hat{q}_{k+1}(\mathbf{x}|\mathbf{y}_{[k]})| \leq 2B\varepsilon_{\text{TV}}^k.$$

Proof of Lemma E.2. It is straightforward that for each $\mathbf{x} \in \mathbb{R}^d$,

$$\begin{aligned} |q_{k+1}(\mathbf{x}|\mathbf{y}_{[k]}) - \hat{q}_{k+1}(\mathbf{x}|\mathbf{y}_{[k]})| & \leq \int \rho_k(\mathbf{x}|\mathbf{x}_k)|\pi_k(\mathbf{x}_k|\mathbf{y}_{[k]}) - \hat{\pi}_k^T(\mathbf{x}_k|\mathbf{y}_{[k]})| d\mathbf{x}_k \\ & \leq 2B \text{TV}(\pi_k(\cdot|\mathbf{y}_{[k]}), \hat{\pi}_k^T(\cdot|\mathbf{y}_{[k]})), \end{aligned}$$

where the first inequality follows from the Jensen's inequality, and the second inequality invokes Assumption 3 (i) and the Hölder's inequality. This completes the proof. \square

Lemma E.3. *Suppose Assumption 3 holds. Then for each $\mathbf{x} \in \mathbb{R}^d$,*

$$\|\nabla_{\mathbf{x}} q_{k+1}(\mathbf{x}|\mathbf{y}_{[k]}) - \nabla_{\mathbf{x}} \hat{q}_{k+1}(\mathbf{x}|\mathbf{y}_{[k]})\|_\infty \leq 2B\varepsilon_{\text{TV}}^k.$$

Proof of Lemma E.3. It is straightforward that for each $\mathbf{x} \in \mathbb{R}^d$,

$$\begin{aligned} & \left| \frac{\partial q_{k+1}}{\partial x_i}(\mathbf{x}|\mathbf{y}_{[k]}) - \frac{\partial \hat{q}_{k+1}}{\partial x_i}(\mathbf{x}|\mathbf{y}_{[k]}) \right| \\ & \leq \int \left| \frac{\partial \rho_k}{\partial x_i}(\mathbf{x}|\mathbf{x}_k) \right| |\pi_k(\mathbf{x}_k|\mathbf{y}_{[k]}) - \hat{\pi}_k^T(\mathbf{x}_k|\mathbf{y}_{[k]})| d\mathbf{x}_k \\ & \leq 2B \text{TV}(\pi_k(\cdot|\mathbf{y}_{[k]}), \hat{\pi}_k^T(\cdot|\mathbf{y}_{[k]})), \end{aligned}$$

where the first inequality follows from the Jensen's inequality, and the second inequality invokes Assumption 3 (ii) and the Hölder's inequality. This completes the proof. \square

With the help of Lemmas E.2 and E.3, we now prove the Lemma E.1.

Proof of Lemma E.1. According to Assumption 3, we find

$$(E.1) \quad \left| \left(\frac{1}{q_{k+1}} \frac{\partial q_{k+1}}{\partial x_i} \right) (\mathbf{x}|\mathbf{y}_{[k]}) \right| \leq BD, \quad \mathbf{x} \in \mathbb{R}^d.$$

Notice that $\hat{q}_{k+1}(\cdot|\mathbf{y}_{[k+1]})$ is close to $q_{k+1}(\cdot|\mathbf{y}_{[k+1]})$ given that $\hat{\pi}_k^T(\cdot|\mathbf{y}_{[k]})$ is close to $\pi_k(\cdot|\mathbf{y}_{[k]})$. Without loss of generality, we assume $\nabla_{\mathbf{x}} \log \hat{q}_{k+1}(\cdot|\mathbf{y}_{[k+1]})$ also satisfies the above inequality. Then it is straightforward that

$$\begin{aligned} & \left| \left(\frac{1}{q_{k+1}} \frac{\partial q_{k+1}}{\partial x_i} \right) (\mathbf{x}|\mathbf{y}_{[k]}) - \left(\frac{1}{\hat{q}_{k+1}} \frac{\partial \hat{q}_{k+1}}{\partial x_i} \right) (\mathbf{x}|\mathbf{y}_{[k]}) \right| \\ & \leq \left| \frac{1}{q_{k+1}(\mathbf{x}|\mathbf{y}_{[k]})} \frac{\partial q_{k+1}}{\partial x_i}(\mathbf{x}|\mathbf{y}_{[k]}) - \frac{1}{q_{k+1}(\mathbf{x}|\mathbf{y}_{[k]})} \frac{\partial \hat{q}_{k+1}}{\partial x_i}(\mathbf{x}|\mathbf{y}_{[k]}) \right| \\ & \quad + \left| \frac{1}{q_{k+1}(\mathbf{x}|\mathbf{y}_{[k]})} \frac{\partial \hat{q}_{k+1}}{\partial x_i}(\mathbf{x}|\mathbf{y}_{[k]}) - \frac{1}{\hat{q}_{k+1}(\mathbf{x}|\mathbf{y}_{[k]})} \frac{\partial \hat{q}_{k+1}}{\partial x_i}(\mathbf{x}|\mathbf{y}_{[k]}) \right| \\ & \leq \frac{1}{q_{k+1}(\mathbf{x}|\mathbf{y}_{[k]})} \left| \frac{\partial q_{k+1}}{\partial x_i}(\mathbf{x}|\mathbf{y}_{[k]}) - \frac{\partial \hat{q}_{k+1}}{\partial x_i}(\mathbf{x}|\mathbf{y}_{[k]}) \right| \\ & \quad + \frac{1}{q_{k+1}(\mathbf{x}|\mathbf{y}_{[k]})} \left| \left(\frac{1}{\hat{q}_{k+1}} \frac{\partial \hat{q}_{k+1}}{\partial x_i} \right) (\mathbf{x}|\mathbf{y}_{[k]}) \right| |\hat{q}_{k+1}(\mathbf{x}|\mathbf{y}_{[k]}) - q_{k+1}(\mathbf{x}|\mathbf{y}_{[k]})| \\ & \leq D \left| \frac{\partial q_{k+1}}{\partial x_i}(\mathbf{x}|\mathbf{y}_{[k]}) - \frac{\partial \hat{q}_{k+1}}{\partial x_i}(\mathbf{x}|\mathbf{y}_{[k]}) \right| + D^2 B |\hat{q}_{k+1}(\mathbf{x}|\mathbf{y}_{[k]}) - q_{k+1}(\mathbf{x}|\mathbf{y}_{[k]})| \\ & \leq 4D^2 B^2 \text{TV}(\pi_k(\cdot|\mathbf{y}_{[k]}), \hat{\pi}_k^T(\cdot|\mathbf{y}_{[k]})), \end{aligned}$$

where the first inequality follows from the triangular inequality, the third inequality is due to Assumption 3, and the last inequality invokes Lemmas E.2 and E.3. This completes the proof. \square

APPENDIX F. SCORE ESTIMATION ERROR

This section focuses on the error of the score matching, which is inspired by the proof of Tang and Yang (2024, Lemma B.4).

Lemma F.1. *Suppose Assumptions 1, 3, 2, and 4 hold. Then*

$$\begin{aligned} & \sum_{\ell=0}^{K-1} h \mathbb{E}_{\bar{\mathbf{Z}}_{\ell h}} \left[\|\nabla_{\mathbf{x}} \log \hat{q}_{k+1}(\bar{\mathbf{Z}}_{\ell h}|\mathbf{y}_{[k]}) - \hat{\mathbf{s}}_{k+1}(\bar{\mathbf{Z}}_{\ell h}, \mathbf{y}_{[k]})\|_2^2 \right] \\ & \leq 28C_{\text{LSI}} \sqrt{GB^3 D^3} \eta_{\chi} \Delta + 8\sqrt{GB^3 D^3} T \Delta, \end{aligned}$$

where the step size $h > 0$ satisfies $400dC_{\text{LSI}}\lambda^2 h \leq 1$.

Lemma F.2. *Suppose Assumptions 3 and 4 hold. Then for each $0 \leq \ell \leq K - 1$,*

$$\begin{aligned} & \mathbb{E}_{\bar{\mathbf{Z}}^{\ell h}} [\|\nabla_{\mathbf{x}} \log \hat{q}_{k+1}(\bar{\mathbf{Z}}^{\ell h} | \mathbf{y}_{[k]}) - \hat{\mathbf{s}}_{k+1}(\bar{\mathbf{Z}}^{\ell h}, \mathbf{y}_{[k]})\|_2^2] \\ & \leq 2\sqrt{GB^3D^3} \Delta (\chi^2(\bar{\pi}_{k+1}^{\ell h}(\cdot | \mathbf{y}_{[k+1]}) \| \pi_{k+1}(\cdot | \mathbf{y}_{[k+1]})) + 1)^{\frac{1}{2}}. \end{aligned}$$

Proof of Lemma F.2. For the simplicity of the notation, we define

$$\varpi_{k+1}^2(\mathbf{x}, \mathbf{y}_{[k]}) := \|\nabla_{\mathbf{x}} \log \hat{q}_{k+1}(\mathbf{x} | \mathbf{y}_{[k]}) - \hat{\mathbf{s}}_{k+1}(\mathbf{x}, \mathbf{y}_{[k]})\|_2^2.$$

According to Assumption 3, the boundedness of the prediction score is derived by (E.1). Without loss of generality, we assume $\nabla_{\mathbf{x}} \log \hat{q}_{k+1}(\cdot | \mathbf{y}_{[k]})$ and $\hat{\mathbf{s}}_{k+1}(\cdot, \mathbf{y}_{[k]})$ also satisfies this inequality. As a consequence, $\varpi_{k+1}^2(\mathbf{x}, \mathbf{y}_{[k]}) \leq 4B^2D^2$ for each $\mathbf{x} \in \mathbb{R}^d$. It is straightforward that

$$\begin{aligned} & \mathbb{E}_{\bar{\mathbf{Z}}^{\ell h}}^2 [\varpi_{k+1}^2(\bar{\mathbf{Z}}^{\ell h}, \mathbf{y}_{[k]})] \\ & = \left(\int \varpi_{k+1}^2(\mathbf{x}, \mathbf{y}_{[k+1]}) \frac{\bar{\pi}_{k+1}^{\ell h}(\mathbf{x} | \mathbf{y}_{[k+1]})}{\pi_{k+1}(\mathbf{x} | \mathbf{y}_{[k+1]})} \pi_{k+1}(\mathbf{x} | \mathbf{y}_{[k+1]}) d\mathbf{x} \right)^2 \\ \text{(F.1)} \quad & \leq \underbrace{\int \varpi_{k+1}^4(\mathbf{x}, \mathbf{y}_{[k]}) \pi_{k+1}(\mathbf{x} | \mathbf{y}_{[k+1]}) d\mathbf{x}}_{\text{(i)}} \underbrace{\int \left(\frac{\bar{\pi}_{k+1}^{\ell h}(\mathbf{x} | \mathbf{y}_{[k+1]})}{\pi_{k+1}(\mathbf{x} | \mathbf{y}_{[k+1]})} \right)^2 \pi_{k+1}(\mathbf{x} | \mathbf{y}_{[k+1]}) d\mathbf{x}}_{\text{(ii)}}, \end{aligned}$$

where the inequality invokes the Cauchy-Schwarz inequality. For the term (i) in (F.1),

$$\begin{aligned} & \int \varpi_{k+1}^4(\mathbf{x}, \mathbf{y}_{[k]}) \pi_{k+1}(\mathbf{x} | \mathbf{y}_{[k+1]}) d\mathbf{x} \\ & = \int \varpi_{k+1}^4(\mathbf{x}, \mathbf{y}_{[k]}) \frac{\pi_{k+1}(\mathbf{x} | \mathbf{y}_{[k+1]})}{q_{k+1}(\mathbf{x} | \mathbf{y}_{[k]})} \frac{q_{k+1}(\mathbf{x} | \mathbf{y}_{[k]})}{\hat{q}_{k+1}(\mathbf{x} | \mathbf{y}_{[k]})} \hat{q}_{k+1}(\mathbf{x} | \mathbf{y}_{[k]}) d\mathbf{x} \\ & \leq GBD \int \varpi_{k+1}^4(\mathbf{x}, \mathbf{y}_{[k]}) \hat{q}_{k+1}(\mathbf{x} | \mathbf{y}_{[k]}) d\mathbf{x} \\ \text{(F.2)} \quad & \leq 4GB^3D^3 \int \varpi_{k+1}^2(\mathbf{x}, \mathbf{y}_{[k]}) \hat{q}_{k+1}(\mathbf{x} | \mathbf{y}_{[k]}) d\mathbf{x} \leq 4GB^3D^3 \Delta^2, \end{aligned}$$

where the first inequality holds from Assumption 3 and the inequalities

$$\left| \frac{q_{k+1}(\mathbf{x} | \mathbf{y}_{[k]})}{\hat{q}_{k+1}(\mathbf{x} | \mathbf{y}_{[k]})} \right| \leq BD, \quad \frac{\pi_{k+1}(\mathbf{x} | \mathbf{y}_{[k+1]})}{q_{k+1}(\mathbf{x} | \mathbf{y}_{[k]})} = g_{k+1}(\mathbf{y}_{k+1} | \mathbf{x}) \leq G,$$

the second inequality is due to the boundedness of $\varpi_{k+1}^2(\mathbf{x}, \mathbf{y}_{[k+1]})$, and the last inequality is owing to Assumption 4. For the term (ii) in (F.1),

$$\begin{aligned} & \int \left(\frac{\bar{\pi}_{k+1}^{\ell h}(\mathbf{x} | \mathbf{y}_{[k+1]})}{\pi_{k+1}(\mathbf{x} | \mathbf{y}_{[k+1]})} \right)^2 \pi_{k+1}(\mathbf{x} | \mathbf{y}_{[k+1]}) d\mathbf{x} \\ \text{(F.3)} \quad & = \chi^2(\bar{\pi}_{k+1}^{\ell h}(\cdot | \mathbf{y}_{[k+1]}) \| \pi_{k+1}(\cdot | \mathbf{y}_{[k+1]})) + 1. \end{aligned}$$

Substituting (F.2) and (F.3) into (F.1) completes the proof. \square

Proof of Lemma F.1. By a same argument as the proof of Lemma D.1, we have

$$\text{(F.4)} \quad \sum_{\ell=0}^{K-1} \exp\left(-\frac{\ell h}{10C_{\text{LSI}}}\right) \leq \frac{20C_{\text{LSI}}}{3h},$$

provided that the step size $h > 0$ satisfies $400dC_{\text{LSI}}\lambda^2h \leq 1$. Summing both sides of Lemma F.2 with respect to $0 \leq \ell \leq K - 1$ yields

$$\begin{aligned} & \sum_{\ell=0}^{K-1} h \mathbb{E}_{\bar{\mathbf{Z}}_{\ell h}} \left[\|\nabla_{\mathbf{x}} \log \hat{q}_{k+1}(\bar{\mathbf{Z}}_{\ell h} | \mathbf{y}_{[k]}) - \hat{\mathbf{s}}_{k+1}(\bar{\mathbf{Z}}_{\ell h}, \mathbf{y}_{[k]})\|_2^2 \right] \\ & \leq 2\sqrt{GB^3D^3}h\Delta \sum_{\ell=0}^{K-1} \left(\exp\left(-\frac{\ell h}{5C_{\text{LSI}}}\right) \chi^2(\pi_{k+1}^0(\cdot | \mathbf{y}_{[k+1]}) \| \pi_{k+1}(\cdot | \mathbf{y}_{[k+1]})) + 2 \right)^{\frac{1}{2}} \\ & \leq 4\sqrt{GB^3D^3}h\Delta \left\{ \sum_{\ell=0}^{K-1} \exp\left(-\frac{\ell h}{10C_{\text{LSI}}}\right) \chi^2(\pi_{k+1}^0(\cdot | \mathbf{y}_{[k+1]}) \| \pi_{k+1}(\cdot | \mathbf{y}_{[k+1]})) \right\}^{\frac{1}{2}} + 2K \\ & \leq 28C_{\text{LSI}}\sqrt{GB^3D^3}\Delta \chi^2(\pi_{k+1}^0(\cdot | \mathbf{y}_{[k+1]}) \| \pi_{k+1}(\cdot | \mathbf{y}_{[k+1]})) \right)^{\frac{1}{2}} + 8\sqrt{GB^3D^3}T\Delta, \end{aligned}$$

where the first inequality invokes Lemmas F.2 and D.1, and the inequality $400dC_{\text{LSI}}\lambda^2h \leq 1$. The second inequality is due to $\sqrt{a+b} \leq 2\sqrt{a} + 2\sqrt{b}$ for $a, b \geq 0$, and the last inequality follows from (F.4) and $T = Kh$. This completes the proof. \square

APPENDIX G. CONVERGENCE ANALYSIS FOR THE INITIAL STEP

In this section, we consider the assimilation in the first time step. The Langevin diffusion is given as

$$(G.1) \quad d\mathbf{Z}_t = \nabla_{\mathbf{x}} \log \pi_1(\mathbf{Z}_t | \mathbf{y}_1) dt + \sqrt{2} d\mathbf{B}_t, \quad \mathbf{Z}_0 \sim \pi_1^0(\cdot | \mathbf{y}_1), \quad t \geq 0.$$

Denote by π_1^t the law of \mathbf{Z}_t for each $t \geq 0$. The Langevin Monte Carlo is defined as the Euler-Maruyama discretization of the Langevin diffusion. The interpolation of the Langevin Monte Carlo is given as, for each $0 \leq \ell \leq K - 1$,

$$(G.2) \quad d\bar{\mathbf{Z}}_t = \nabla_{\mathbf{x}} \log \pi_1(\bar{\mathbf{Z}}_{\ell h} | \mathbf{y}_{[k+1]}) dt + \sqrt{2} d\mathbf{B}_t, \quad \ell h \leq t \leq (\ell + 1)h,$$

where $\bar{\mathbf{Z}}_0 \sim \pi_1^0(\cdot | \mathbf{y}_1)$. Denote by $\bar{\pi}_1^t$ the law of $\bar{\mathbf{Z}}_t$ for each $0 \leq t \leq Kh = T$. We next introduce the interpolation of the score-based Langevin Monte Carlo

$$(G.3) \quad d\hat{\mathbf{Z}}_t = \hat{\mathbf{b}}_1(\hat{\mathbf{Z}}_{\ell h} | \mathbf{y}_{[k+1]}) dt + \sqrt{2} d\mathbf{B}_t, \quad \ell h \leq t \leq (\ell + 1)h,$$

where $\hat{\mathbf{Z}}_0 \sim \pi_1^0(\cdot | \mathbf{y}_1)$, and the estimator of posterior score function is given as

$$\hat{\mathbf{b}}_1(\mathbf{x} | \mathbf{y}_1) = \nabla_{\mathbf{x}} \log g_1(\mathbf{y}_1 | \mathbf{x}) + \hat{\mathbf{s}}_1(\mathbf{x}).$$

Here $\hat{\mathbf{s}}_1$ is an estimator of $\nabla_{\mathbf{x}} \log \hat{q}_1$. Denote by $\hat{\pi}_{k+1}^t$ the law of $\hat{\mathbf{Z}}_t$ for each $0 \leq t \leq Kh = T$.

The main result in this section is stated as the following lemma.

Lemma G.1. *Suppose Assumptions 1, 2, 3, and 4 hold. Then for each terminal time $T = Kh$,*

$$\begin{aligned} (\varepsilon_{\text{TV}}^1)^2 & \lesssim \exp\left(-\frac{T}{5C_{\text{LSI}}}\right) \eta_{\chi}^2 + dC_{\text{LSI}}\lambda^2h + \sqrt{GB^3D^3}(T + C_{\text{LSI}}\eta_{\chi})\Delta \\ & \quad + T \|\nabla_{\mathbf{x}} \log q_1 - \nabla_{\mathbf{x}} \log \hat{q}_1\|_{L^\infty(\mathbb{R}^d)}^2, \end{aligned}$$

where the step size h and the initial distribution $\pi_k^0(\cdot | \mathbf{y}_{[k]})$ satisfies

$$h \leq \mathcal{O}\left(\frac{1}{dC_{\text{LSI}}\lambda^2}\right), \quad \chi^2(\pi_1^0(\cdot | \mathbf{y}_1) \| \pi_1(\cdot | \mathbf{y}_1)) \leq \eta_{\chi}^2.$$

By an argument similar to Lemma C.1, we decompose the error of the initial time step of the assimilation as the following lemma.

Lemma G.2. Let π_1 be the stationary distribution of the Langevin diffusion (G.1), and let $\widehat{\pi}_1^T$ be the law of the score-based Langevin Monte Carlo (G.3). Then

$$\begin{aligned} & \text{TV}^2(\pi_1(\cdot|\mathbf{y}_1), \widehat{\pi}_1^T(\cdot|\mathbf{y}_1)) \\ & \leq 2 \underbrace{\text{TV}^2(\pi_1(\cdot|\mathbf{y}_1), \bar{\pi}_1^T(\cdot|\mathbf{y}_1))}_{\text{convergence of Langevin Monte Carlo}} + 4T \underbrace{\|\nabla_{\mathbf{x}} \log q_1 - \nabla_{\mathbf{x}} \log \widehat{q}_1\|_{L^\infty(\mathbb{R}^d)}^2}_{\text{prior error}} \\ & \quad + 4 \underbrace{\sum_{\ell=0}^{K-1} h \mathbb{E}_{\bar{\mathbf{Z}}_{\ell h}} \left[\|\nabla_{\mathbf{x}} \log \widehat{q}_1(\bar{\mathbf{Z}}_{\ell h}) - \widehat{\mathbf{s}}_1(\bar{\mathbf{Z}}_{\ell h})\|_2^2 \right]}_{\text{score estimation error}}, \end{aligned}$$

where the expectation $\mathbb{E}_{\bar{\mathbf{Z}}_{\ell h}}[\cdot]$ is taken with respect to $\bar{\mathbf{Z}}_{\ell h} \sim \bar{\pi}_{k+1}^{\ell h}(\cdot|\mathbf{y}_{[k+1]})$.

The convergence of the Langevin Monte Carlo can be obtained by Lemma D.1, while the score estimation error can be estimated by an argument similar to Lemma F.1 as follows.

Lemma G.3. Suppose Assumptions 1, 2, 3, and 4 hold. Then

$$\begin{aligned} & \sum_{\ell=0}^{K-1} h \mathbb{E}_{\bar{\mathbf{Z}}_{\ell h}} \left[\|\nabla_{\mathbf{x}} \log \widehat{q}_1(\bar{\mathbf{Z}}_{\ell h}) - \widehat{\mathbf{s}}_1(\bar{\mathbf{Z}}_{\ell h})\|_2^2 \right] \\ & \leq 28C_{\text{LSI}} \sqrt{GB^3 D^3} \eta_\chi \Delta + 8\sqrt{GB^3 D^3} T \Delta, \end{aligned}$$

where the step size $h > 0$ satisfies $400dC_{\text{LSI}}\lambda^2 h \leq 1$.

Proof of Lemma G.1. For the simplicity of the notation, we define

$$\varpi_1^2(\mathbf{x}) := \|\nabla_{\mathbf{x}} \log \widehat{q}_1(\mathbf{x}) - \widehat{\mathbf{s}}_1(\mathbf{x})\|_2^2.$$

According to Assumption 3, $\|\nabla_{\mathbf{x}} q_1(\mathbf{x})\|_\infty \leq BD$. Without loss of generality, we assume $\nabla_{\mathbf{x}} \log \widehat{q}_1(\mathbf{x})$ and $\widehat{\mathbf{s}}_1(\mathbf{x})$ also satisfies this inequality. As a consequence, $\varpi_1^2(\mathbf{x}) \leq 4B^2 D^2$ for each $\mathbf{x} \in \mathbb{R}^d$. It is straightforward that

$$\begin{aligned} \mathbb{E}_{\bar{\mathbf{Z}}_{\ell h}}^2 [\varpi_1^2(\bar{\mathbf{Z}}_{\ell h})] & = \left(\int \varpi_1^2(\mathbf{x}) \frac{\bar{\pi}_1^{\ell h}(\mathbf{x}|\mathbf{y}_1)}{\pi_1(\mathbf{x}|\mathbf{y}_1)} \pi_1(\mathbf{x}|\mathbf{y}_1) \, d\mathbf{x} \right)^2 \\ & \leq \int \varpi_1^4(\mathbf{x}) \pi_1(\mathbf{x}|\mathbf{y}_1) \, d\mathbf{x} \int \left(\frac{\bar{\pi}_1^{\ell h}(\mathbf{x}|\mathbf{y}_1)}{\pi_1(\mathbf{x}|\mathbf{y}_1)} \right)^2 \pi_1(\mathbf{x}|\mathbf{y}_1) \, d\mathbf{x}, \\ \text{(G.4)} \quad & = \underbrace{\int \varpi_1^4(\mathbf{x}) \pi_1(\mathbf{x}|\mathbf{y}_1) \, d\mathbf{x}}_{(*)} (\chi^2(\bar{\pi}_1^{\ell h}(\cdot|\mathbf{y}_1) \|\pi_1(\cdot|\mathbf{y}_1)) + 1), \end{aligned}$$

where the inequality invokes the Cauchy-Schwarz inequality. For the term $(*)$ in (G.4),

$$\begin{aligned} & \int \varpi_1^4(\mathbf{x}) \pi_1(\mathbf{x}|\mathbf{y}_1) \, d\mathbf{x} \\ & = \int \varpi_1^4(\mathbf{x}) \frac{\pi_1(\mathbf{x}|\mathbf{y}_1)}{q_1(\mathbf{x})} \frac{q_1(\mathbf{x})}{\widehat{q}_1(\mathbf{x})} \widehat{q}_1(\mathbf{x}) \, d\mathbf{x} \leq GBD \int \varpi_1^4(\mathbf{x}) \widehat{q}_1(\mathbf{x}) \, d\mathbf{x} \\ \text{(G.5)} \quad & \leq 4GB^3 D^3 \int \varpi_1^2(\mathbf{x}) \widehat{q}_1(\mathbf{x}) \, d\mathbf{x} \leq 4GB^3 D^3 \Delta^2, \end{aligned}$$

where the first inequality holds from Assumption 3 and the inequalities

$$\left| \frac{q_1(\mathbf{x})}{\widehat{q}_1(\mathbf{x})} \right| \leq BD, \quad \frac{\pi_1(\mathbf{x}|\mathbf{y}_1)}{q_1(\mathbf{x})} = g_k(\mathbf{y}_1|\mathbf{x}) \leq G,$$

the second inequality is due to the boundedness of $\varpi_1^2(\mathbf{x})$, and the last inequality is owing to Assumption 4. Substituting (G.5) into (G.4) implies

$$\mathbb{E}_{\bar{\mathbf{Z}}_{\ell h}} \left[\|\nabla_{\mathbf{x}} \log \hat{q}_1(\bar{\mathbf{Z}}_{\ell h}) - \hat{\mathbf{s}}_1(\bar{\mathbf{Z}}_{\ell h})\|_2^2 \right] \leq 2\sqrt{GB^3D^3} \Delta \left(\chi^2(\bar{\pi}_1^{\ell h}(\cdot|\mathbf{y}_1) \|\pi_1(\cdot|\mathbf{y}_1)) + 1 \right)^{\frac{1}{2}}.$$

Finally, by the same argument as the proof of Lemma F.1, we completes the proof. \square

APPENDIX H. AUXILIARY DEFINITIONS AND LEMMAS

We first introduce total variation (TV) distance, χ^2 -divergence, and the Kullback-Leibler (KL) divergence.

Definition H.1 (Total variation distance). The total variation (TV) distance between two distributions μ and π is defined as

$$\text{TV}(\mu, \pi) = \frac{1}{2} \int |\mu(\mathbf{x}) - \pi(\mathbf{x})| \, d\mathbf{x}.$$

Definition H.2 (Chi-squared divergence). The χ^2 -divergence between two distributions μ and π is defined as

$$\chi^2(\mu \|\pi) = \int \left(\frac{\mu(\mathbf{x})}{\pi(\mathbf{x})} \right)^2 \pi(\mathbf{x}) \, d\mathbf{x} - 1 = \int \left(\frac{\mu(\mathbf{x})}{\pi(\mathbf{x})} - 1 \right)^2 \pi(\mathbf{x}) \, d\mathbf{x}.$$

Definition H.3 (Kullback-Leibler divergence). The KL-divergence between two distributions μ and π is defined as

$$\text{KL}(\mu \|\pi) = \int \mu(\mathbf{x}) \log \frac{\mu(\mathbf{x})}{\pi(\mathbf{x})} \, d\mathbf{x}.$$

We then show the relationships between them.

Lemma H.4. For two distributions μ and π ,

$$\text{TV}^2(\mu, \pi) \leq \frac{1}{4} \chi^2(\mu \|\pi).$$

Proof of Lemma H.4. It is straightforward that

$$\begin{aligned} \text{TV}^2(\mu, \pi) &= \frac{1}{4} \left(\int |\mu(\mathbf{x}) - \pi(\mathbf{x})| \, d\mathbf{x} \right)^2 \\ &\leq \frac{1}{4} \left(\int \frac{(\mu(\mathbf{x}) - \pi(\mathbf{x}))^2}{\pi(\mathbf{x})} \, d\mathbf{x} \right) \left(\int \pi(\mathbf{x}) \, d\mathbf{x} \right) \\ &= \frac{1}{4} \int \left(\frac{\mu(\mathbf{x})}{\pi(\mathbf{x})} - 1 \right)^2 \pi(\mathbf{x}) \, d\mathbf{x} = \frac{1}{4} \chi^2(\mu \|\pi), \end{aligned}$$

where the inequality follows from the Cauchy-Schwarz inequality. The proof is complete. \square

The proof of Lemmas H.5 and H.6 can be found in Tsybakov (2009, Lemmas 2.5 and 2.7).

Lemma H.5 (Pinsker's inequality). For two distributions μ and π ,

$$\text{TV}^2(\mu, \pi) \leq \frac{1}{2} \text{KL}(\mu \|\pi).$$

Lemma H.6. For two distributions μ and π ,

$$\text{KL}(\mu \|\pi) \leq \log(1 + \chi^2(\mu \|\pi)) \leq \chi^2(\mu \|\pi).$$

Proof of Lemma H.6. It is straightforward that

$$\begin{aligned} \text{KL}(\mu\|\pi) &= \int \mu(\mathbf{x}) \log \frac{\mu(\mathbf{x})}{\pi(\mathbf{x})} d\mathbf{x} = \mathbb{E}_{\mathbf{X}\sim\mu} \left[\log \frac{\mu(\mathbf{X})}{\pi(\mathbf{X})} \right] \\ &\leq \log \mathbb{E}_{\mathbf{X}\sim\mu} \left[\frac{\mu(\mathbf{X})}{\pi(\mathbf{X})} \right] = \log \int \left(\frac{\mu(\mathbf{x})}{\pi(\mathbf{x})} \right)^2 \pi(\mathbf{x}) d\mathbf{x} \\ &= \log(1 + \chi^2(\mu\|\pi)) \leq \chi^2(\mu\|\pi), \end{aligned}$$

where the inequality follows from the Jensen's inequality. The proof is complete. \square

Definition H.7 (Poincaré inequality). A distribution π satisfies a Poincaré inequality with constant C_{PI} , that is, for each function $f \in C_0^\infty(\mathbb{R}^d)$,

$$\text{Var}(f) \leq C_{\text{PI}} \mathbb{E} [\|\nabla f\|_2^2],$$

where the expectation and variance are taken with respect to the distribution π .

Notice that the log-Sobolev inequality implies a Poincaré inequality with the same constant. Thus Lee et al. (2022, Lemma E.5) gives the following lemma.

Lemma H.8. Let π be a distribution such that $\log \pi$ is C^1 and λ -smooth. Further, π satisfies the log-Sobolev inequality with constant C_{LSI} . Then $\lambda C_{\text{LSI}} \geq 1$.

Lemma H.9. For two distributions μ and π , it holds that

$$\int \Delta \mu(\mathbf{x}) \frac{\mu(\mathbf{x})}{\pi(\mathbf{x})} d\mathbf{x} + \int \mu(\mathbf{x}) \nabla \log \pi(\mathbf{x}) \cdot \nabla \frac{\mu(\mathbf{x})}{\pi(\mathbf{x})} d\mathbf{x} = \mathbb{E}_\pi \left[\left\| \nabla \frac{\mu}{\pi} \right\|_2^2 \right].$$

Proof of Lemma H.9. It is straightforward that

$$\begin{aligned} & - \int \Delta \mu(\mathbf{x}) \frac{\mu(\mathbf{x})}{\pi(\mathbf{x})} d\mathbf{x} - \int \mu(\mathbf{x}) \nabla \log \pi(\mathbf{x}) \cdot \nabla \frac{\mu(\mathbf{x})}{\pi(\mathbf{x})} d\mathbf{x} \\ &= \int \nabla \mu(\mathbf{x}) \cdot \nabla \frac{\mu(\mathbf{x})}{\pi(\mathbf{x})} d\mathbf{x} - \int \frac{\mu(\mathbf{x})}{\pi(\mathbf{x})} \nabla \pi(\mathbf{x}) \cdot \nabla \frac{\mu(\mathbf{x})}{\pi(\mathbf{x})} d\mathbf{x} \\ &= \int \pi(\mathbf{x}) \left(\frac{\nabla \mu(\mathbf{x})}{\pi(\mathbf{x})} - \frac{\mu(\mathbf{x}) \nabla \pi(\mathbf{x})}{\pi(\mathbf{x})^2} \right) \cdot \nabla \frac{\mu(\mathbf{x})}{\pi(\mathbf{x})} d\mathbf{x} \\ &= \int \left\| \nabla \frac{\mu(\mathbf{x})}{\pi(\mathbf{x})} \right\|_2^2 \pi(\mathbf{x}) d\mathbf{x} = \mathbb{E}_\pi \left[\left\| \nabla \frac{\mu}{\pi} \right\|_2^2 \right], \end{aligned}$$

where the first equality holds from Green's formula. This completes the proof. \square

Lemma H.10. Let π be a distribution satisfies the log-Sobolev inequality with constant C_{LSI} . Then for each distribution μ , it holds that

$$\frac{1}{2C_{\text{LSI}}} \chi^2(\mu\|\pi) \leq \mathbb{E}_\pi \left[\left\| \nabla \frac{\mu}{\pi} \right\|_2^2 \right].$$

Proof of Lemma H.10. Recall the log-Sobolev inequality

$$(H.1) \quad \text{Ent}_\pi(f^2) \leq 2C_{\text{LSI}} \mathbb{E}_\pi [\|\nabla f\|_2^2].$$

Substituting $f(\mathbf{x}) = (\mu(\mathbf{x})/\pi(\mathbf{x}))^{q/2}$ into the left-hand side of (H.4) deduces

$$\begin{aligned} \text{Ent}_\pi \left(\frac{\mu^q}{\pi^q} \right) &= q \int \frac{\mu(\mathbf{x})^q}{\pi(\mathbf{x})^q} \log \frac{\mu(\mathbf{x})}{\pi(\mathbf{x})} \pi(\mathbf{x}) d\mathbf{x} - \int \frac{\mu(\mathbf{x})^q}{\pi(\mathbf{x})^q} \pi(\mathbf{x}) d\mathbf{x} \log \int \frac{\mu(\mathbf{x})^q}{\pi(\mathbf{x})^q} \pi(\mathbf{x}) d\mathbf{x} \\ &= q \partial_q \int \frac{\mu(\mathbf{x})^q}{\pi(\mathbf{x})^q} \pi(\mathbf{x}) d\mathbf{x} - \int \frac{\mu(\mathbf{x})^q}{\pi(\mathbf{x})^q} \pi(\mathbf{x}) d\mathbf{x} \log \int \frac{\mu(\mathbf{x})^q}{\pi(\mathbf{x})^q} \pi(\mathbf{x}) d\mathbf{x}, \end{aligned}$$

where the last equality used the chain rule. As a consequence,

$$\begin{aligned}
& \left(\int \frac{\mu(\mathbf{x})^q}{\pi(\mathbf{x})^q} \pi(\mathbf{x}) \, d\mathbf{x} \right)^{-1} \text{Ent}_\pi \left(\frac{\mu^q}{\pi^q} \right) \\
&= q \partial_q \log \int \frac{\mu(\mathbf{x})^q}{\pi(\mathbf{x})^q} \pi(\mathbf{x}) \, d\mathbf{x} - \log \int \frac{\mu(\mathbf{x})^q}{\pi(\mathbf{x})^q} \pi(\mathbf{x}) \, d\mathbf{x} \\
&= q \partial_q \left\{ (q-1) \left(\frac{1}{q-1} \log \int \frac{\mu(\mathbf{x})^q}{\pi(\mathbf{x})^q} \pi(\mathbf{x}) \, d\mathbf{x} \right) \right\} - \log \int \frac{\mu(\mathbf{x})^q}{\pi(\mathbf{x})^q} \pi(\mathbf{x}) \, d\mathbf{x} \\
&= \frac{q}{q-1} \log \int \frac{\mu(\mathbf{x})^q}{\pi(\mathbf{x})^q} \pi(\mathbf{x}) \, d\mathbf{x} - \log \int \frac{\mu(\mathbf{x})^q}{\pi(\mathbf{x})^q} \pi(\mathbf{x}) \, d\mathbf{x} \\
&\quad + q(q-1) \partial_q \left(\frac{1}{q-1} \log \int \frac{\mu(\mathbf{x})^q}{\pi(\mathbf{x})^q} \pi(\mathbf{x}) \, d\mathbf{x} \right) \\
&\geq \frac{1}{q-1} \log \int \frac{\mu(\mathbf{x})^q}{\pi(\mathbf{x})^q} \pi(\mathbf{x}) \, d\mathbf{x},
\end{aligned}$$

where the inequality invokes the fact that the Rényi divergence is monotonic in the order q (Vempala and Wibisono, 2019, Lemma 11). Hence by setting $q = 2$,

$$\begin{aligned}
\text{Ent}_\pi \left(\frac{\mu^2}{\pi^2} \right) &\geq \left(\int \frac{\mu(\mathbf{x})^2}{\pi(\mathbf{x})^2} \pi(\mathbf{x}) \, d\mathbf{x} \right) \log \int \frac{\mu(\mathbf{x})^2}{\pi(\mathbf{x})^2} \pi(\mathbf{x}) \, d\mathbf{x} \\
\text{(H.2)} \quad &\geq (\chi^2(\mu \parallel \pi) + 1) \log (\chi^2(\mu \parallel \pi) + 1) \geq \chi^2(\mu \parallel \pi),
\end{aligned}$$

where the last inequality holds from $(x+1) \log(x+1) \geq x$ for each $x \geq 0$. Combining (H.1) and (H.2) completes the proof. \square

We next introduce Donsker-Varadhan variational principle Rassoul-Agha and Seppäläinen (2015, Theorem 5.4).

Lemma H.11. *Let μ and π be two distributions. Then for each function $\phi : \mathbb{R}^d \rightarrow \mathbb{R}$,*

$$\mathbb{E}_\mu[\phi] \leq \text{KL}(\mu \parallel \pi) + \log \mathbb{E}_\pi[\exp(\phi)].$$

The following lemma provides the Chernoff bound for χ^2 -distribution, which can be found in (Wainwright, 2019, Example 2.8) and Duchi (2024, Example 4.1.13).

Lemma H.12. *Let $\mathbf{X} = (X_1, \dots, X_d)$ be a vector of independent Gaussian random variables with zero mean and σ^2 -variance. Then*

$$\log \mathbb{E}[\exp\{s(\|\mathbf{X}\|_2^2 - \mathbb{E}[\|\mathbf{X}\|_2^2])\}] \leq 2ds\sigma^2.$$

Proof of Lemma H.12. Before proceeding, we consider the Chernoff bound for the Z^2 with $Z \sim N(0, 1)$. For $4\lambda < 1$, we have

$$\begin{aligned}
\mathbb{E}[\exp(\lambda(Z^2 - \mathbb{E}[Z^2]))] &= \frac{1}{\sqrt{2\pi}} \int \exp(\lambda(z^2 - 1)) \exp\left(-\frac{z^2}{2}\right) dz \\
\text{(H.3)} \quad &= \frac{\exp(-\lambda)}{\sqrt{1-2\lambda}} \leq \exp(2\lambda^2),
\end{aligned}$$

where the inequality holds from $-\log(1-2\lambda) \leq 2\lambda + 4\lambda^2$ for $4\lambda \leq 1$.

We next turn to verify the Chernoff bound for the χ^2 random variable with d degrees of freedom, denoted by $Y \sim \chi_n^2$. Note that $Y \stackrel{d}{=} \sum_{i=1}^d Z_i^2$ where $Z_1, \dots, Z_d \sim^{\text{i.i.d.}} N(0, 1)$. Then

for $4\lambda < 1$,

$$\begin{aligned} & \log \mathbb{E} \left[\exp \{ \lambda (Y - \mathbb{E}[Y]) \} \right] \\ &= \log \mathbb{E} \left[\exp \left\{ \sum_{i=1}^d \lambda (Z_i^2 - \mathbb{E}[Z_i^2]) \right\} \right] = \sum_{i=1}^d \log \mathbb{E} [\lambda (Z_i^2 - \mathbb{E}[Z_i^2])] \leq 2d\lambda^2, \end{aligned}$$

where the inequality follows from (H.3). Setting $\lambda = s\sigma^2$ completes the proof. \square

The next lemma shows that the KL divergence can be bounded by the Fisher information.

Lemma H.13. *Suppose the distribution π satisfies the log-Sobolev inequality with constant C_{LSI} . Then for each distribution μ ,*

$$\text{KL}(\mu \parallel \pi) \leq 2C_{\text{LSI}} \mathbb{E}_\pi \left[\left\| \nabla \sqrt{\frac{\mu}{\pi}} \right\|_2^2 \right].$$

Proof of Lemma H.13. Recall the log-Sobolev inequality

$$(H.4) \quad \text{Ent}_\pi(f^2) \leq 2C_{\text{LSI}} \mathbb{E}_\pi \left[\left\| \nabla f \right\|_2^2 \right].$$

Substituting $f^2(\mathbf{x}) = \mu(\mathbf{x})/\pi(\mathbf{x})$ into the left-hand side of (H.4) deduces

$$\begin{aligned} \text{Ent}_\pi \left(\frac{\mu}{\pi} \right) &= \int \frac{\mu(\mathbf{x})}{\pi(\mathbf{x})} \log \frac{\mu(\mathbf{x})}{\pi(\mathbf{x})} \pi(\mathbf{x}) \, d\mathbf{x} - \int \frac{\mu(\mathbf{x})}{\pi(\mathbf{x})} \pi(\mathbf{x}) \, d\mathbf{x} \log \int \frac{\mu(\mathbf{x})}{\pi(\mathbf{x})} \pi(\mathbf{x}) \, d\mathbf{x} \\ &= \int \mu(\mathbf{x}) \log \frac{\mu(\mathbf{x})}{\pi(\mathbf{x})} \, d\mathbf{x} = \text{KL}(\mu \parallel \pi). \end{aligned}$$

As a consequence,

$$\text{KL}(\mu \parallel \pi) = \text{Ent}_\pi \left(\frac{\mu}{\pi} \right) \leq 2C_{\text{LSI}} \mathbb{E}_\pi \left[\left\| \nabla \sqrt{\frac{\mu}{\pi}} \right\|_2^2 \right].$$

This completes the proof. \square

Lemma H.14. *For two distributions μ and π , it holds that*

$$\mathbb{E}_\mu \left[\left\| \nabla \log \frac{\mu}{\pi} \right\|_2^2 \right] = 4\mathbb{E}_\pi \left[\left\| \nabla \sqrt{\frac{\mu}{\pi}} \right\|_2^2 \right].$$

Proof of Lemma H.14. It is straightforward that

$$\begin{aligned} \mathbb{E}_\mu \left[\left\| \nabla \log \frac{\mu}{\pi} \right\|_2^2 \right] &= \int \left\| \nabla \log \frac{\mu(\mathbf{x})}{\pi(\mathbf{x})} \right\|_2^2 \mu(\mathbf{x}) \, d\mathbf{x} = \int \frac{\pi(\mathbf{x})}{\mu(\mathbf{x})} \left\| \nabla \frac{\mu(\mathbf{x})}{\pi(\mathbf{x})} \right\|_2^2 \pi(\mathbf{x}) \, d\mathbf{x} \\ &= 4 \int \left\| \frac{1}{2} \sqrt{\frac{\pi(\mathbf{x})}{\mu(\mathbf{x})}} \nabla \frac{\mu(\mathbf{x})}{\pi(\mathbf{x})} \right\|_2^2 \pi(\mathbf{x}) \, d\mathbf{x} = 4 \int \left\| \nabla \sqrt{\frac{\mu(\mathbf{x})}{\pi(\mathbf{x})}} \right\|_2^2 \pi(\mathbf{x}) \, d\mathbf{x} \\ &= 4\mathbb{E}_\pi \left[\left\| \nabla \sqrt{\frac{\mu}{\pi}} \right\|_2^2 \right], \end{aligned}$$

which completes the proof. \square

Lemma H.15. *Let μ and π be two distributions. Define ϕ as $d\mu = \phi \, d\pi$, and define $\psi \mathbb{E}_\pi[\phi^2] = \phi$. Then the following equality holds*

$$\mathbb{E}_\mu \left[\psi \left\| \nabla \log(\psi\phi) \right\|_2^2 \right] = \frac{4\mathbb{E}_\pi \left[\left\| \nabla_{\mathbf{x}} \phi \right\|_2^2 \right]}{\mathbb{E}_\pi[\phi^2]}.$$

Proof of Lemma H.15. It is straightforward that

$$\|\nabla \log(\psi\phi)\|_2^2 = \|\nabla \log \frac{\phi^2}{\mathbb{E}_\pi[\phi^2]}\|_2^2 = 4\|\nabla \log \phi\|_2^2 = \frac{4\|\nabla_{\mathbf{x}}\phi\|_2^2}{\phi^2}.$$

As a consequence,

$$\mathbb{E}_\mu[\psi\|\nabla \log(\psi\phi)\|_2^2] = \frac{4}{\mathbb{E}_\pi[\phi^2]} \int \frac{\|\nabla_{\mathbf{x}}\phi(\mathbf{x})\|_2^2}{\phi(\mathbf{x})} \mu(\mathbf{x}) \, d\mathbf{x} = \frac{4\mathbb{E}_\pi[\|\nabla_{\mathbf{x}}\phi\|_2^2]}{\mathbb{E}_\pi[\phi^2]},$$

which completes the proof. \square

APPENDIX I. EXPERIMENTAL DETAILS

I.1. Double-well problem. For the first problem, we adopt a residual neural network with 2 hidden layers to learn for the prior score. The width of each hidden layer is set as 128, and the activation functions is chosen as the sigmoid function. During the learning procedure, we apply the denoising score match method [Vincent \(2011\)](#) with a noise level 0.1 to improve the training efficiency. After that, the gradient of log posterior can be explicitly evaluated.

In the implementation of APF and EnKF, the ensemble size is set as $n = 1000$, same to the sample size used in SSLS. Among all the three methods, the initial state distribution is defined as the normal distribution $N(-1, 0.15^2)$.

I.2. Lorenz 96 model. For the Lorenz 96 problem, we adopt a 1D UNet to learn for the prior score. The channels are 32, 64 and 128, and the activation functions is chosen as the ReLU function. During the learning procedure, we apply the denoising score match method [Vincent \(2011\)](#) with a noise level 0.1 to improve the training efficiency. After that, the gradient of log posterior can be explicitly evaluated.

In the implementation of APF, if unspecified, the ensemble size is set as $n = 500$, same to the sample size used in SSLS. The initial state distribution is defined as the normal distribution $N(\mathbf{0}, \mathbf{I}_{20})$.

The superiority of SSLS in [Figure 6](#) can also be understood using [Figure 12](#). Starting from a bad initial guess, the width of assimilation band of the APF ensemble (the maximum difference between any two samples in the ensemble) becomes narrowing rapidly, due to the imbalanced distribution of the likelihood value. This phenomenon greatly reduces the efficiency of APF. On the contrary, SSLS adopts a continues network function to approximate

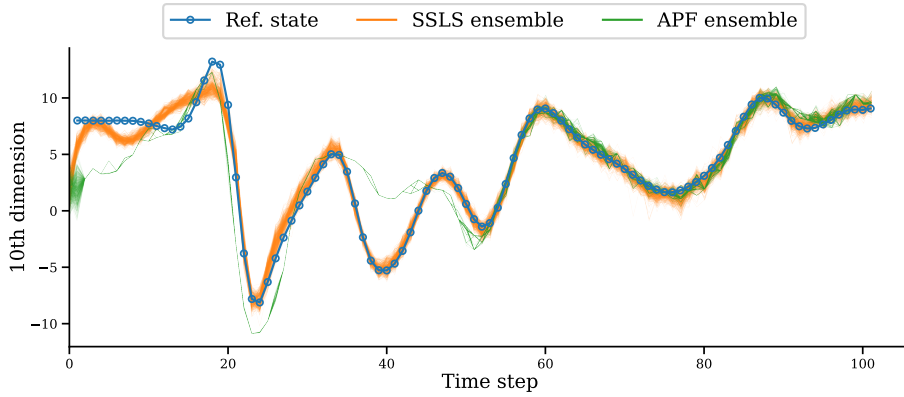


FIGURE 12. Evolution of x_{10} of the true states, the SSLS ensemble and the APF ensemble on REFERENCE LORENZ.

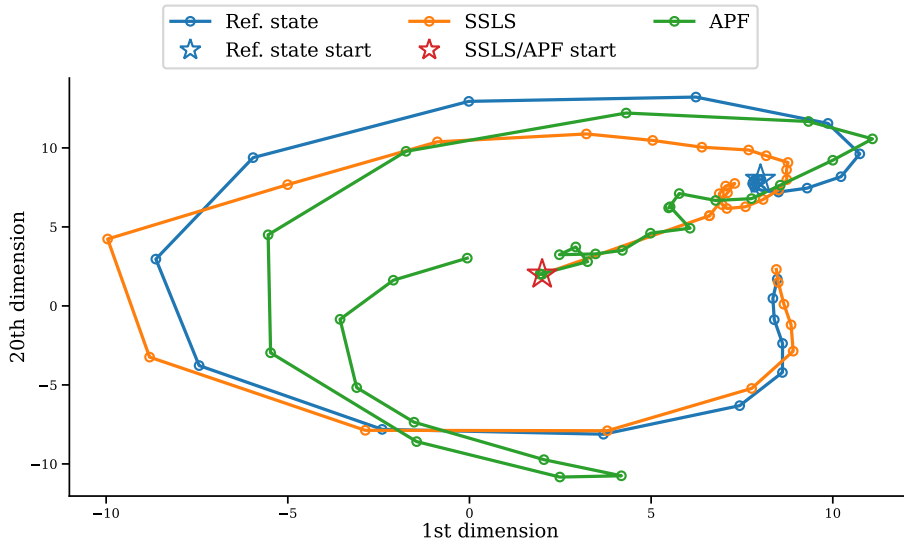


FIGURE 13. Trajectory of the true states, the SSSL estimation and the APF estimation for a Lorenz 96 system. The trajectory is visualized in the x_1 - x_{20} space.

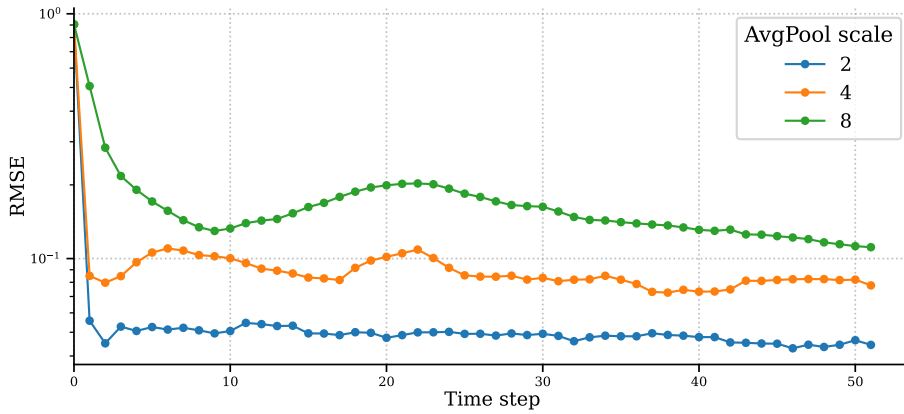


FIGURE 14. RMSE of SSSL assimilated states at different average pooling scale. Time 0 corresponds to RMSE from the expectation of the prior distribution, when the assimilation has not taken place. The three lines share the same starting RMSE as they share the same guess on the prior distribution.

the prior distribution, the better generalization ability increases the coverage probability for the true state. In Figure 13, we compare the predicted trajectories of SSSL and APF with true state in the x_1 - x_{20} space, which again verifies this advantage.

I.3. Kolmogorov flow. For the Kolmogorov flow problem, we adopt a 2D UNet to learn for the prior score. During the learning procedure, we apply the denoising score match method Vincent (2011) with a noise level 0.2 to improve the training efficiency. After that, the gradient of log posterior can be explicitly evaluated. The sample size used in SSSL is set as $n = 500$.

To further study the evolution of error, we also compare the RMSE of SSSL under different average pooling scale in Figure 14, which demonstrates at the early stage of assimilation

(eliminating the effect of initial lag error), the RMSE would decrease rapidly to a small value, and then maintain stable. Furthermore, a larger pooling scale would make the problem more difficult, resulting in a slower decrease of RMSE, converging to a higher value.

I.4. Numerical stability improvements. Throughout our numerical experiments, we mainly adopt two numerical improvements on the original algorithm for stability.

The first improvement is that, before matching the score function of the prior distribution at each step, we normalize the samples to zero mean and identity covariance. Then we match the score function on the normalized distribution, from which we obtain the original score function after affine transformation. In general, denote the prior distribution by $p_{\mathbf{X}}$, and its mean and standard deviation by μ and σ . Then for random variable $X \sim p_{\mathbf{X}}$ and its normalized version $\mathbf{Y} = \frac{\mathbf{X} - \mu}{\sigma}$. The definition of score function yields

$$\nabla_{\mathbf{x}} \log p_{\mathbf{X}}(\mathbf{x}) = \frac{\nabla_{\mathbf{y}} \log p_{\mathbf{Y}}(\mathbf{y})}{\sigma}, \quad \mathbf{y} = \frac{\mathbf{x} - \mu}{\sigma}.$$

Another improvement is that, we manually clip the score function of estimated posterior score by its L^2 -norm to ensure the stability of the Langevin Monte Carlo.

We provide a python-like pseudocode of SSLS in Listing 1 and Listing 2.

```
prior = sample_from_prior()
for i in range(k+1):
    prior_score = score_matching(prior) # sliced / implicit / denoising
    posterior_score = lambda x: grad_log_likelihood(x, y[i]) + prior_score(x)
    posterior = langevin(prior, posterior_score) # any Langevin-type sampling
    method
    prior = dynamics_transition(posterior)
```

LISTING 1. Pseudocode of SSLS with LMC

```
prior = sample_from_prior()
for i in range(k+1):
    prior_score = score_matching(prior) # sliced / implicit / denoising
    for m in range(M):
        posterior_score = lambda x: beta[m] * grad_log_likelihood(x, y[i]) +
        prior_score(x)
        posterior = langevin(prior, posterior_score) # any Langevin-type sampling
        method
    prior = posterior
    prior = dynamics_transition(posterior)
```

LISTING 2. Pseudocode of SSLS with ALMC